

**PETROGRAPHIC, MINERALOGIC, AND GEOCHEMICAL STUDIES OF  
HYDROCARBON-DERIVED AUTHIGENIC CARBONATE ROCK FROM GAS  
VENTING, SEEPAGE, FREE GAS, AND GAS HYDRATE SITES IN THE GULF  
OF MEXICO AND OFFSHORE INDIA**

A Dissertation

by

WOODONG JUNG

Submitted to the Office of Graduate Studies of  
Texas A&M University  
in partial fulfillment of the requirements for the degree of

DOCTOR OF PHILOSOPHY

December 2008

Major Subject: Geology

**PETROGRAPHIC, MINERALOGIC, AND GEOCHEMICAL STUDIES OF  
HYDROCARBON-DERIVED AUTHIGENIC CARBONATE ROCK FROM GAS  
VENTING, SEEPAGE, FREE GAS, AND GAS HYDRATE SITES IN THE GULF  
OF MEXICO AND OFFSHORE INDIA**

A Dissertation

by

WOODONG JUNG

Submitted to the Office of Graduate Studies of  
Texas A&M University  
in partial fulfillment of the requirements for the degree of

DOCTOR OF PHILOSOPHY

Approved by:

Chair of Committee,	Andrew Hajash, Jr.
Committee Members,	Mark E. Everett
	Mitchell J. Malone
	Stuart L. Scott
Head of Department,	Andreas Kronenberg

December 2008

Major Subject: Geology

## ABSTRACT

Petrographic, Mineralogic, and Geochemical Studies of Hydrocarbon-derived Authigenic Carbonate Rock from Gas Venting, Seepage, Free Gas, and Gas Hydrate Sites in the Gulf of Mexico and Offshore India. (December 2008)

Woodong Jung, B.S., Hanyang University;

M.S., Chungang University;

M.S., Texas A&M University

Chair of Advisory Committee: Dr. Andrew Hajash, Jr.

Authigenic carbonate rock (ACR) is derived from microbial oxidation of methane, biodegradation of crude oil, and oxidation of sedimentary organic matter. The precipitation of ACR was characterized petrographically, mineralogically, and geochemically. ACR collected from the seafloor in the Gulf of Mexico (GOM) and ACR recovered from drilled cores in the Krishna-Godawari (KG) basin offshore India were used. All study sites are associated with hydrocarbon gas venting, seepage, free gas, or gas hydrate. ACR from the GOM is densely cemented and extremely irregular in shape, whereas ACR from offshore India is generally an oval-shaped smooth nodule and also densely cemented. The dominant mineral in ACR is authigenic calcite.

ACR contains carbon derived from sedimentary organic carbon oxidation that geologically sequesters much fossil carbon. Bulk carbon and oxygen isotopes of ACR were measured. ACR from the GOM is strongly depleted in  $^{13}\text{C}$  with  $\delta^{13}\text{C}$  of  $-42.5\%$  and enriched in  $^{18}\text{O}$  with  $\delta^{18}\text{O}$  of  $+4.67\%$ . The  $\delta^{13}\text{C}$  of hydrocarbon is typically more depleted in  $^{13}\text{C}$  than in the associated ACR. The reason is that authigenic carbonate cements from hydrocarbon oxidation generally enclose skeletal material characterized by normal marine carbonate. Three groups that represent different hydrocarbon sources to ACR were classified in this study: primary carbon sources to ACR from (1) methane plus biodegraded oil, (2) methane, or (3) biodegraded oil.

Wide ranges in  $\delta^{13}\text{C}$  ( $-49.12$  to  $+14.06\text{‰}$ ) and  $\delta^{18}\text{O}$  ( $+1.27$  to  $+14.06\text{‰}$ ) were observed in ACR from offshore India. In sediments, the  $\delta^{13}\text{C}$  may be affected by differences in the rate of organic carbon oxidation, which generate varying  $\delta^{13}\text{C}$  with depth during methanogenesis. Based on the wide range in  $\delta^{13}\text{C}$ , ACR from offshore India was classified: (1)  $\delta^{13}\text{C}$  may reflect high rates of organic carbon oxidation, (2) ACR may be derived primarily from methane oxidation, and (3)  $\delta^{13}\text{C}$  may reflect low rates of organic carbon oxidation.

$\delta^{18}\text{O}$  values are heavier than those of normal marine carbonates. The  $\delta^{18}\text{O}$  may be caused by reaction with deep-sourced water that was isotopically heavier than ambient seawater. Some samples may reflect heavy  $\delta^{18}\text{O}$  from gas hydrate decomposition, but it would not cause significant heavy oxygen isotopes.

## DEDICATION

I dedicate this dissertation to:

My wife, SungAe Yoo

My son, Heejae Jung (“Tony”)

and

my father, Moon-Dal Jung and my late mother, Myung-Doo Lee  
for their love and support.

my father-in-law, Bum-Ho Yoo and my mother-in-law, Ju-Wha Kim  
for their love and support.

and

my uncle and my aunt for their love and support.

and

all of my family for their love and support.

and

all who love me.

Thank you.

## ACKNOWLEDGEMENTS

I would like to express my deep appreciation to Dr. Andrew Hajash for his guidance and encouragement with his warmth. I am especially thankful to Dr. Roger Sassen for his support, guidance, and patience through my graduate program. I also wish to thank my committee members, Drs. Mark Everett, Mitchell Malone, and Stuart Scott for their time, guidance, and advice.

My study was a part of the National Gas Hydrates Program India (NGHP) (2006) project offshore India under U.S. Geological Survey (USGS). I am thankful to the Directorate General of Hydrocarbons (DGH) NGHP and USGS, who gave me a great scientific experience on shipboard for research. The experience at sea motivates me to be a good researcher all the time.

Important and expensive rock samples recovered from great deep sediments in the Gulf of Mexico for this study were provided by the Geochemical and Environment Research Group (GERG) at Texas A&M University. I sincerely appreciate it.

Special appreciations are given to Drs. Bobb Popp, Ethan Grossman, and Ray Guillemette for precious teaching, lab work, and their guidance.

Last, I want to thank the Department of Geology and Geophysics and Texas A&M University for my graduate teaching assistantship and their support. I would never have finished without them.

**NOMENCLATURE**

$\alpha$	Fractionation factor
ACR	Authigenic carbonate rock
ALVIN	Deep submergence vehicle
AROM	Aromatic hydrocarbon
ASPH	Asphaltenes
BSE	Backscattered electron
BSR	Bottom simulating reflector
C <sub>1</sub>	Methane
C <sub>2</sub>	Ethane
C <sub>3</sub>	Propane
C <sub>4</sub>	Butane
C <sub>5</sub>	Pentane
DIC	Dissolved inorganic carbon
EDS	Energy dispersive X-ray spectroscopy
EOM	Total extractable organic matter
FPC	Fugro pressure corer
GHSZ	Gas hydrate stability zone
GOM	Gulf of Mexico
HRC	HYACE rotary corer
ICP	Integrated Chemistry-Physics
IR	Infrared
JSL	Johnson Sea-Link
KG	Krishna-Godawari
mbsf	Meters below sea floor
NBS-19	National Bureau of Standards-19
NGHP	National Gas Hydrate Program India
NSO	Nitrogen, sulfur, and oxygen compounds also known as resins

P	Pressure
PCS	Pressure core sampler
PDB	Pee Dee belemnite
RAB	Resistivity at bit
SAT	Saturated hydrocarbon
SMI	Sulfate-methane Interface
SMOW	Standard mean ocean water
STP	Standard temperature and pressure
T	Temperature
UCM	Unresolved complex mixture
V	Volume
VPDB	Vienna Pee Dee belemnite



## TABLE OF CONTENTS

	Page
ABSTRACT .....	iii
DEDICATION .....	v
ACKNOWLEDGEMENTS .....	vi
NOMENCLATURE.....	vii
TABLE OF CONTENTS .....	ix
LIST OF FIGURES.....	xi
LIST OF TABLES .....	xv
 CHAPTER	
I INTRODUCTION.....	1
Background .....	2
Carbonate carbon sources to ACR .....	10
Sedimentary organic matter .....	11
Microbial methane.....	12
Thermogenic hydrocarbon gases.....	13
CO <sub>2</sub> .....	14
Gas hydrate.....	14
Origin of waters at great depth in the Gulf of Mexico .....	16
II GEOLOGIC SETTING AND STUDY SITES .....	19
Gulf of Mexico .....	19
Offshore India .....	23
III METHODS.....	27

CHAPTER	Page
IV RESULTS: PETROGRAPHIC, MINERALOGIC, AND GEOCHEMICAL STUDIES OF HYDROCARBON-DERIVED AUTHIGENIC CARBONATE ROCK .....	30
Authigenic carbonate rock from the Gulf of Mexico.....	30
Mississippi Canyon (MC) 118 .....	30
Florida Escarpment at Vernon (VN) 945 .....	40
The Elbow (EL) 711 .....	45
Atwater Valley (AT) 425 .....	51
Authigenic carbonate rock from the Krishna-Godawari basin offshore India .....	57
Site 3 (NGHP-01-03, GDGH05-A).....	57
Site 5 (NGHP-01-05, KGGH02-A).....	69
Site 10 (NGHP-01-10, GD-3-1).....	80
Site 14 (NGHP-01-14, GDGH14-A).....	93
V DISCUSSION .....	103
Gulf of Mexico .....	103
Offshore India .....	112
VI CONCLUSIONS AND SUGGESTIONS FOR FUTURE RESEARCH.....	121
REFERENCES.....	125
APPENDIX A .....	135
APPENDIX B .....	137
VITA .....	139

## LIST OF FIGURES

FIGURE	Page
1.1 Generalized biogeochemical processes at hydrocarbon vent, seep, gas hydrate, and chemosynthetic community sites .....	6
1.2 Crystal structures of gas hydrates .....	15
1.3 $\delta^{18}\text{O}$ value profiles of interstitial waters at (A) Site 994 and (B) Site 997, Leg 164 in Blake Ridge .....	17
2.1 A conceptualized north-south cross section of central Gulf slope from the shelf to the abyssal plains .....	19
2.2 Location of study sites (MC 118, VN 945, EL 711, and AT 425) in the Gulf of Mexico slope.....	21
2.3 Location of Krishna-Godawari (KG) basin offshore India .....	23
2.4 Bathymetry and topography of northeastern Indian Ocean.....	24
2.5 Location of study sites in the Krishna-Godawari (KG) basin offshore India.....	25
4.1 Bathymetry image of the MC 118 site by side-scan sonar surveys .....	33
4.2 Seafloor imagery of the MC 118 site .....	33
4.3 Authigenic carbonate rock and thin section images from the MC 118 site	34
4.4 Point count analyses of a thin section of ACR-2 (MC 118) .....	37
4.5 Authigenic carbonate rock from hydrocarbon oxidation outcrops on the seafloor at the VN 945 site in the Florida Escarpment .....	41
4.6 Tube worms, mussels, and other organisms in a complex chemosynthetic community from the Florida Escarpment.....	41
4.7 Authigenic carbonate rock from the seafloor at the VN 945 site in the Florida Escarpment chemosynthetic community .....	42
4.8 Thin section images of authigenic carbonate rock from the VN 945 site ..	42
4.9 Point count analyses of thin sections of (a) ACR-3 (VN 945) and (b) ACR-4 (VN 945) .....	44
4.10 Authigenic carbonate rock and thin section images from the EL 711 site.	46

FIGURE	Page
4.11 Back Scattered Electron image (600X) of ACR from the EL 711 site .....	47
4.12 Back Scattered Electron image (100X) of ACR from the EL 711 site .....	48
4.13 Back Scattered Electron image (300X) of ACR from the EL 711 site .....	48
4.14 Energy dispersive X-ray spectroscopy (EDS) images of ACR from the EL 711 site .....	49
4.15 Authigenic carbonate rock and thin section images from the AT 425 site	53
4.16 Whole-oil chromatogram of bacterially oxidized crude oil from the AT 425 site showing hydrocarbons in the approximate C <sub>9</sub> to C <sub>20</sub> range.....	55
4.17 Multichannel seismic reflection line across Site 3 (GDGH05-A) in the Krishna-Godawari basin .....	57
4.18 Lithostratigraphic summary of Hole NGHP-01-03B .....	59
4.19 Authigenic carbonate bands and rock typical of those observed in core sections from Site 3 .....	60
4.20 Concentration depth profile of sulfate and methane at Site 3 .....	61
4.21 Plot of headspace methane gas concentration with depth at Site 3 .....	62
4.22 Plot of headspace carbon dioxide gas concentration with depth at Site 3.....	63
4.23 Authigenic carbonate rock and thin section images of ACR-1 (Site 3).....	64
4.24 Diagram illustrating effect of varying sedimentation rate and rate of organic-carbon oxidation on $\delta^{13}\text{C}$ values with depth .....	66
4.25 Multichannel seismic reflection line across Site 5 (KGGH02-A) in the Krishna-Godawari basin.....	69
4.26 Lithostratigraphic summary of Hole NGHP-01-05C .....	70
4.27 Nodules of authigenic carbonate rock from Site 5 .....	71
4.28 Concentration depth profile of sulfate and methane at Site 5 .....	72
4.29 Plot of headspace methane gas concentration with depth at Site 5 .....	73
4.30 Plot of headspace carbon dioxide gas concentration with depth at Site 5.....	74
4.31 Authigenic carbonate rock from Site 5 in the Krishna-Godawari basin offshore India .....	75

FIGURE	Page
4.32 Thin section images of ACR from Site 5 in the Krishna-Godawari basin offshore India .....	76
4.33 Multichannel seismic reflection line across Site 10 (NGHP-01-10) in the Krishna-Godawari basin .....	81
4.34 Lithostratigraphic summary of Hole NGHP-01-10B .....	82
4.35 Lithostratigraphic summary of Hole NGHP-01-10D .....	83
4.36 Authigenic carbonate rock and possible fossil chemosynthetic communities at Site 10 .....	84
4.37 Concentration depth profile of sulfate and methane at Site 10 .....	86
4.38 Plot of headspace methane gas concentration with depth at Site 10 .....	87
4.39 Plot of headspace carbon dioxide gas concentration with depth at Site 10 .....	88
4.40 Authigenic carbonate rock from Site 10 in the Krishna-Godawari basin offshore India .....	90
4.41 Thin section images of ACR from Site 10 in Krishna-Godawari basin offshore India .....	91
4.42 Multichannel seismic reflection line across Site 14 (GDGH14-A) in the Krishna-Godawari basin .....	94
4.43 Terrestrial organic matter (circled) and large broken authigenic carbonate rock from Site 14 .....	95
4.44 Lithostratigraphic summary of Hole NGHP-01-14A .....	96
4.45 Sulfate and alkalinity concentrations from Hole NGHP-01-14A .....	98
4.46 Plot of headspace methane gas concentration with depth at Site 14, Hole A .....	99
4.47 Plot of headspace carbon dioxide gas concentration with depth at Site 14, Hole A .....	100
4.48 Authigenic carbonate rock and thin section image of ACR-10 (Site 14)...	101
5.1 Authigenic carbonate rock from the Gulf of Mexico .....	103
5.2 Petrographic thin section images of authigenic carbonate rock from the Gulf of Mexico .....	105
5.3 Plot of $\delta^{13}\text{C}$ versus $\delta^{18}\text{O}$ of ACR from the Gulf of Mexico .....	106

FIGURE	Page
5.4 Petrographic thin section images of authigenic carbonate rock from the Krishna-Godawari basin offshore India .....	112
5.5 Plot of $\delta^{13}\text{C}$ versus $\delta^{18}\text{O}$ of authigenic carbonate rock from the Krishna-Godawari basin offshore India .....	115

## LIST OF TABLES

TABLE	Page
2.1 Summary of study sites in the Gulf of Mexico .....	22
2.2 Summary of study sites in the Krishna-Godawari basin offshore India.....	26
3.1 List of ACR samples from the Gulf of Mexico.....	28
3.2 List of ACR samples from the Krishna-Godawari basin offshore India....	29
4.1 Molecular and isotopic composition of vent gas and gas hydrate samples from the MC 118 site .....	32
4.2 Isotopic composition of authigenic carbonate rock from the MC 118 site	34
4.3 Isotopic composition of authigenic carbonate rock from the VN 945 site.	43
4.4 Isotopic composition of authigenic carbonate rock from the EL 711 site .	46
4.5 Molecular and isotopic composition of gas hydrate sample from the AT 425 site.....	52
4.6 Isotopic composition of authigenic carbonate rock of ACR-6 from the AT 425 site.....	53
4.7 Isotopic composition of authigenic carbonate rock from Site 3.....	65
4.8 Oxygen isotopic composition of ACR-1 (Site 3).....	68
4.9 Isotopic composition of authigenic carbonate rock from Site 5.....	75
4.10 Oxygen isotopic properties of authigenic carbonate rock from Site 5.....	79
4.11 Molecular and isotopic composition of gas hydrates from Site 10.....	80
4.12 Isotopic composition of authigenic carbonate rock from Site 10.....	89
4.13 Oxygen isotopic properties of authigenic carbonate rock from Site 10.....	93
4.14 Isotopic composition of ACR-10 (Site 14) .....	101
4.15 Oxygen isotopic properties of authigenic carbonate rock from Site 14.....	102
5.1 Isotopic composition of authigenic carbonate rock from the Gulf of Mexico.....	111
5.2 Isotopic composition of authigenic carbonate rock from the KG basin offshore India .....	119

TABLE	Page
5.3 Calculated oxygen isotopes and temperatures of authigenic carbonate rock from the KG basin offshore India .....	120



## CHAPTER I

### INTRODUCTION

The objective of this study is to characterize the precipitation of hydrocarbon-derived authigenic carbonate rock (ACR). It is important to study ACR because ACR sequesters enormous quantities of carbon as part of the global carbon cycle (Houghton et al., 1996; Judd et al., 2002; Dickens, 2003; Sassen et al., 2006). ACR may also be a valuable guide to petroleum exploration. Microbial processes related to the formation of ACR may contribute to the development and stability of chemosynthetic communities on the deep seafloor (Roberts and Aharon, 1994; Aharon and Fu, 2000; Sassen et al., 2004a). Also, designing programs to sequester carbon dioxide (CO<sub>2</sub>) as carbonate rock may be an outstanding issue for industrial processes.

ACR is abundant globally and has been discovered mainly in areas of sediments containing methane and other hydrocarbons. The global abundance and distribution of ACR in marine sediments depends on the flux of methane and other hydrocarbons over time in response to environmental changes. ACR typically occurs as massive pavements, slabs, crusts, nodules, and cements on the seafloor and within the sediment column (Sassen and Roberts, 2004).

In this study, sixteen samples of ACR were studied: six samples recovered from the seafloor in the Gulf of Mexico (GOM) and ten samples collected from drilled cores in the Krishna-Godawari (KG) basin offshore India. Eight study sites (four in the GOM and four in the KG basin offshore India) are characterized by hydrocarbon gas venting, seepage, free gas, or gas hydrate associated with ACR.

---

This dissertation follows the style of Chemical Geology.

Petrographic, mineralogic, and geochemical studies characterized ACR. Petrographic thin sections were used to describe textures and to identify carbonate phases of ACR. A microprobe was also used to provide backscattered electron (BSE) images to identify chemical elements in ACR. Bulk carbon and oxygen isotopes ( $\delta^{13}\text{C}$  and  $\delta^{18}\text{O}$ ) of ACR were measured and documented. Carbon isotopes reflect carbon sources, whereas oxygen isotopes reflect temperatures of initial formation of ACR (Friedman and O'Neil, 1977; Bohrmann et al., 1998). The measured  $\delta^{13}\text{C}$  values of ACR are different from those of normal marine carbonates. The  $\delta^{13}\text{C}$  of ACR rarely corresponds to the  $\delta^{13}\text{C}$  of source carbon in this study. ACR derived from several different sources of carbon with different  $\delta^{13}\text{C}$  values is characterized.

### **Background**

A major discovery by Feely and Kulp (1957) focused on the origin of elemental sulfur in association with carbonate host rock in the cap rocks of oil-productive Gulf Coast salt domes. The precipitation of gulf salt-dome carbonate cap rock and elemental sulfur is the result of microbial processes at shallow depths and low temperatures. Previously, some scientists had thought the cap rock was the result of thermochemical processes at great depth and high temperature (Feely and Kulp, 1957).

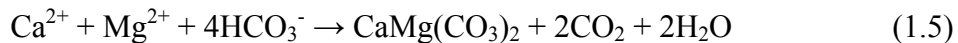
Posey et al. (1987) reviewed principal papers on carbon and oxygen isotopes of Gulf Coast salt domes located in the East Texas basin and in the Northern Louisiana basin. They reported that calcite cap rocks are highly depleted in  $^{13}\text{C}$  ranging from  $-5$  to  $-51\text{‰}$  compared to normal marine carbonates such as limestone ( $\delta^{13}\text{C} = 0 \pm 5\text{‰}$  PDB, Hudson, 1977). Calcite cap rock  $\delta^{18}\text{O}$  values are in the range of  $-4$  to  $+11.2\text{‰}$ .

The microbial origin of carbonate mineralization has become increasingly well documented. Gas vents, seeps, and gas hydrates in marine sediments are associated with ACR. The precipitation of ACR depends on oxidation of methane, sulfate reduction, hydrocarbon oxidation, and methanogenesis via  $\text{CO}_2$  reduction (Mozley and Burns,

1993; Roberts and Aharon, 1994; Sassen et al., 2004a), and biodegradation of crude oil (Sassen et al., 2004b).

ACR is defined as a carbonate rock formed by in-situ inorganic precipitation on the seafloor and within the sediment column (Kastner, 1999). ACR is typically depleted in  $^{13}\text{C}$  because it is derived from the microbial oxidation of methane and other hydrocarbons. In contrast, the carbon skeletal material from bivalves and other calcareous organisms is characterized by  $\delta^{13}\text{C}$  similar to normal marine carbonates (Sassen et al., 2004b).

Carbonates are anionic complexes of  $\text{CO}_3^{2-}$  and divalent metallic cations such as Ca, Mg, Fe, Ba, Sr, Mn, Cu, and Zn. Common carbonates are grouped on the basis of their crystal lattice structures: calcite (hexagonal), dolomite (hexagonal), and aragonite (orthorhombic). A carbonate rock is classified as a sedimentary rock composed primarily of carbonate minerals. Limestone and dolomite are two major types of carbonate rock. They are composed of calcite ( $\text{CaCO}_3$ ) and dolomite [ $\text{CaMg}(\text{CO}_3)_2$ ] minerals, respectively. Calcite (Eq. 1.4) and dolomite (Eq. 1.5) precipitation reactions are given below.



In some marine environments, hydrocarbon and nonhydrocarbon gases produced in subsurface sediments migrate vertically and naturally vent from the seafloor to the water column. Vent gas is important because it is the source of carbon from which ACR precipitates. Vent gas also drives microbial processes that result in build-ups of ACR, and supports chemosynthetic organisms such as tube worms and mussels on the seafloor. Most free gas in sediment is rapidly oxidized in situ by microbial processes at shallow sediment depths, leading to sequestration of carbon as the precipitation of ACR (Sassen, 2004).

At selected sites where ACR occurs, methane ( $C_1$ ) is the main component of vent gas. Ethane ( $C_2$ ), propane ( $C_3$ ), normal butane ( $n-C_4$ ), isobutane ( $i-C_4$ ), normal pentane ( $n-C_5$ ), isopentane ( $i-C_5$ ), and neo-pentane (neo- $C_5$ ) are also present.  $CO_2$  is also found in vent gas. For example, vent gas was collected and analyzed from the Mississippi Canyon (MC) 118 site in the Gulf of Mexico, where  $C_1$  was 93.0 to 96.5% of the normalized hydrocarbon gas ( $C_1$  through  $C_5$ ). Ethane, propane, and other hydrocarbon gases are present in lesser relative abundance. Nonhydrocarbon gas such as  $CO_2$  was a relatively minor component with a relative concentration of ~1% of the concentration of methane (Sassen, 2004; Sassen et al., 2006).

The vent gases related to oil from the deep subsurface petroleum system are of thermogenic origin. These gases are characterized by  $\delta^{13}C$  values that vary. For example, at the Mississippi Canyon (MC) 118 site in the GOM the  $\delta^{13}C$  value of  $C_1$  is  $-45.7\text{‰}$ ,  $C_2$  is  $-26.9\text{‰}$ , and  $C_3$  is  $-24.2\text{‰}$ . The  $\delta^{13}C$  of  $CO_2$  is  $-20.2\text{‰}$  (Sassen et al., 2006).

The vent gases produced by bacteria, archaea, fungi, etc. are of microbial origin. Microbial gases are characterized by  $\delta^{13}C$  values of  $C_1$  that are strongly depleted in  $^{13}C$ . For example, microbial  $C_1$  may be defined as about  $-70\text{‰}$  (Sassen, 2004), ranging between  $-60$  and  $-80\text{‰}$  (Kvenvolden, 1995; Whiticar et al., 1986).

Many scientists use  $\delta^{13}C$  to distinguish ACR from normal marine carbonate. ACR associated with carbon derived from methane oxidation is strongly depleted in  $^{13}C$  (Barker and Fritz, 1981; MacDonald et al., 1989; Roberts and Aharon, 1994; Roberts and Carney, 1997; Bohrmann et al., 1998; Aharon and Fu, 2000; Thomsen et al., 2001;

Gieskes et al., 2005; Sassen et al., 1999, 2004a, 2006). Therefore, if  $C_1$  was the primary source of carbon to ACR, one would expect it also to be highly depleted in  $^{13}\text{C}$  with  $\delta^{13}\text{C}$  of  $\sim -70\text{‰}$  (microbial origin methane) (Whiticar et al., 1986; Kvenvolden, 1995; Sassen, 2004) or  $\sim -45\text{‰}$  (thermogenic origin methane) (Sassen, 2004; Sassen et al., 2006).

At the Elbow (EL) 711 site offshore Florida, sampling and analysis of microbial  $C_1$  has shown it to be highly depleted in  $^{13}\text{C}$  with  $\delta^{13}\text{C}$  of  $-80\text{‰}$  (Sassen et al., 2004b). ACR from the EL 711 site has been shown to be depleted in  $^{13}\text{C}$  with  $\delta^{13}\text{C}$  of  $-34.8\text{‰}$ . In addition,  $C_1$  has a mean  $\delta^{13}\text{C}$  of  $-45.7\text{‰}$  at the MC 118 site (Sassen et al., 2006). ACR from the MC 118 site is depleted in  $^{13}\text{C}$  with  $\delta^{13}\text{C}$  of  $-30.7\text{‰}$ . If the primary source of carbon to ACR is  $C_1$ , then one would expect it also to be highly depleted in  $^{13}\text{C}$ . Why are those rock samples so enriched in  $^{13}\text{C}$  with  $\delta^{13}\text{C}$  of  $-34.8\text{‰}$  and  $-30.7\text{‰}$  when compared to  $^{13}\text{C}$  with  $\delta^{13}\text{C}$  of  $-80\text{‰}$  at the EL 711 site and  $-45.7\text{‰}$  at the MC 118 site of  $C_1$ ? The hypothesis is that the carbonate is derived from several different sources of carbon with different  $\delta^{13}\text{C}$  values. Sources of carbon to ACR may include normal marine carbonates (e.g., foraminifera, planktonic organisms, and other skeletal carbonates), oxidation of  $C_1$  from methanogenesis, oxidation of other hydrocarbons ( $C_2$  through  $C_5$ ), oxidation of sedimentary organisms, dissolved inorganic carbon ( $\text{CO}_2$ ), and biodegradation of crude oil.

Sassen et al. (2001b) analyzed the  $\delta^{13}\text{C}$  of ACR recovered from Atwater Valley (AT) 425 site in the Gulf of Mexico (GOM), suggesting that oil may be a dominant contributor of ACR depleted in  $^{13}\text{C}$  with  $\delta^{13}\text{C}$  of  $-28.6\text{‰}$ . They also suggested that ACR contains carbonate carbon from several sources. Possible sources of carbon include oil, thermogenic methane, and normal marine carbonates. Other main sources of carbonate carbon include microbial processes of methane oxidation and sulfate reduction and methanogenesis.

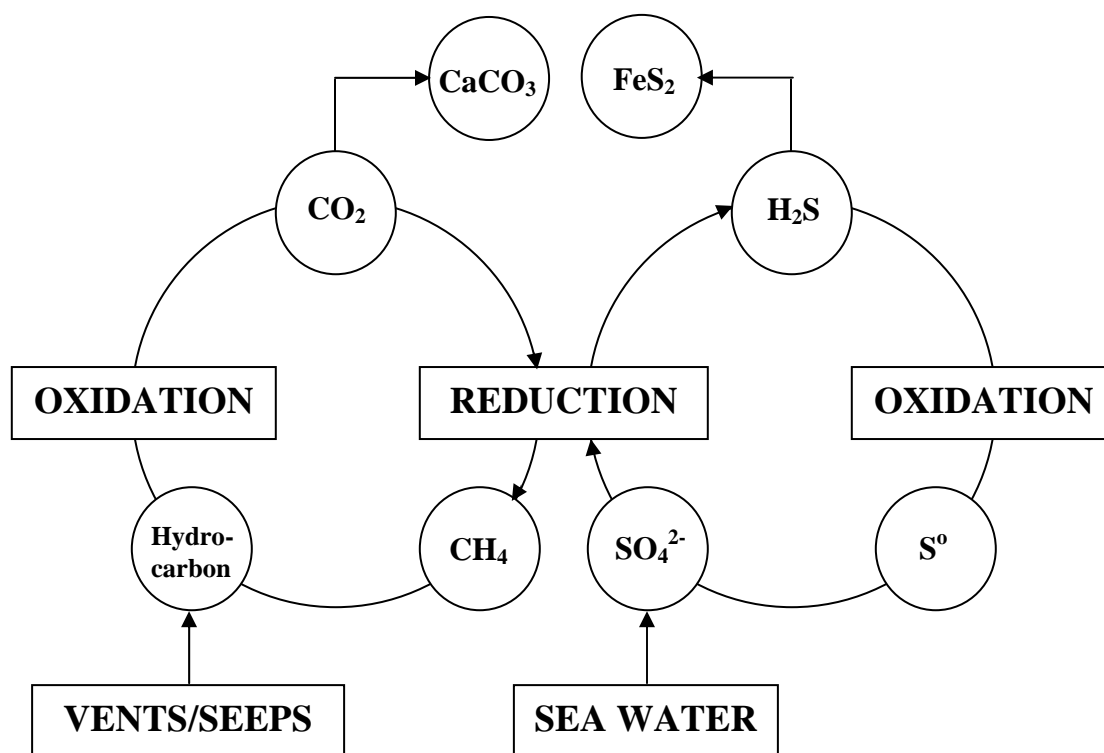


Fig. 1.1. Generalized biogeochemical processes at hydrocarbon vent, seep, gas hydrate, and chemosynthetic community sites (modified from Sassen, 1980; 2004).

Methane oxidation and sulfate reduction increases alkalinity in sediment pore water, favoring the precipitation of ACR (Fig. 1.1). Aharon and Fu (2000) studied microbial sulfate reduction rates at oil and gas seeps in deepwater Gulf of Mexico. They found that sulfate reduction and anaerobic methane oxidation are the dominant microbial processes occurring in gas hydrate-bearing sediments where crude oil and methane are present. The crude oil and gas seep sites are generally characterized by well-developed seafloor chemosynthetic communities. In their study, push cores (0 to 0.5 mbsf) were recovered in seep sediments at chemosynthetic communities. Profiles ( $\text{SO}_4^{2-}$  vs. depth) from pore fluids of the sediments show that estimated sulfate reduction rates are higher

in crude oil seeps (up to 50 times) and methane seeps (up to 600 times) relative to a nonseep sediment.

Methane oxidation, fueled by a flux of methane, and the oxidation of organic matter determine the rate of degree of sulfate reduction (Iverson and Jørgensen, 1985; Reeburgh, 1976, 1980). Carbon isotopes of dissolved inorganic carbon (DIC) and methane may be used to estimate the relative amount of sulfate reduction occurring by methane oxidation or oxidation of sedimentary organic matter. This is because oxidation of sedimentary organic matter produces carbon dioxide ( $\text{CO}_2$ ) in the zone of sulfate reduction. Subsequently, the microbial processes between the  $\text{CO}_2$  and methane through the mineralization of organic carbon are accompanied by carbon isotope fractionations and can be measured.

Common  $\delta^{13}\text{C}_{\text{CO}_2}$  values from oxidation of sedimentary organic matter decrease from surface values of  $\sim 0\text{‰}$  to the base of sulfate reduction zone of  $\sim -20\text{‰}$  (Reeburgh, 1980; Whiticar et al., 1986; Kvenvolden, 1995; Burns, 1998). In contrast, the values of  $\delta^{13}\text{C}_{\text{CO}_2}$  from Amazon Fan sediments were recorded as low as  $-49.6\text{‰}$  (Burns, 1998). The values suggest that a large portion of the dissolved  $\text{CO}_2$  in the sediments may be sourced by the anaerobic oxidation of microbial methane. This is because the  $\delta^{13}\text{C}$  values of microbial methane are between  $-60$  and  $-80\text{‰}$  (Whiticar et al., 1986; Kvenvolden, 1995; Sassen et al., 2004a) near the base of the sulfate reduction zone. Then, typically below the zone of sulfate reduction, methanogenesis takes place by the microbial process of  $\text{CO}_2$  reduction (Claypool and Kaplan, 1974; Whiticar et al., 1986; Kvenvolden, 1995), increasing  $\delta^{13}\text{C}_{\text{CO}_2}$  values to  $\sim +5\text{‰}$  (Burns, 1998).

Mozley and Burns (1993) studied the  $\delta^{18}\text{O}$  of authigenic marine carbonates from recent published data. The  $\delta^{18}\text{O}$  values for calcite ( $\text{CaCO}_3$ ), siderite ( $\text{FeCO}_3$ ), and dolomite [ $\text{CaMg}(\text{CO}_3)_2$ ] are highly variable. For calcite,  $\delta^{18}\text{O}$  values range from  $-10$  to  $0\text{‰}$ . For siderite,  $\delta^{18}\text{O}$  values range from  $-12$  to  $+1\text{‰}$ . For dolomite,  $\delta^{18}\text{O}$  values range from  $-7$  to  $+8\text{‰}$ .

In contrast, Bohrmann et al. (1998) recovered ACR from the upper 50 cm of sediments from the Hydrate Ridge in the Cascadia subduction zone. The mineralogy of

ACR includes microcrystalline high-magnesium calcite ( $\text{CaCO}_3$ ) and aragonite. They measured  $\delta^{18}\text{O}$  of high-magnesium calcite ( $\text{CaCO}_3$ ) with a value of +4.86‰ and an aragonite sample with a value of +3.86‰. Hudson (1977) generalized values of  $\delta^{18}\text{O}$  from many measurements of methane-derived ACR ranging from +1.5 to +5.0‰.

Large quantities of carbon may be sequestered, because ACR was investigated by side-scan sonar surveys that strongly modify the seafloor over an area of  $\sim 1 \text{ km}^2$  at the MC 118 site in the GOM (Sassen et al., 2006). ACR is estimated to sequester  $\sim 3$  billion  $\text{m}^3$  of  $\text{CO}_2$  gas (STP) at the MC 118 site. The magnitude of the volume of  $\text{CO}_2$  involved suggests that microbial processes appear to sequester  $\text{CO}_2$  as ACR over long periods of geologic time.

ACR forms by in situ precipitation. Associated authigenic minerals of ACR include sulfides (pyrite), sulfates (barite and gypsum), and oxides. The main minerals of ACR are carbonates (Roberts et al., 1990; Roberts and Aharon, 1994; Bohrmann et al., 1998; Malone et al., 2002; Sassen, 2004; Jung and Sassen, 2006) such as calcite, aragonite (Sassen et al., 2004b; Sassen, 2004; Mazzini et al., 2006), dolomite (Baker and Burns, 1985; Malone et al., 1990; Mazzini et al., 2006), and siderite (Taylor and Curtis, 1995; Rodriguez et al., 2000). Pyrite (Berner, 1964, 1970; Peckmann et al., 2001; Chen et al., 2006) and barite (Fu et al., 1994; Torres et al., 1996a,b; Dickens, 2001; Castellini et al., 2006) are in trace quantities of ACR. Oxides (Fe and Mn) often coat carbonates on the seafloor (Roger Sassen).

In this study, ACR samples were recovered from eight sites: four sites in the GOM and four sites in the KG basin offshore India. Each site is characterized by hydrocarbon gas venting, free gas, seepage, well-developed seafloor chemosynthetic communities, or gas hydrate deposits. The four study sites in the GOM include Mississippi Canyon (MC) 118, Florida Escarpment at Vernon Basin (VN) 945, Elbow (EL) 711, and Atwater Valley (AT) 425. These sites are summarized as follows.

MC 118: Hydrocarbon gas venting, gas hydrate, and chemosynthetic communities.



VN 945: Microbial methane seeps, chemosynthetic communities, oil seeps, and no gas hydrate.

EL 711: Microbial methane in high concentration in sediment, well-developed chemosynthetic communities, and no gas hydrate.

AT 425: Thermogenic hydrocarbon gas venting, gas hydrate, oil stained sediment, and chemosynthetic communities.

The other four sites, from the KG basin offshore India, are Site 3 (NGHP-01-03), Site 5 (NGHP-01-05), Site 10 (NGHP-01-10), and Site 14 (NGHP-01-14) on the east coast of India at the Krishna-Godawari (KG) basin on the passive margins of the Indian Peninsula, which are the areas of seismically inferred gas hydrate occurrences. The occurrence of gas hydrate with deeper microbial free gas may be controlled by methane, other hydrocarbon gases, oil, and nonhydrocarbon fluxes through vertical migration systems.

Each site from the KG basin offshore India is summarized as follows.

Site 3: Seafloor-parallel to slightly inclined beds to a depth of ~125 mbsf, structural unconformity. Free gas trapping is indicated by the strong seismic reflectivity below bottom simulating reflector (BSR) (209 mbsf). Disseminated gas hydrates are observed.

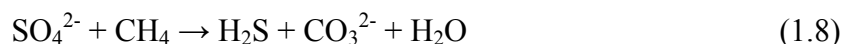
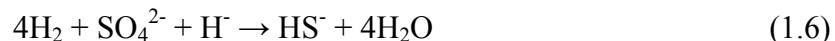
Site 5: Well-developed faulting is observed. Free gas trapping below ~120 mbsf and no gas hydrate.

Site 10: Distinct BSR is observed at ~170 mbsf. Well-developed gas trapping under BSR, free gas with anticline structure, possible cold vent, and mud-volcanism at the seafloor were observed. Gas hydrate site.

Site 14: Typical sediment sequences of basin and ridge. Each ridge associated with a deep-rooted fault. Basins are characterized by seafloor parallel to subparallel and sedimentary sequences, whereas the ridge flanks are dominated by layers of large dips. Free gas is indicated below a BSR. Disseminated gas hydrates are present.

### Carbonate carbon sources to ACR

In this study, ACR samples contain carbonate carbon derived from hydrocarbons. Some source of carbon is degradation of sedimentary organic matter. In most environments, including marine sediments, the remineralization of carbon proceeds through microbial consortia. In the zone of sulfate reduction or in the upper portion of sediment sections, sulfate reducing bacteria compete against methanogenic bacteria for available electron donors such as hydrogen (H<sub>2</sub>) and acetate (CH<sub>3</sub>COOH) (Burns, 1998). The chemical reactions of sulfate reduction are given in Eqs. (1.6) and (1.7). Both carbonate and hydrogen sulfide (H<sub>2</sub>S) derived from microbial sulfate reduction have also been documented in cold submarine seeps, where methane donates as the reduced carbon source (Sansone and Martens, 1982; Iversen and Jørgensen, 1985; Aharon, 2000; Valentine and Reeburgh, 2000; Valentine, 2002; Sassen, 2004) in Eq. (1.8).



Consequently, CH<sub>4</sub> production or accumulation proceeds in the zone of sulfate reduction until the sulfate is substantially depleted, whereas oxidation of sedimentary organic matter (CH<sub>2</sub>O) may produce CO<sub>2</sub>. The chemical reaction of sulfate reduction is given in Eq. (1.9) (Aharon and Fu, 2000).



Typically methane is generated microbially in marine sediments after the concentrations of oxidants (electron acceptors) such as SO<sub>4</sub>, O<sub>2</sub>, and NO<sub>3</sub> (Cavagna et

al., 1999; Valentine and Reeburgh, 2000; Thomsen et al., 2001) are depleted. Once concentrations of oxidants are depleted, organisms use CO<sub>2</sub> as an oxidant to decompose for methane production through microbial methanogenesis. The chemical reaction of methane production is given in Eq. (1.10) (Thauer, 1998).



CH<sub>4</sub> production begins to occur near the bottom of the sulfate/methane interface (SMI), increasing the production of CH<sub>4</sub> with increasing depth. Methane may also be generated at greater depths by thermal hydrocarbon cracking (Tissot and Welte, 1984; Sassen, 2004).

ACR is often composed of carbon from several different sources. Each carbon source separately will be discussed: sedimentary organic matter, microbial methane, thermogenic hydrocarbon gases, CO<sub>2</sub>, and gas hydrate.

### **Sedimentary organic matter**

Geological sections contain clay, mud, and sand sediments that accumulate in thick sections of Tertiary deltas at study sites in the GOM and in the KG basin offshore India. The main type of organic matter in both basins is terrestrially derived. It is carried into the basins by great river systems (Collett et al., 2006; Sassen, 2004; Roger Sassen).

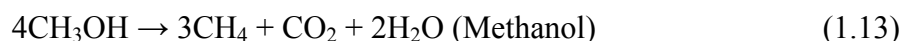
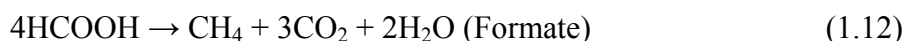
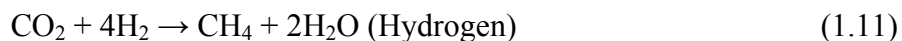
In marine sediments, sedimentary organic matter may produce CO<sub>2</sub> in the zone of sulfate reduction and also produce CH<sub>4</sub> in the zone of methanogenesis (Burns, 1998; Paull et al., 2000). Those microbial processes result in organic carbon remineralization accompanied by large fractionations of carbon isotopes between carbon reservoirs. The fractionations of carbon isotopes may be controlled by a flux of methane (Borowski et al., 1996), the rate of organic carbon oxidation, and sedimentation rate (Mozley and Burns, 1993), leading to depth-related differences in the mineralogy and carbon isotopes.

In general, organic carbon derived from oxidation of sedimentary organic matter has a δ<sup>13</sup>C value of around -20‰ at the base of sulfate reduction zone. The δ<sup>13</sup>C of

dissolved inorganic carbon (DIC) is in the range of around 0‰ at the seafloor to –20‰. The  $\delta^{13}\text{C}$  value of DIC may be enriched in  $^{13}\text{C}$  in the zone of methanogenesis. Thus, the DIC may also be isotopically heavier with depth as methanogenesis proceeds (Burns, 1998).

### Microbial methane

Methanogenic reactions involving hydrogen, formate, methanol, and carbon monoxide drive microbial methane production from sedimentary organic matter (Valentine, 2002).



The hydrogen methanogenic process primarily dominates in marine sediments (Chapelle et al., 2002). The  $\text{CO}_2$  reduction process depends on dissolved  $\text{H}_2$  molecules that are derived from compounds of sedimentary organic matter. Microbial gases predominantly contain methane ( $\text{C}_1$ ) with minor amounts of ethane ( $\text{C}_2$ ) and traces of propane ( $\text{C}_3$ ). They are characterized by  $\delta^{13}\text{C}$  and  $\delta\text{D}$  values of methane that is strongly depleted in  $^{13}\text{C}$  and D. The  $\delta^{13}\text{C}$  and  $\delta\text{D}$  values of microbial methane are isotopically lighter than –55‰ and –200‰, respectively (Bernard et al., 1978; Whiticar, 1999).

Sassen et al. (2002) and Milkov (2005) studied carbon isotopic properties of methane from 160 high flux seep sites at the seafloor across the GOM from the outer shelf to the lower slope. These sites represent the intersection of a major migration conduit from the deep subsurface to the seafloor related to salt or faults. Their mean  $\delta^{13}\text{C}$

value of methane is  $-74\text{‰}$ , whereas the range is from  $-30.1$  to  $-116.6\text{‰}$ . Isotopically light methane represents microbial origin methane, whereas isotopically heavy methane probably implies thermogenic origin methane. Sassen et al. (2002) and Milkov (2005) suggest that high-flux gas seeps across the GOM are a mixture of microbial and thermogenic hydrocarbons. Therefore, the carbon isotopic properties between microbial and thermogenic methane often may not be defined because of considerable overlap. For example, the mean  $\delta^{13}\text{C}$  value of microbial methane is  $-69.0\text{‰}$  from gas hydrate samples collected from Site 10 offshore India (Data from Oil and Natural Gas Corporation India, ONGC),  $-57$  to  $-73\text{‰}$  from gas hydrate samples collected in subaquatic settings from around the world (Kvenvolden, 1995),  $-60$  to  $-110\text{‰}$  in marine sediments and  $-50$  to  $-65\text{‰}$  in freshwater sediments (Whiticar et al., 1986), and  $-68.4\text{‰} \pm 7\text{‰}$  (mean) from methane samples collected on Ocean Drilling Program (ODP) Leg 164 in the Blake Ridge (Rodriguez et al., 2000).

### **Thermogenic hydrocarbon gases**

Hydrocarbon gases related to oil from the deep subsurface petroleum systems are of thermogenic origin. Thermogenic gas is produced by the degradation of kerogen at temperatures over  $\sim 120^\circ\text{C}$  and burial depths greater than  $\sim 1$  km (Tissot and Welte, 1984). Methane is the primary component of microbial origin gases, whereas thermogenic origin gases contain a considerable amount of  $\text{C}_{2+}$  hydrocarbons (Schoell, 1983; Sassen et al., 1999, 2001b, 2001d; Milkov, 2005).

Thermogenic gas is characterized by  $\delta^{13}\text{C}$  values that vary but are closer to those of its original sedimentary organic matter (Paull et al., 2000) because of low fractionation during thermal cracking of kerogen (Schoell, 1980). The  $\delta^{13}\text{C}$  and  $\delta\text{D}$  values of thermogenic methane are isotopically heavier than  $-55\text{‰}$  and  $-200\text{‰}$ , respectively (Bernard et al., 1978; Whiticar, 1999). For example, thermogenic gases at the MC 118 site are characterized by  $\delta^{13}\text{C}$  of methane with a mean value of  $-45.7\text{‰}$  from gas hydrate samples (Sassen et al., 2006).

## **CO<sub>2</sub>**

CO<sub>2</sub> derived from anaerobic oxidation of sedimentary organic matter has  $\delta^{13}\text{C}$  of  $\sim -20\text{‰}$  in the SMI, the value of marine sedimentary organic carbon (Burns, 1998). Consequently, the  $\delta^{13}\text{C}$  values of DIC decrease from  $\sim 0\text{‰}$  at the seafloor to  $-20\text{‰}$  near the SMI (Claypool and Kaplan, 1974; Mozley and Burns, 1993). Below the SMI,  $^{12}\text{C}$  from CO<sub>2</sub> is preferentially fractionated into methane, and hence residual DIC becomes enriched in  $^{13}\text{C}$ .

## **Gas hydrate**

Natural gas hydrates are found from the seafloor to ocean sediment depths, in thick permafrost regions, in deep water sediments of inland lakes, and in polar sediment (Kvenvolden and Lorenson, 2001). Gas hydrates are crystalline compounds. Gas and fresh water combine to form the ice-like crystalline solids at temperatures above the normal freezing point of water. Gas molecules are trapped by hydrogen bonding inside well-defined cages formed by the water molecules.

There are three representative crystal structures of natural gas hydrates: Structure I (body-centered cubic lattice), Structure II (diamond lattice), or Structure H (hexagonal lattice) (Sloan, 1998). Structure I may form from methane, ethane, carbon dioxide, hydrogen sulfide, and nitrogen. Structure II may form with larger, single-guest molecules than those of Structure I, such as propane or isobutane. Larger molecules such as isopentane or neohexane form Structure H (Fig. 1.2).

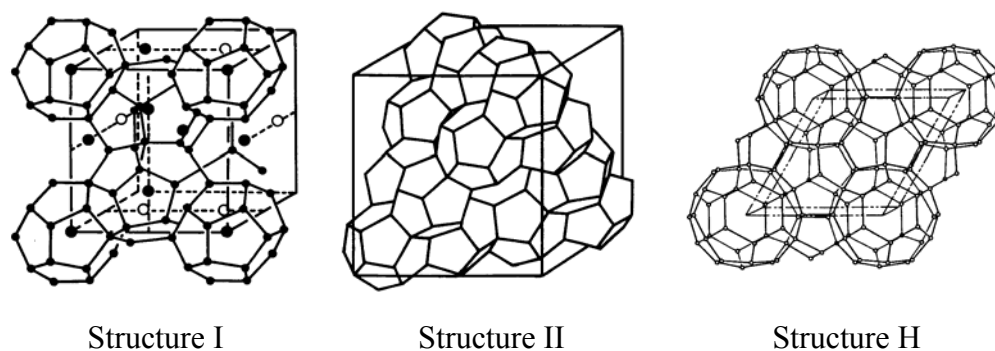


Fig. 1.2. Crystal structures of gas hydrates (Structure I and II, Ripmeester et al., 1987; Structure H, von Stackelberg and Müller, 1954).

Sassen et al. (2001a) have provided interesting evidence for molecular fractionation of  $^{13}\text{C}$  related to gas hydrates. In their study, a gas hydrate mound that contains massive, vein-filling, Structure II gas hydrates occurs on the upper continental slope of the GOM, southwest of the Mississippi Delta. The mound is located in the Green Canyon (GC) 185, adjacent to Jolliet field in GC 184. The Jolliet field is characterized by oil and gas that filled fault traps by salt deformation. Sassen et al. (2001a) measured molecular and isotopic properties of  $\text{C}_1$  to  $\text{C}_5$  hydrocarbons collected from vent gas and gas hydrates. Methane collected from vent gas is the primary component (mean = 93.2%). The methane is thermogenic in origin with mean  $\delta^{13}\text{C}$  of  $-45.5\text{‰}$  and mean  $\delta\text{D}$  of  $-190\text{‰}$ . Mean relative abundance of  $\text{C}_{2+}$  hydrocarbons from vent gas is ethane (3.7%), propane (2.1%), isobutane (0.5%), normal butane (0.5%), isopentane (0.2%), and normal pentane ( $<0.1\%$ ). The mean  $\delta^{13}\text{C}$  values of  $\text{C}_{2+}$  hydrocarbons from vent gas are ethane ( $-29.8\text{‰}$ ), propane ( $-25.8\text{‰}$ ), isobutane ( $-28.9\text{‰}$ ), and normal butane ( $-23.4\text{‰}$ ). Methane collected from gas hydrates is also the primary component (mean = 77.5%). Hydrate-bound methane from GC 185 is enriched in  $^{13}\text{C}$  (mean  $\delta^{13}\text{C} = -42.9\text{‰}$ ) and D (mean  $\delta\text{D} = -168\text{‰}$ ). Mean relative abundance of  $\text{C}_{2+}$  hydrocarbons collected from gas hydrates is propane (9.7%), ethane (9.2%), isobutane (1.8%), normal butane (1.2%), isopentane (0.5%), and normal pentane ( $<0.1\%$ ). The mean  $\delta^{13}\text{C}$  values of hydrate-bound ethane ( $-29.2\text{‰}$ ), propane ( $-25.6\text{‰}$ ),

and mean  $\delta^{13}\text{C}$  of the pentanes is within  $<1\%$  of the vent gas. The mean  $\delta^{13}\text{C}$  values of ethane and propane in vent gas and gas hydrates are identical, but the mean  $\delta^{13}\text{C}$  values of methane from gas hydrates are slightly enriched in  $^{13}\text{C}$  when compared to vent gas. The  $\delta^{13}\text{C}$  values of methane collected from vent gas and gas hydrates are almost the same. It appears that no obvious isotopic fractionation of  $^{13}\text{C}$  occurs during gas hydrate crystallization in the complex natural settings of the deep sea.

Also, several scientists have proposed molecular fractionation of  $^{18}\text{O}$  regarding gas hydrates. They propose that gas hydrate crystallization preferentially favors  $^{18}\text{O}$  in the crystal lattice (Hesse and Harrison, 1981; Ussler and Paull, 1995; Matsumoto and Borowski, 2000). Thus, hydrogen bonding combined with water molecules within gas hydrates is enriched in isotopically heavy oxygen ( $^{18}\text{O}$ ) relative to ambient waters. Therefore, residual water from hydrate crystallization may become depleted in  $^{18}\text{O}$ . In contrast, gas hydrate decomposition may also enrich the water in  $^{18}\text{O}$ .

Matsumoto and Borowski (2000) have reported molecular fractionation of  $\delta^{18}\text{O}$  values from interstitial waters in the gas hydrate stability zone (GHSZ) at Sites 994 and 997 in the Blake Ridge as gas hydrates decomposed during core recovery. The magnitude of the fractionation in  $^{18}\text{O}$  from Site 997 is 0.3 to 0.6‰ SMOW (Fig. 1.3). No obvious isotopic fractionation of  $^{18}\text{O}$  appears to occur during gas hydrate decomposition in complex natural settings.

### **Origin of waters at great depth in the Gulf of Mexico**

The main structural features of the northern Gulf of Mexico are salt basins, which formed during Late Triassic rifting and were generated by salt during Middle Jurassic marine incursions (Salvador, 1987). In this study, geological sections contain clay, mud, and sand sediments that accumulate in thick sections of Tertiary deltas in the Gulf of Mexico (GOM) and in the Krishna-Godawari (KG) basin offshore India. The



main type of organic matter in both basins is terrestrially derived. It is carried into the basins by great river systems (Sassen, 2004; Collett et al., 2006).

Land and Macpherson (1992) proposed that three types of water (Na-acetate type, NaCl type, and Ca-rich type) dominate Cenozoic hydrocarbon reservoirs in the Gulf of Mexico sedimentary basin. The water is derived from dewatering of the clastic sediments, and vertically migrates into Cenozoic section from underlying Mesozoic strata. Concomitantly, aqueous solutes are derived almost entirely from the interactions between water and rock such as dissolution and recrystallization.

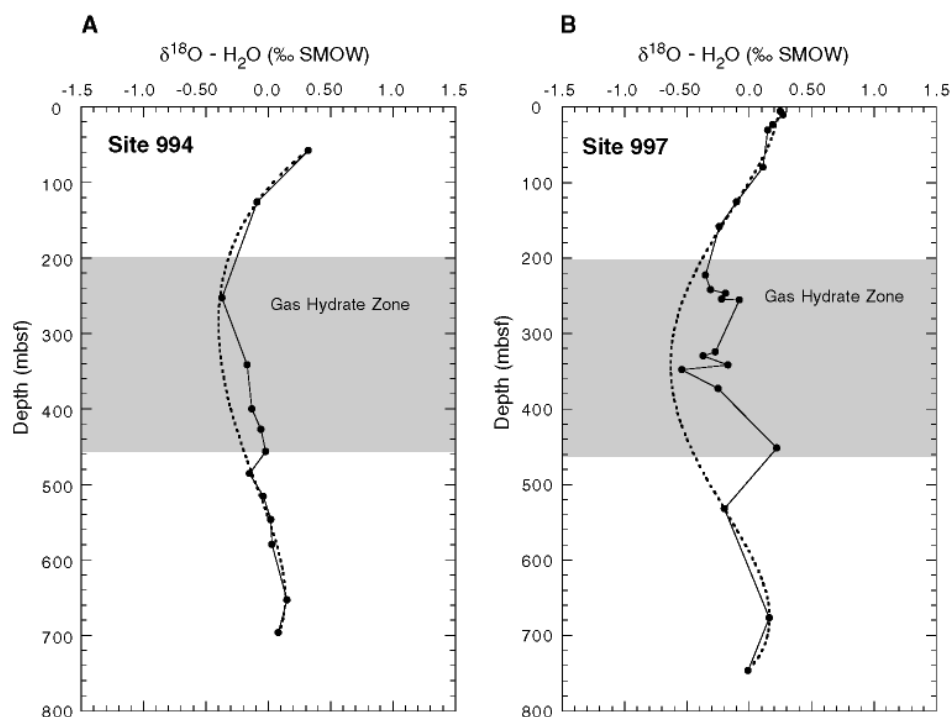


Fig. 1.3.  $\delta^{18}\text{O}$  value profiles of interstitial waters at (A) Site 994 and (B) Site 997, Leg 164 in Blake Ridge. Dotted lines represent baselines for the interstitial waters likely unaffected by gas hydrate decomposition (Matsumoto and Borowski, 2000).

Morton and Land (1987) proposed that three major water types (Na-acetate, NaCl, and Ca-rich) characterize reservoirs in the Oligocene Frio formation, Texas Gulf Coast. They evaluated regional compositional variations in different formation waters

encountered in fields of Portland (Na-acetate water), West Alta Loma (NaCl water), and Candelaria (Ca-rich water) in the Oligocene Frio Formation, Texas Gulf Coast. They collected 90 water samples from three wells: Portland well (2,963 mbsf), West Alta Loma well (3,741 mbsf), and Candelaria well (2,890 mbsf). Their study and laboratory data (Morton et al., 1983) showed that Na-acetate water is internally derived from the geopressured zone sediments by mineral reactions that release water and by interaction between water and rock. Na-acetate water is characterized by Cl concentrations between about 6,000 and 20,000 mg/L. Na-acetate water has  $\delta^{18}\text{O}$  of +6.9‰ SMOW. NaCl water ( $\delta^{18}\text{O} = +4.3\text{‰}$  SMOW) is derived by dissolution of diapiric salt. NaCl water is characterized by Cl concentrations between about 30,000 and 70,000 mg/L, less than about 2,000 mg/L Ca concentration, and dominated by NaCl. This water type is slightly affected by water/rock interaction. Ca-rich water is characterized by high Cl and high Ca concentrations. This water type ( $\delta^{18}\text{O} = +5.5\text{‰}$  SMOW) is derived from underlying Mesozoic strata.

Although Ca-rich water is most typical of the Oligocene Frio formation, it is least common in Cenozoic hydrocarbon reservoirs in the Gulf of Mexico sedimentary basin (Land and Macpherson, 1992). Land and Macpherson (1992) proposed that Na-acetate water is typical of many shale-rich sections not associated with diapiric salt. The water originated as seawater, but was modified by microbial reactions such as sulfate reduction or methanogenesis. The most abundant water is NaCl water in the Gulf basin, which consists of more than 90% NaCl. They studied  $\delta^{18}\text{O}$  values of three types of formation water in the Gulf Coast Cenozoic section: Eocene Wilcox, Oligocene Frio, and Miocene. In their study, Na-acetate water has  $\delta^{18}\text{O}$  values of +5.1‰, +4.8‰, and +3.3‰ SMOW. NaCl water has  $\delta^{18}\text{O}$  values of +3.5‰, +4.3‰, +4.0‰, and -1.6‰ SMOW. Influx of meteoric water in shallow formations was recognized by  $\delta^{18}\text{O}$  values isotopically lighter than seawater.

## CHAPTER II

### GEOLOGIC SETTING AND STUDY SITES

#### Gulf of Mexico

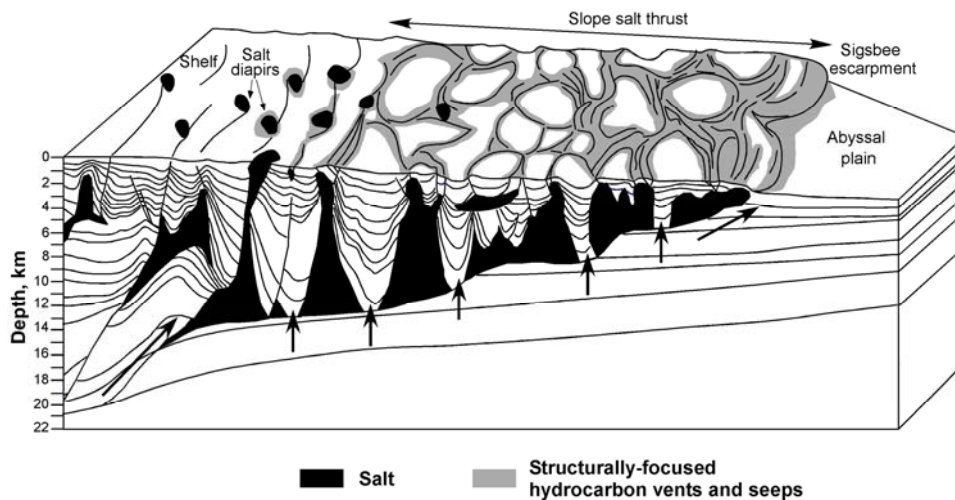


Fig. 2.1. A conceptualized north-south cross section of central Gulf slope from the shelf to the abyssal plains. Numerous geologically young basins formed by salt withdrawal pierce the slope salt thrust. Fluids migrate upward through openings in the salt thrust (arrows). Hydrocarbon vents and seeps are focused by the structure near the rims of salt withdrawal basins (Sassen et al., 2004a).

The Gulf of Mexico (GOM) is an ideal region to study authigenic carbonate rock (ACR). The geology of the GOM continental slope is characterized by hydrocarbon seepage, migration, and venting. The hydrocarbon sources come from sedimentary organic matter either by microbial degradation or by thermal cracking of kerogen. Numerous geologically young basins formed by salt withdrawal. Fluids migrate upward through the openings in the salt thrusts. Hydrocarbon venting and seepage are focused by the structure near the rims of salt withdrawal basins (Sassen et al., 2004a).

The fluids, methane ( $C_1$ ) and other hydrocarbons (mostly  $C_2$  through  $C_5$ ), vent at numerous mud volcanoes and seeps from the seafloor in the GOM (Neurauter and

Bryant, 1990; Roberts et al., 1990; Sassen et al., 1993). The GOM continental shelf is also characterized by numerous salt domes, whereas the continental slope is affected by large sheet-like salt thrusts (Worrall and Snelson, 1989; Sassen, 2004).

The main structural features of the northern Gulf of Mexico are salt basins, which formed during Late Triassic rifting and were generated by salt during Middle Jurassic marine incursions (Salvador, 1987). In this area, the large Gulf of Mexico Salt Basin extends from the coastal salt dome province to the lower continental slope. A number of smaller interior salt basins also extend onshore from south Texas to Alabama (Sassen et al., 2004a).

The framework of deep hydrocarbon involves vertical migration through salt withdrawal basins that pierce the large salt thrusts (Fig. 2.1). A series of structural fracture areas associated with active salt sheets and faults provides migration conduits for penetration upward through openings from greater depth to the seafloor of fluids including gas, crude oil, and brines. In some brine seeps, which may be associated with limited chemosynthetic communities, minerals include strontium-rich barite (Fu and Aharon, 1998; Sassen et al., 2004a).

ACR forms rapidly, modifying enormous seafloor structures including massive irregular pavements, bunches of slabs, cemented crusts, and many nodules. The seafloor shows irregular bathymetry from structural deformation, faulting, fracturing, and slumping (Roberts and Carney, 1997). Widely distributed and massive hydrocarbon seepages result in gas hydrate formation, oil-stained sediments, ACR precipitation depleted in  $^{13}\text{C}$ , and hydrocarbon-driven chemosynthetic communities (MacDonald et al., 1989; Roberts and Aharon, 1994; Aharon et al., 1997; Roberts and Carney, 1997). Many seepages and irregular venting are widely distributed across the Gulf slope. Fluid migration and movement from great depth are structurally controlled (Sassen et al., 2004a). Gas hydrates and chemosynthetic communities are concentrated along the rims of salt-withdrawal basins, over salt ridges, and near the faulted and folded margin of the Sigsbee (deepest part of the Gulf of Mexico) Escarpment at the downdip limit of the Gulf of Mexico Salt Basin (Fig. 2.1).

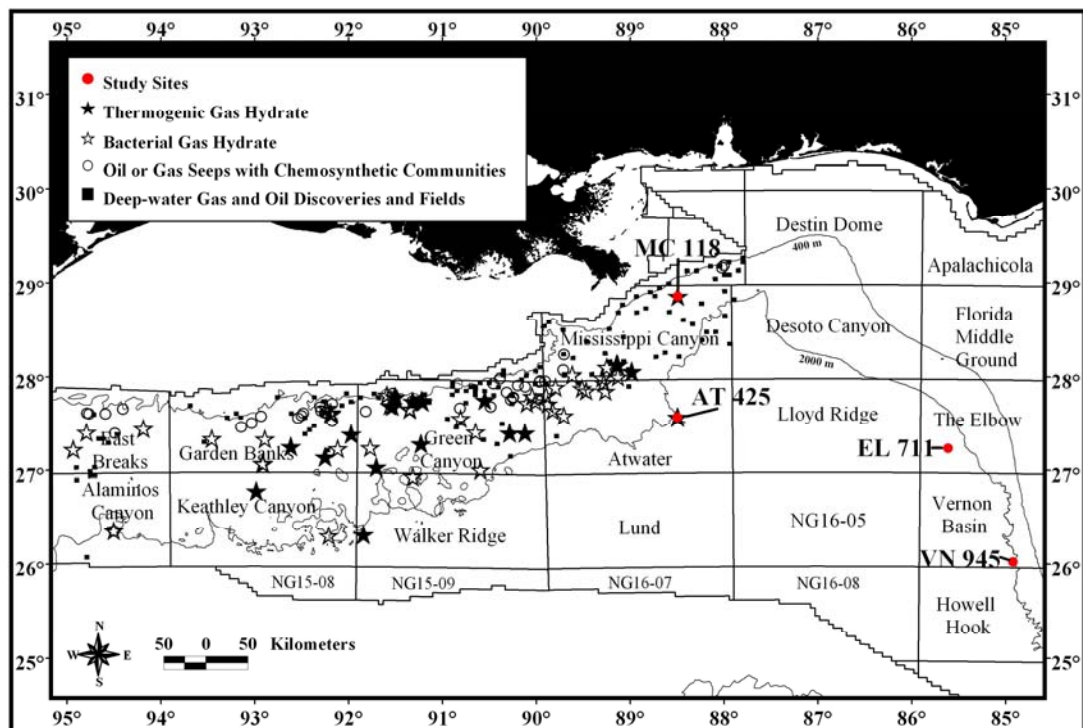


Fig. 2.2. Location of study sites (MC 118, VN 945, EL 711, and AT 425) in the Gulf of Mexico slope (Sassen et al, 2004a).

Samples of ACR were collected from sites in the GOM during submersible dives using either the Johnson Sea-Link (JSL) research submarine or a deep submergence vehicle (ALVIN) (Sassen, 2004). The samples from four sites in the GOM were studied petrographically, mineralogically, and geochemically. The four sites are Mississippi Canyon (MC) 118, Florida Escarpment at Vernon (VN) 945, Elbow (EL) 711, and Atwater Valley (AT) 425 (Fig. 2.2). The description of the study sites is summarized in Table 2.1.

Table 2.1  
Summary of study sites in the Gulf of Mexico

Sites	Seafloor temperature (°C)	Water depth (m)	Site description
MC 118	5.7	890	Hydrocarbon gas vents, gas hydrate, chemosynthetic communities
VN 945	–	3,300	Microbial methane seeps, chemosynthetic communities, gas hydrate not found
EL 711	4.0	3,220	Microbial methane in high concentration in sediment, well developed chemosynthetic communities, gas hydrate not found
AT 425	6.0	1,920 – 1,930	Thermogenic hydrocarbon gas vents, oil stained sediment, chemosynthetic communities, gas hydrate

## Offshore India

Study sites are located on the Krishna-Godawari (KG) basin in the eastern passive continental margin of the Indian Peninsula (Fig. 2.3). This continental margin formed as the result of rifting between India and the rest of East Gondwanaland (Australia/Antarctica) in the Late Jurassic and Early Cretaceous (Powell et al., 1988; Scotese et al., 1988). Since 2006, the Indian National Gas Hydrate Program (NGHP) has studied gas hydrate occurrences with geologic and geochemical research in the area.

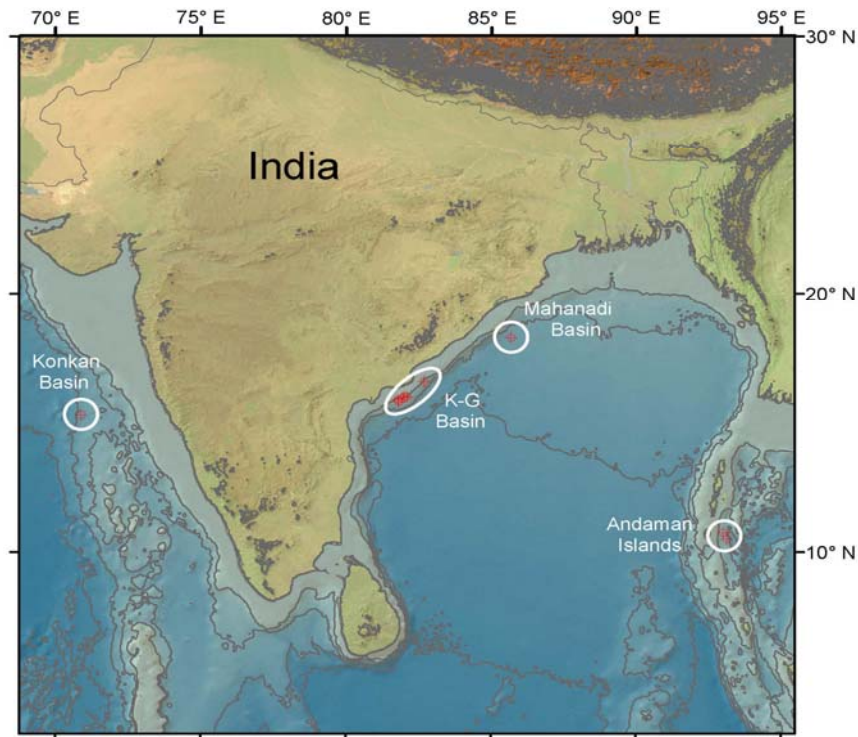


Fig. 2.3. Location of Krishna-Godawari (KG) basin offshore India (Collett et al., 2006).

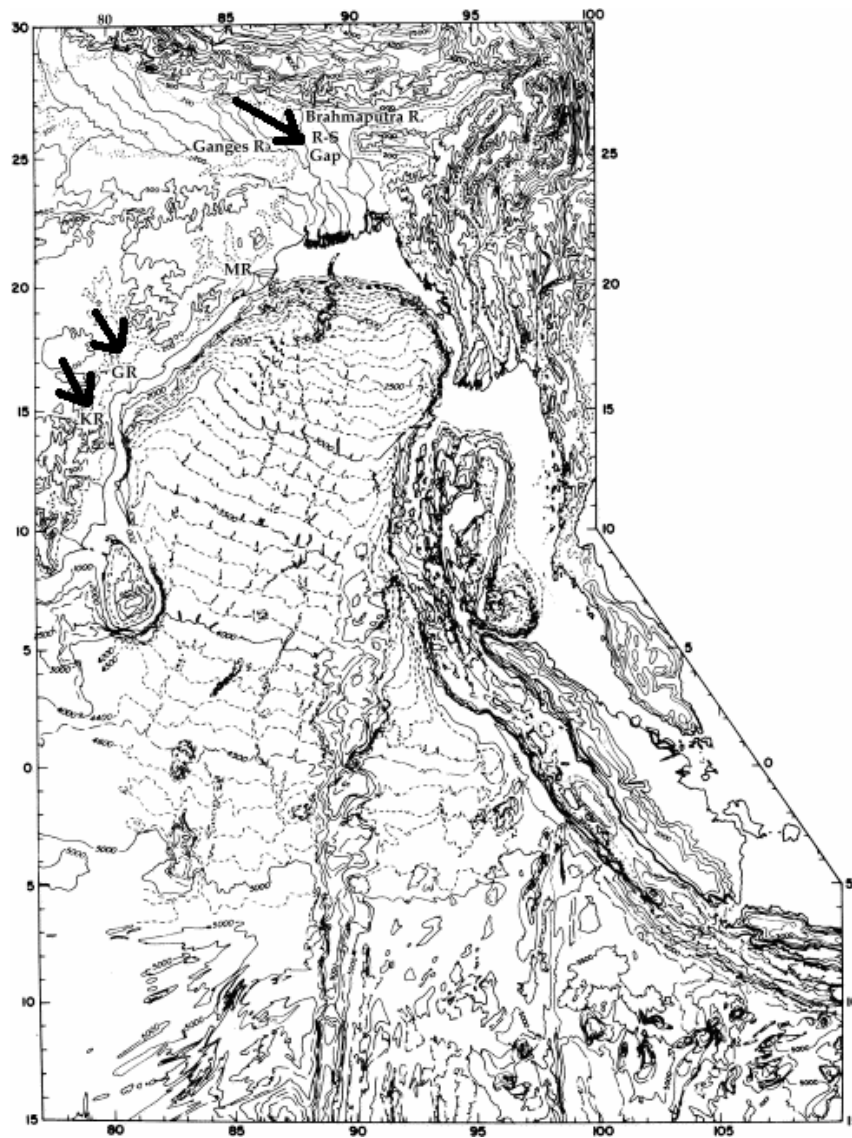


Fig. 2.4. Bathymetry and topography of northeastern Indian Ocean. KR is Krishna River. GR is Godawari River. R-S is Rajmahal-Shillong Gap (Curry et al., 2003).

Sediment input to the continental margin of the Bay of Bengal is dominated by the Ganges-Brahmaputra River system, which drains much of the Himalayas (Fig. 2.4). This sediment input has built the Bengal Fan, which is the largest submarine fan in the world, with a length of  $\sim 3,000$  km to the south, a width of  $\sim 1,000$  km (Curry et al.,



2003). The depth to basement reaches a maximum of over 22 km on the Bangladesh shelf (Curry, 1991) and over 2 km of fan sediments are found there (Curry et al., 1982).

At study sites, the depth to basement is 8 to 10 km with the contributions of sediment from Krishna and Godawari rivers. Krishna and Godawari rivers have a high sediment transport. Both rivers have built substantial deltas. The sedimentation is dominated by the river input with smaller contributions from the Bengal Fan (Sastri et al., 1981; Biksham and Subrahmanyam, 1988).

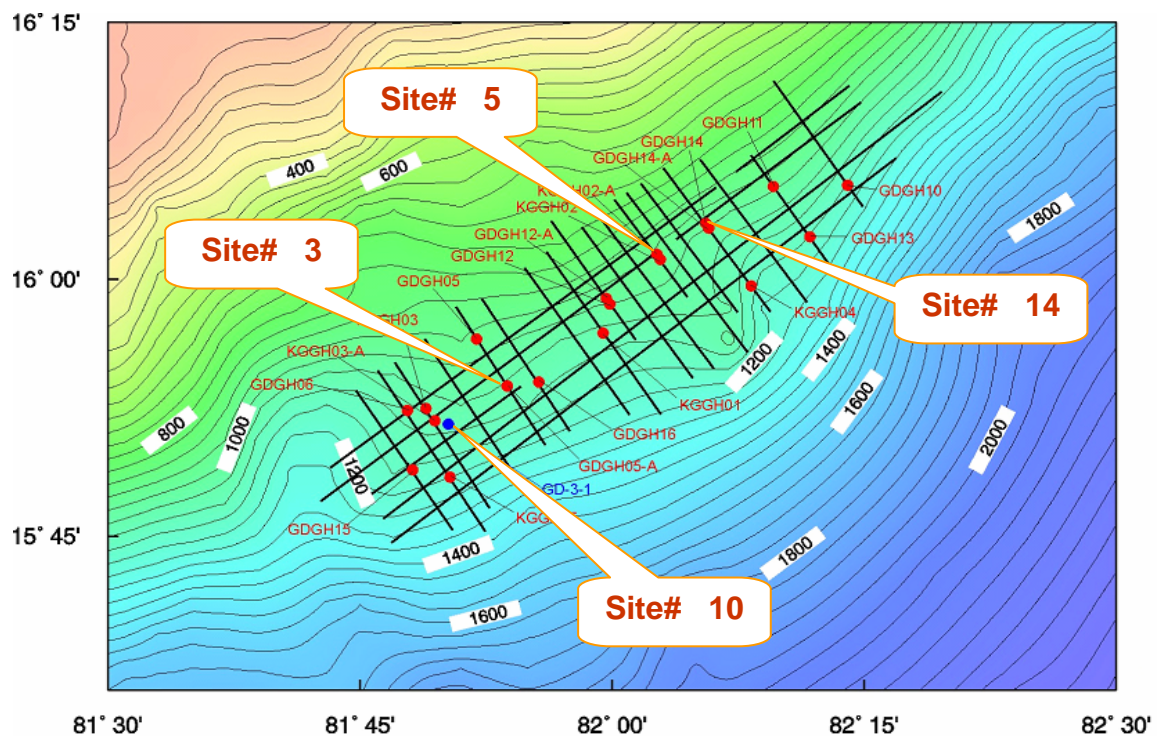


Fig. 2.5. Location of study sites in the Krishna-Godawari (KG) basin offshore India (Collett et al., 2006).

The KG basin shows typical features of fans including cut and filled channels and abundant growth faulting. Thus, the sediments drilled are mostly clays with well-defined horizon sediment layers. Study sites are characterized by microbial methane gas (Collett et al., 2006). Seismic data suggest gas hydrate occurrences. Microbial methane has also been discovered by industry oil and gas exploration drilling at the study sites.

The samples of gas hydrate were collected from cores drilled during the NGHP. The molecular compositions and isotopes of gas hydrate samples from Site 10 (NGHP-01-10) in the KG basin offshore India were measured. Methane ( $C_1$ ) is the main component of gas hydrate from Site 10. The mean concentrations of  $C_1$  and ethane ( $C_2$ ) were 99.6% and 0.2%, respectively, whereas  $CO_2$  is a relatively minor component. In relative terms, the concentration of  $CO_2$  is ~0.1%. The gases from gas hydrate may be of microbial origin, with  $\delta^{13}C$  values with  $-69.0\text{‰}$  of  $C_1$  and  $-50.8\text{‰}$  of  $C_2$  (data from Oil and Natural Gas Corporation India, ONGC).

ACR samples from four study sites in the KG basin offshore India were studied (Fig. 2.5). Four study sites include Site 3 (NGHP-01-03, GDGH05-A), Site 5 (NGHP-01-05, KGGH02-A), Site 10 (NGHP-01-10, GD-3-1), and Site 14 (NGHP-01-14, GDGH14-A). The samples were collected at the sediment depths between 16.2 and 173.2 meter below seafloor (mbsf). Water depth, seafloor temperature, and geothermal gradient of study sites are summarized in Table 2.2.

Table 2.2. Summary of study sites in the Krishna-Godawari basin offshore India

Sites	Water depth (m)	Seafloor temperature ( $^{\circ}C$ )	Geothermal gradient ( $^{\circ}C/100m$ )	BSR (mbsf)	Drilled depth (mbsf)
Site 3	1,076	6.50	3.9	209	300.0
Site 5	945	6.89	4.6	125	201.0
Site 10	1,038	6.50	4.5	160	204.9
Site 14	895	7.92	3.7	109	180.0

## CHAPTER III

### METHODS

Sixteen ACR samples were collected from eight study sites. Six samples are from four sites in the GOM: two samples from MC 118, two samples from VN 945, one sample from EL 711, and one sample from AT 425 (Table 3.1). The other ten samples are from four sites offshore India: one sample from Site 3, three samples from Site 5, five samples from Site 10, and one sample from Site 14 (Table 3.2).

For petrographic and mineralogical studies, thin sections of ACR samples were used to describe textures and identify carbonates and other minerals. Highly polished thin sections of ACR samples using a CAMECA SX50 electron microprobe were analyzed. The CAMECA SX50 provides backscattered electron (BSE) images and chemical element mapping of thin sections from energy dispersive X-ray spectroscopy (EDS). Main chemical elements detected were Ca, Mg, Si, Fe, K, Al, Ba, C, S, and O. Thin sections were also studied using a petrographic microscope under transmitted, reflected, and polarized light.

Carbon isotopes reflect the carbon sources, whereas oxygen isotopes reflect the temperature of initial formation of ACR. In this study, all carbon and oxygen isotopes of ACR samples are given on the Pee Dee Belemnite (PDB) scale, unless otherwise noted. Isotopic composition is reported as per mil (‰) difference in the isotopic ratio relative to the standard. This is referred to as “delta” or “δ” notation.

$$\delta(\text{‰}) = \left( \frac{R_x - R_{\text{std}}}{R_{\text{std}}} \right) \times 1000 = \left( \frac{R_x}{R_{\text{std}}} - 1 \right) \times 1000 \quad (3.1)$$

where  $R_x$  is the isotopic ratio of the samples, and  $R_{\text{std}}$  is the isotopic ratio of the standard.

For isotopic measurements, 150 to 200  $\mu\text{g}$  (0.15 to 0.20 mg) powder from each sample was converted into  $\text{CO}_2$  gas by reaction with 100%  $\text{H}_3\text{PO}_4$  (phosphoric acid) at  $70^\circ\text{C}$ . Then, the gas was automatically transferred to a Thermo-Finnigan DeltaPlus XP isotope-ratio mass spectrometer coupled with a Finnigan GasBench II for analysis, with results calibrated to Vienna Pee Dee Belemnite (VPDB) standard using the National Bureau of Standards NBS-19 reference standard ( $\delta^{13}\text{C} = +1.95\text{‰}$  PDB,  $\delta^{18}\text{O} = -2.20\text{‰}$  PDB). Replicates were run for each sample to determine internal precision. Typical reproducibility is  $\pm 0.05\text{‰}$  for  $\delta^{13}\text{C}$  and  $\pm 0.06\text{‰}$  for  $\delta^{18}\text{O}$ .

Table 3.1  
List of ACR samples from the Gulf of Mexico

ACR sample#	Sites	JSL dive#
ACR-1	MC 118	L53693 (BC 8)
ACR-2	MC 118	L53686 (BC 3)
ACR-3	VN 945	3916
ACR-4	VN 945	3916
ACR-5	EL 711	3918
ACR-6	AT 425	3918

Table 3.2  
List of ACR samples from the Krishna-Godawari basin offshore India

ACR sample#	Sites	Core#	Depth (mbsf)	Volume (cc)
ACR-1	Site 3	NGHP-01-03B-7H3	56.2	4
ACR-2	Site 5	NGHP-01-05C-5H	37.1	7
ACR-3	Site 5	NGHP-01-05C-5H	40.0	5
ACR-4	Site 5	NGHP-01-05C-15X	110.2	5
ACR-5	Site 10	NGHP-01-10B-4X	22.3	50
ACR-6	Site 10	NGHP-01-10B-6X	31.4	2
ACR-7	Site 10	NGHP-01-10D-3H	16.2	50
ACR-8	Site 10	NGHP-01-10D-3H	16.5	37
ACR-9	Site 10	NGHP-01-10D-7X	43.2	40
ACR-10	Site 14	NGHP-01-14A-16X	109.5	10

## CHAPTER IV

### **RESULTS: PETROGRAPHIC, MINERALOGIC, AND GEOCHEMICAL STUDIES OF HYDROCARBON-DERIVED AUTHIGENIC CARBONATE ROCK**

#### **Authigenic carbonate rock from the Gulf of Mexico**

##### **Mississippi Canyon (MC) 118**

The MC 118 site is located at 28° 51.4'N and 88° 29.5'W in the Gulf of Mexico (GOM) (Fig. 2.2). This site is the easternmost gas hydrate and hydrocarbon gas venting site in the GOM. It was discovered using the Johnson Sea-Link (JSL) research submersible in 2002. Maximum water depth at the site during the JSL dives is around 890 m and measured seafloor temperature is ~5.7°C (Sassen et al., 2006).

Sassen et al. (2006) presented the preliminary results of multidisciplinary studies at the MC 118 site. The MC 118 site is characterized by an enormous volume of ACR that strongly modifies the seafloor. Side-scan sonar surveys show that the seafloor is highly modified by the precipitation of ACR across an area of ~1 km<sup>2</sup> (Figs. 4.1 and 4.2). The enormous volume of ACR is the result of complex consortia of microbes that drive carbon and sulfur cycles. This site is also characterized by complex chemosynthetic communities. Those chemosynthetic communities have developed in association with gas vents, gas hydrates, and ACR.

Vent gas formed in the deep subsurface petroleum system migrates vertically and vents from the seafloor to the water column along faults at the MC 118 site (Sassen et al., 2001a). The vent gas in sediments drives microbial processes that result in the formation of ACR. It also nourishes seafloor chemosynthetic communities. Gas bubbles were observed at the sea surface. As oil-lined bubbles of gas burst, they give rise to natural oil slicks at the sea surface almost directly over the site (Sassen et al., 2006).

Three samples of vent gas were collected from the MC 118 site during the JSL dives in 2002. Hydrocarbon gas ( $C_1$  to  $C_5$ ) is the main component of vent gas, whereas  $CO_2$  is a relatively minor component. In relative terms, the  $CO_2$  concentration is  $\sim 1\%$  of the methane ( $C_1$ ) concentration in the vent gas (Sassen et al., 2006). Methane (94.4 to 96.5%) is the main component of the hydrocarbon vent gas. Methane from vent gas has a mean  $\delta^{13}C$  of  $-45.7\text{‰}$  and a mean  $\delta D$  of  $-163\text{‰}$ . Vent gas also contains  $CO_2$ , which is strongly enriched in  $^{13}C$  with  $\delta^{13}C$  of  $+21.5\text{‰}$  as typical of a deeply buried oil source (Sassen et al., 2006).

This site also contains gas hydrates. Intact gas hydrate was recovered by Sassen et al. (2006) from a crater-like depression using the JSL. Molecular and isotopic compositions of gas hydrate are reported in Table 4.1. Methane from gas hydrate is the primary component (70.0%) of hydrocarbon ( $C_1$  to  $C_5$ ). Methane has  $\delta^{13}C$  of  $-46.7\text{‰}$  and  $\delta D$  of  $-169\text{‰}$ .  $CO_2$  has  $\delta^{13}C$  of  $-15.3\text{‰}$ . The  $\delta^{13}C_1$  from gas hydrate is consistent with that of methane from vent gas (Table 4.1). Thus, methane gas hydrate may be crystallized from the vent gas. Ethane ( $C_2$ ) is present in lower relative abundance (7.5%,  $\delta^{13}C$  of  $-29.2\text{‰}$ ) than propane ( $C_3$ ) (15.9%,  $\delta^{13}C$  of  $-26.5\text{‰}$ ) as Structure II gas hydrate (Table 4.1). Propane is in high relative abundance when compared to most other gas hydrates from the Gulf (Milkov, 2005). Butanes are relatively abundant ( $i-C_4 = 4.4\%$ ,  $n-C_4 = 1.1\%$ ) whereas pentanes are trace components. The  $\delta^{13}C$  of hydrate-bound  $CO_2$  is  $-15.3\text{‰}$  (Table 4.1). Gas and oil in mud from MC 118 are altered by microbial oxidation (Sassen et al., 2006).

Table 4.1

Molecular and isotopic composition of vent gas and gas hydrate samples from the MC 118 site (Sassen et al., 2006)

Sample	C <sub>1</sub> (%)	δ <sup>13</sup> C <sub>1</sub> (‰)	δD (‰)	C <sub>2</sub> (%)	δ <sup>13</sup> C <sub>2</sub> (‰)	C <sub>3</sub> (%)	δ <sup>13</sup> C <sub>3</sub> (‰)	<i>i</i> -C <sub>4</sub> (%)	δ <sup>13</sup> <i>i</i> -C <sub>4</sub> (‰)	<i>n</i> -C <sub>4</sub> (%)	δ <sup>13</sup> <i>n</i> -C <sub>4</sub> (‰)	neo-C <sub>5</sub> (%)	<i>i</i> -C <sub>5</sub> (%)	<i>n</i> -C <sub>5</sub> (%)	δ <sup>13</sup> C <sub>CO2</sub> (‰)
Vent gas															
Dive 4414	94.6	-45.8	-164	3.1	-27.1	1.4	-24.5	0.3	-	0.4	-	0.0	0.1	0.1	+21.2
Dive 4415	94.4	-45.7	-162	3.1	-26.8	1.4	-24.1	0.4	-	0.4	-	0.0	0.2	0.1	+21.5
Dive 4415	96.5	-45.7	-163	2.4	-26.8	0.5	-24.1	0.1	-	0.3	-	0.0	0.1	0.1	+17.8
Gas hydrate															
	70.0	-46.7	-169	7.5	-29.2	15.9	-26.5	4.4	-27.5	1.1	-25.5	0.0	1.0	0.1	-15.3



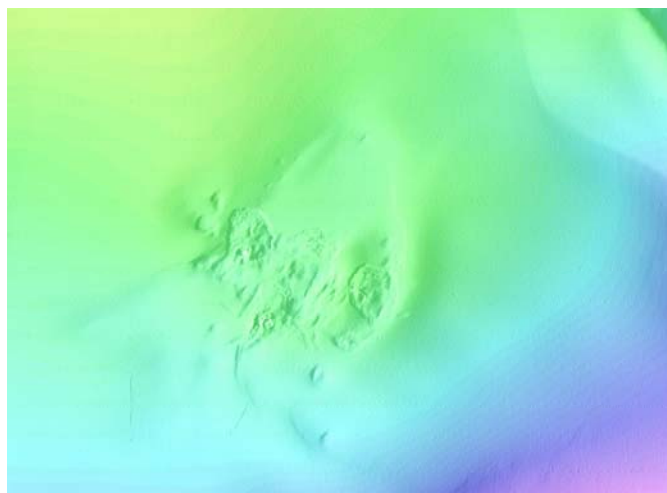


Fig. 4.1. Bathymetry image of the MC 118 site by side-scan sonar surveys. It shows irregular seafloor affected by the formation of authigenic carbonate rock. Complex morphology of the site suggests a long history of episodic seepage and venting of gas and oil (Sassen et al., 2006). This figure was created by Paul Mitchell (CMRET) using a 3-D swath bathymetry shaded relief map produced by Alessandro Bosman (University of Rome, La Sapienza) and Leonardo Macelloni (CMRET) from acoustic data acquired by C&C Technologies using the Hugin 3000 AUV. Note that CMRET is the Center for Marine Resources and Environmental Technology.

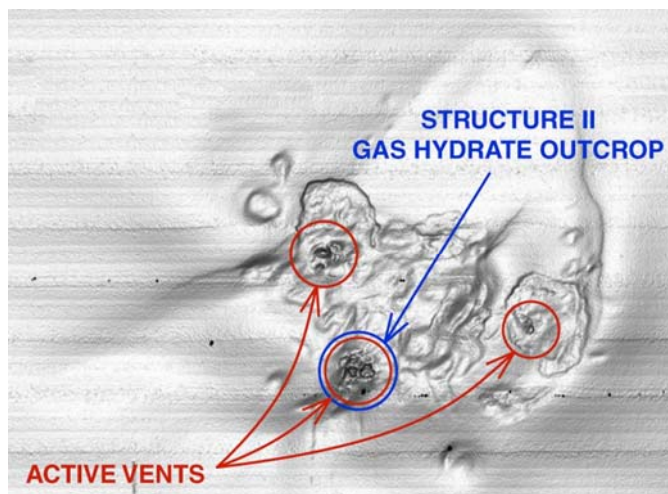


Fig. 4.2. Seafloor imagery of the MC 118 site. Structure II gas hydrate was recovered from a crater-like depression (Sassen et al., 2006). This figure was created by Paul Mitchell (CMRET) using a 3-D swath bathymetry shaded relief map produced by Alessandro Bosman (University of Rome, La Sapienza) and Leonardo Macelloni (CMRET) from acoustic data acquired by C&C Technologies using the Hugin 3000 AUV. Note that CMRET is the Center for Marine Resources and Environmental Technology.

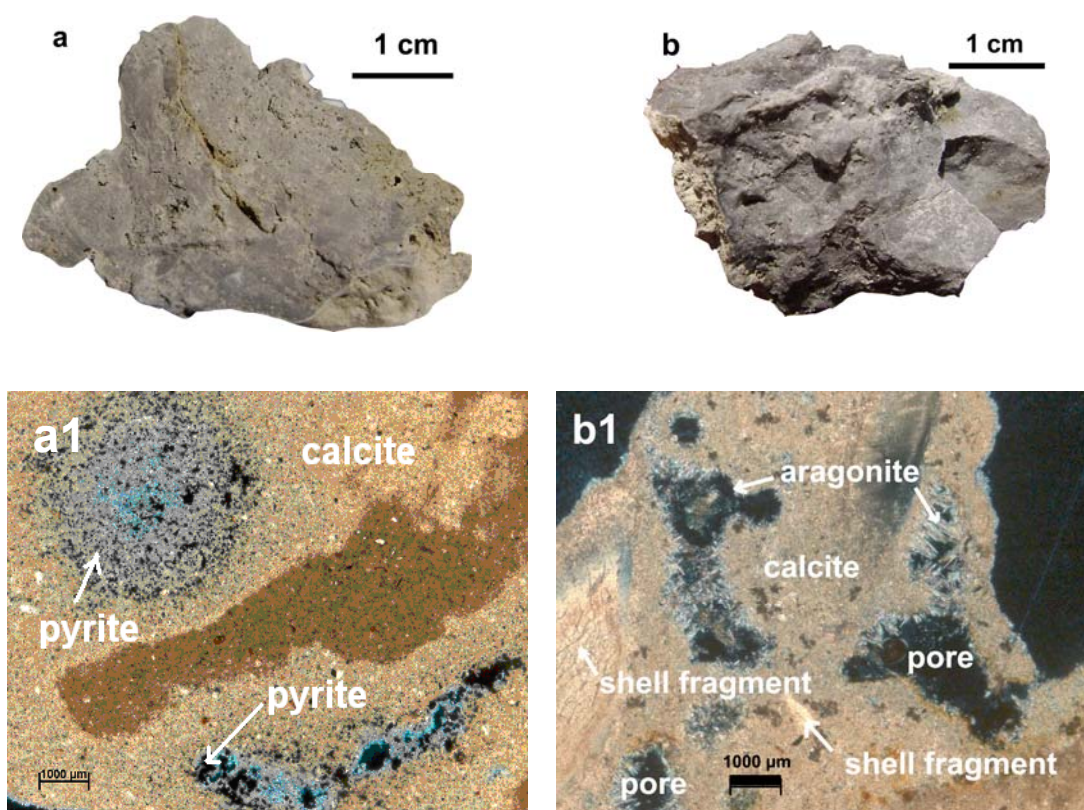


Fig. 4.3. Authigenic carbonate rock and thin section images from the MC 118 site. Note that (a) is ACR-1 (oil stained) and (b) is ACR-2 (oil stained) in Table 4.2. The thin section image (a1) comes from ACR-1 and is fine-grained calcite with the inclusions of pyrite. The thin section image (b1) comes from ACR-2 and it contains fine-grained calcite and aragonite with the inclusions of bioclastic (shell fragments and debris) organisms comprised of carbonate mud matrix with pore spaces.

Table 4.2

Isotopic composition of authigenic carbonate rock from the MC 118 site

ACR sample# from Table 3.1	Measured (n)	Sample depth (mbsf)	Sediment#	Core#	$\delta^{13}\text{C}$ (‰, PDB)	$\delta^{18}\text{O}$ (‰, PDB)
ACR-1	MC118-1	0-0.3	L53693	BC 8	-39.96	+4.42
ACR-1	MC118-2	0-0.3	L53693	BC 8	-42.50	+4.67
ACR-2	MC118-3	0-0.3	L53686	BC 3	-24.07	+3.94
ACR-2	MC118-4	0-0.3	L53686	BC 3	-26.06	+4.12
ACR-2	MC118-5	0-0.3	L53686	BC 3	-20.68	+3.60

Two samples of ACR (ACR-1 and ACR-2) were collected from 30 cm push cores of gassy mud from the MC 118 site during JSL dives in 2002 (Sassen, 2004; Sassen et al., 2006). ACR-1 (MC 118) collected from the JSL core #BC 8 is a smooth rocky nodule with evidence of oil stain. ACR-2 (MC 118) collected from the JSL core #BC 3 is a densely cemented nodule with evidence of oil stain (Fig. 4.3). Both ACR-1 and ACR-2 contain visible evidence of oil stain.

Petrographic thin section images show that ACR-1 (MC 118) (Fig. 4.3a) contains almost totally fine-grained calcite with the inclusions of pyrite, whereas ACR-2 (MC 118) (Fig. 4.3b) contains fine-grained calcite and aragonite with the inclusions of shell fragments associated with chemosynthetic communities.

Bulk carbon and oxygen ( $\delta^{13}\text{C}$  and  $\delta^{18}\text{O}$ ) isotopes of ACR samples from the MC 118 site were measured. ACR samples are highly depleted in  $^{13}\text{C}$ . ACR-1 (MC 118) has  $\delta^{13}\text{C}$  values of  $-39.96\text{‰}$  and  $-42.50\text{‰}$ . ACR-2 (MC 118) has  $\delta^{13}\text{C}$  values of  $-24.07\text{‰}$ ,  $-26.06\text{‰}$ , and  $-20.68\text{‰}$ . The mean  $\delta^{13}\text{C}$  values are  $-41.2\text{‰}$  for ACR-1 (MC 118) and  $-23.6\text{‰}$  for ACR-2 (MC 118) (Table 4.2).

The  $\delta^{13}\text{C}$  values of ACR are different from those of normal marine carbonates such as limestone. At this site, if methane (mean  $\delta^{13}\text{C} = -45.7\text{‰}$ , Sassen et al., 2006) from vent gas is the primary source of carbon to ACR, one would expect it to be also highly depleted in  $^{13}\text{C}$ . However, the  $\delta^{13}\text{C}$  of ACR does not closely correspond to that of the methane. ACR samples are enriched in  $^{13}\text{C}$  when compared to the methane, which is highly depleted in  $^{13}\text{C}$ . The enrichment in  $^{13}\text{C}$  of ACR may be better understood by study of petrographic thin section images (Fig.4.3). Thin sections show that several different carbon sources may affect the bulk carbon isotopes of ACR samples. Each ACR sample will be discussed separately.

For ACR-1 (MC 118),  $\delta^{13}\text{C}$  values (mean =  $-41.2\text{‰}$ ) suggest that the primary source of carbonate carbon to ACR may be methane oxidation from hydrocarbon vent gas. The mean  $\delta^{13}\text{C}$  value of ACR-1 (MC 118) appears to be consistent with that of methane (mean  $\delta^{13}\text{C} = -45.7\text{‰}$ , Sassen et al., 2006) from the vent gas at the MC 118 site.

For the purpose of a mass balance calculation, a mean  $\delta^{13}\text{C}$  of methane from vent gas is used to calculate the percentage of methane oxidation. The mean  $\delta^{13}\text{C}$  of methane from vent gas is  $-45.7\text{‰}$  (Sassen et al., 2006). The mean  $\delta^{13}\text{C}$  of ACR-1 (MC 118) is  $-41.2\text{‰}$  (Table 4.2). The  $\delta^{13}\text{C}$  of normal marine carbonate is  $\sim 0\text{‰}$  (Hudson, 1977). The fraction of methane oxidation in ACR was calculated:  $X(-45.7\text{‰}) + (1 - X)(0\text{‰}) = -41.2\text{‰}$ , where  $X$  is the fraction of methane oxidation, Here  $X = 0.90$  or 90%.

As calculated, methane oxidation has contributed to  $\sim 90\%$  of ACR-1 (MC 118). A petrographic thin section of ACR-1 (MC 118) (Fig. 4.3a) was studied to check out the calculation. The petrographic thin section shows that ACR-1 (MC 118) contains almost totally fine-grained calcite. ACR-1 (MC 118) is a smooth rocky nodule with visible evidence of oil stain. The  $\delta^{13}\text{C}$  value of ACR-1 does not correspond to that of methane. Why is the ACR-1 (MC 118) enriched in  $^{13}\text{C}$  with a mean  $\delta^{13}\text{C}$  of  $-41.2\text{‰}$  when compared to  $\delta^{13}\text{C}$  of  $-45.7\text{‰}$  of methane? Various carbon sources may affect the bulk  $\delta^{13}\text{C}$  values of ACR-1 (MC 118). Further, the  $\delta^{13}\text{C}$  of ACR-1 (MC 118) enriched in  $^{13}\text{C}$  may reflect a mixture of (1) methane oxidation, (2) normal marine carbonate, or (3) oxidation of isotopically heavy biodegraded oil.

Bulk  $\delta^{13}\text{C}$  values of ACR-2 (MC 118) with a range of  $-20.68$  to  $-26.06\text{‰}$  (mean =  $-23.6\text{‰}$ ) (Sassen et al., 2006) do not closely correspond to those of methane, which is highly depleted in  $^{13}\text{C}$ . Why is the ACR-2 (MC 118) so enriched in  $^{13}\text{C}$  with a mean  $\delta^{13}\text{C}$  of  $-23.6\text{‰}$  when compared to  $\delta^{13}\text{C}$  of  $-45.7\text{‰}$  of methane from vent gas that is highly depleted in  $^{13}\text{C}$ ? Marine skeletal materials such as shell fragments and debris (Fig. 4.3b) may affect the bulk carbon isotopic composition of ACR-2 (MC 118). As calculated above, the percentage of methane oxidation contributed to the  $\delta^{13}\text{C}$  of ACR-2 (MC 118) was calculated. Thus, the 52% methane oxidation and the 48% marine carbonate carbon may contribute to ACR-2 (MC 118). The petrographic thin section (Fig. 4.3b) shows that ACR-2 (MC 118) contains fine-grained calcite and aragonite with the inclusion of skeletal material. To examine and quantify carbon sources to ACR-2 (MC 118), a point count technique in the thin section image of ACR-2 (MC 118) was used. The thin section image is classified as the features of normal marine carbonates (69 grids) and

pore spaces (85 grids) out of the total 256 grids (Fig. 4.4). Thus, the point count analysis shows that ACR-2 (MC 118) may have 41% normal marine carbonate. However, the 41% marine carbonate carbon in ACR-2 (MC 118) through the point count analysis does not correspond to the 48% marine carbonate carbon calculated by the mass balance. ACR-2 (MC 118) may form in approximately 59% methane oxidation and 41% normal marine carbonate. In addition, the  $\delta^{13}\text{C}$  of ACR-2 (MC 118) enriched in  $^{13}\text{C}$  may also reflect oxidation of isotopically heavier biodegraded oil.

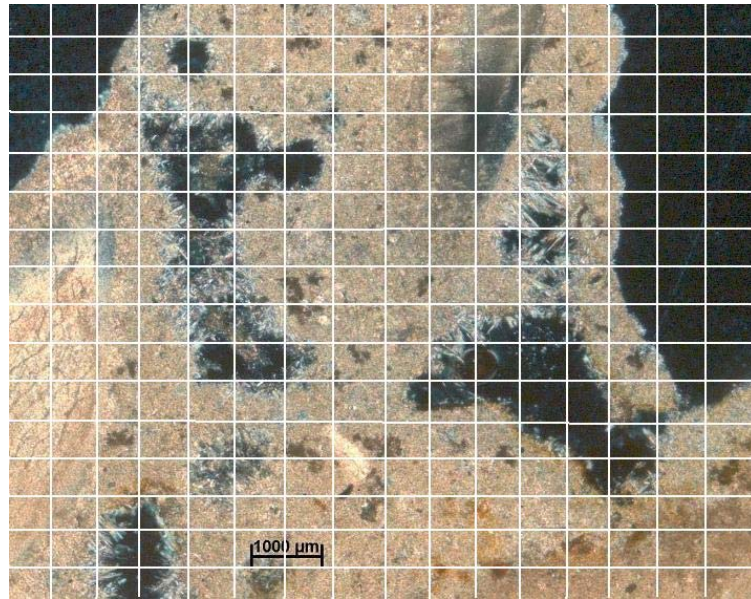


Fig. 4.4. Point count analyses of a thin section of ACR-2 (MC 118). Note that the thin section image is classified as the features of normal marine carbonates (69 grids) and pore spaces (85 grids) out of the total 256 grids. Thus, 41% of normal marine carbonate has contributed to ACR-2 (MC 118).

Bulk  $\delta^{18}\text{O}$  values of ACR-1 and ACR-2 (MC 118) are in the range of +3.60 to +4.67‰ (mean  $\delta^{18}\text{O} = +4.15\%$ ). The  $\delta^{18}\text{O}$  values are isotopically heavier than those of normal marine carbonates. Mozley and Burns (1993) reviewed  $\delta^{13}\text{C}$  and  $\delta^{18}\text{O}$  values for marine calcite, siderite, and dolomite from a large number of previous studies. From their review for marine calcite,  $\delta^{18}\text{O}$  is in the range of -10 to 0‰. Why are ACR samples enriched in  $^{18}\text{O}$  with a mean  $\delta^{18}\text{O}$  of +4.15‰? Isotopically heavy values of  $\delta^{18}\text{O}$  from ACR will be discussed.

There are three likely hypotheses for the isotopically heavier  $\delta^{18}\text{O}$  values: (1) they reflect the temperature of initial formation of ACR; (2) they reflect isotopically heavy  $\delta^{18}\text{O}$  values from gas hydrate decomposition; or (3) they reflect the movement of isotopically heavier water than ambient seawater from greater depth. Some combination of these hypotheses may be reasonable, but each hypothesis separately for clearer explanation will be discussed.

First, measured  $\delta^{18}\text{O}$  values (mean  $\delta^{18}\text{O} = +4.15\%$ ) may reflect the temperature of initial formation of ACR. To calculate the temperature, the measured  $\delta^{18}\text{O}$  value of +4.15‰ in PDB to the value of +35.14‰ in SMOW was converted using the relation of  $\delta^{18}\text{O}_{\text{SMOW}} = 1.03086 \delta^{18}\text{O}_{\text{PDB}} + 30.86$  (Friedman and O'Neil, 1977). Then, using an equilibrium oxygen isotope equation (Kim and O'Neil, 1997) of  $1000 \times \ln(\alpha) = 18.03 \times (10^3 \text{ T}^{-1}) - 32.42$ , the temperature of -3.1°C was calculated.

The calculated temperature of -3.1°C is unrealistic. The first hypothesis can be eliminated. Then, it is suggested to calculate  $\delta^{18}\text{O}$  of water using the measured  $\delta^{18}\text{O}$  value and temperature of ACR for the second hypothesis. Using the equation of Kim and O'Neil (1997), the  $\delta^{18}\text{O}$  water value of +2.3‰ SMOW (APPENDIX A) was calculated. For the calculations,  $\delta^{18}\text{O}$  value of +0.2‰ SMOW was used for seawater in the GOM (<http://data.giss.nasa.gov/o18data>; GEOSECS Grossman and Ku, 1986) at a nearest location (latitude: 27.52°N and longitude: 95.00°E, water depth: 799 m) to the study site of MC 118 (latitude: 28° 51.4'N and longitude: 88° 29.5'E, water depth: 890 m). Therefore, ACR may form in heavier water of +2.3‰ SMOW.

As discussed in the introduction, gas hydrate formation preferentially favors  $^{18}\text{O}$ , leaving the residual water  $^{16}\text{O}$  enriched (Hesse and Harrison, 1981; Ussler and Paull, 1995; Matsumoto and Borowski, 2000). The water within the gas hydrates is enriched in heavy oxygen ( $^{18}\text{O}$ ) relative to ambient waters. Hence, gas hydrate decomposition enriches the water with  $^{18}\text{O}$ . Although gas hydrate water may cause an isotopically heavy  $\delta^{18}\text{O}$  value, the second hypothesis for the isotopically heavy  $\delta^{18}\text{O}$  water values from gas hydrate decomposition may be eliminated because gas hydrate water would not cause significantly heavy oxygen isotopes from +0.2 to +2.3‰ SMOW (Matsumoto and Borowski, 2000; Greinert et al., 2001; Sassen and Roberts, 2004). To eliminate the second hypothesis, two examples of isotopically heavy  $\delta^{18}\text{O}$  values from gas hydrate water were identified. As discussed in Chapter I, the magnitude of the isotopically heavier values of  $\delta^{18}\text{O}$  was 0.3 to 0.6‰ SMOW at Blake Ridge Site 997 (Matsumoto and Borowski, 2000), and 0.86‰ SMOW at Hydrate Ridge (Greinert et al., 2001).

With the preceding explanation as most likely, it remains for the third hypothesis that isotopically heavy  $\delta^{18}\text{O}$  values should reflect the movement of isotopically heavier water than ambient seawater from greater depth. Below explanation supports the third hypothesis: (1) A series of structural fractures associated with active salt sheets and faults provides migration conduits for fluid penetration upward through openings from greater depth to the seafloor (Fu and Aharon, 1998; Sassen et al., 2004b), (2) personal discussion with Sassen who visited the MC 118 site using the JSL research submersible in 2002 and 2006, and (3) most water,  $\delta^{18}\text{O}$  values ranging +3.3 to +5.1‰, produced from Cenozoic hydrocarbon reservoirs in the Gulf of Mexico sedimentary basin is derived from dewatering of clastic sediments (Morton et al., 1983; Morton and Land, 1987; Land and Macpherson, 1992). In addition, locally, the water enters the Cenozoic section from underlying Mesozoic strata (Land and Macpherson, 1992). The main structural features of the northern Gulf of Mexico are salt basins, which formed during Late Triassic rifting and were generated by salt during Middle Jurassic marine incursions (Salvador, 1987).

### **Florida Escarpment at Vernon (VN) 945**

The VN 945 site is located at 26°N and 85°W in the Florida Escarpment at a water depth of 3,300 meters (Fig. 2.2). The site was visited by the ALVIN in 2003 during dives 3915, 3916, and 3918. Two samples of ACR were recovered from the VN 945 site (dive 3916) in the lower GOM slope. This site was described by Paull et al. (1984 and 1985) as a number of chemosynthetic communities, no gas hydrate, no evidence of crude oil, and hydrocarbon seeps along the Florida Escarpment in Vernon basin area of the far eastern Gulf of Mexico. Paull et al. (1985) also reported that microbial methane from the VN 945 site is highly depleted in  $^{13}\text{C}$  with  $\delta^{13}\text{C}$  of  $\sim -80\%$ , and  $\text{H}_2\text{S}$  is also produced at the site.

Several years later in 2003, the ALVIN explored the Florida Escarpment area (dives 3915, 3916, and 3918) again. Sassen (2004) proposed that hydrocarbon (gas and oil) seeps come from vertical migration from a deeply buried subsurface petroleum system. He analyzed gas chromatography for samples of oil seeps, finding anomalous total Unresolved Complex Mixture (UCM) concentrations in the range of 42 to 61 ppm. The UCM represents anomalous elevated chromatographic baseline. Sassen (2004) proposed the presence of highly degraded crude oil along the Florida Escarpment through  $\text{C}_{15+}$  gas chromatography analysis. At the VN 945 site, the  $\delta^{13}\text{C}$  values of oil from oil-stained carbonate rock are in the range of  $-31.3$  to  $-31.4\%$  of saturated hydrocarbons (SAT) and  $-30.2$  to  $-32.0\%$  of aromatic hydrocarbons (AROM) (Sassen, 2004).

Fig. (4.5) shows ACR from hydrocarbon oxidation outcrops on the seafloor in the Florida Escarpment. Fig. (4.6) also shows tube worms, mussels, and other organisms in a complex chemosynthetic community.





Fig. 4.5. Authigenic carbonate rock from hydrocarbon oxidation outcrops on the seafloor at the VN 945 site in the Florida Escarpment. The area shown is ~1.5 m across (photograph by Lisa Levin).



Fig. 4.6. Tube worms, mussels, and other organisms in a complex chemosynthetic community from the Florida Escarpment (photograph by Lisa Levin).

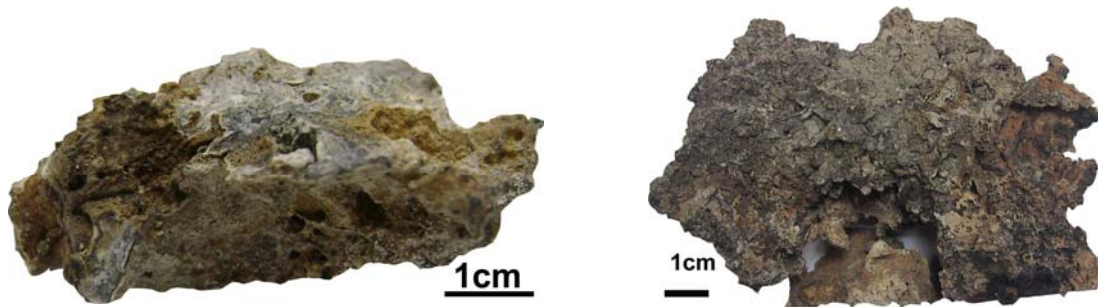


Fig. 4.7. Authigenic carbonate rock from the seafloor at the VN 945 site in the Florida Escarpment chemosynthetic community. Note that the left image is ACR-3 (VN 945) and the right image is ACR-4 (VN 945) in Table 4.3.

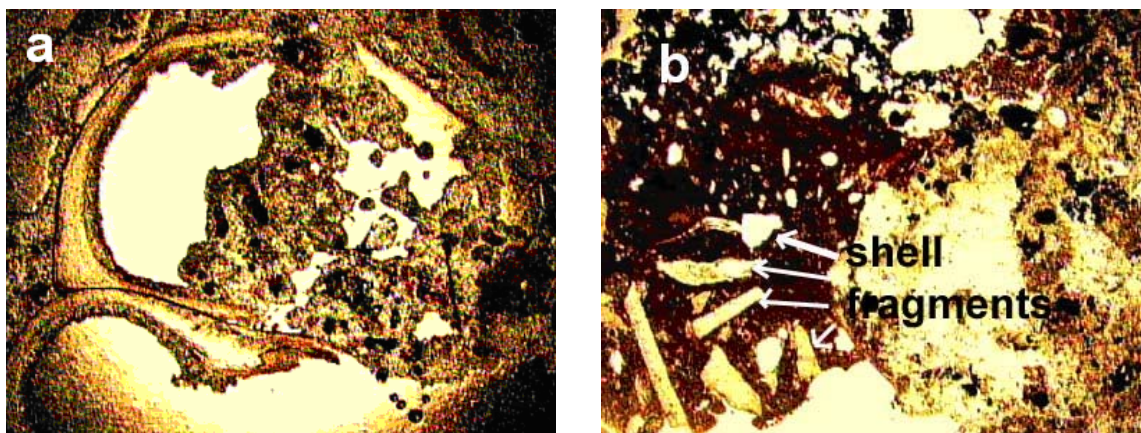


Fig. 4.8. Thin section images of authigenic carbonate rock from the VN 945 site. Each image is ~6 mm across. Note that the left image (a) from ACR-3 (VN 945) contains the structured feature (gastropod section) of normal marine carbonate embedded in hydrocarbon-derived authigenic carbonate rock. The right image (b) from ACR-4 (VN 945) contains structured features which are fragments of chemosynthetic mussels and other carbonate skeletal remains of normal marine carbonate embedded in isotopically-light authigenic carbonate rock.

Table 4.3  
Isotopic composition of authigenic carbonate rock from the VN 945 site (Sassen, 2004)

ACR sample# from Table 3.1	Measured (n)	Sample depth (mbsf)	Dive#	$\delta^{13}\text{C}$ (‰, PDB)	$\delta^{18}\text{O}$ (‰, PDB)
ACR-3	VN 945-1	0-0.3	3916	-41.63	+3.04
ACR-4	VN 945-2	0-0.3	3916	-30.11	+3.59

Two samples of ACR were collected from 30 cm push cores from the VN 945 site. ACR-3 (VN 945) is a hard-cemented carbonate without visible evidence of oil stain, whereas ACR-4 (VN 945) is a rocky nodule with visible oil stain (Fig. 4.7).

A petrographic thin section image shows that ACR-3 (VN 945) contains the structured feature (gastropod section) of a normal marine carbonate embedded in fine-grained sediments. ACR-4 (VN 945) contains structured features formed from fragments of chemosynthetic mussels and other carbonate skeletal remains of a normal marine carbonate embedded in fine-grained sediments (Fig. 4.8).

Bulk  $\delta^{13}\text{C}$  and  $\delta^{18}\text{O}$  isotopes of ACR samples from the VN 945 site were measured (Table 4.3). The  $\delta^{13}\text{C}$  is  $-41.63\text{‰}$  for ACR-3 (VN 945) and  $-30.11\text{‰}$  for ACR-4 (VN 945). The  $\delta^{13}\text{C}$  values of ACR are highly depleted in  $^{13}\text{C}$ .

Various carbon sources may affect the bulk  $\delta^{13}\text{C}$  value of ACR. Three likely hypotheses may explain the depletion in  $^{13}\text{C}$ : (1) if methane from the VN 945 site is the primary source of carbon to the ACR, one would expect it also to be highly depleted in  $^{13}\text{C}$ ; (2) if the  $\delta^{13}\text{C}$  of ACR does not closely correspond to that of the microbial methane, normal marine carbonates such as marine skeletal materials and gastropods may affect the carbon isotopic composition of ACR as identified by petrographic thin section study of point count technique (Fig. 4.9); or (3) the  $\delta^{13}\text{C}$  reflects the oxidation of biodegraded crude oil with the range of  $-30.2$  to  $-32.0\text{‰}$ . Each hypothesis will be discussed separately.

The first and second hypotheses for ACR-4 (VN 945) may be eliminated by petrographic thin section study (Fig. 4.8), which shows lack of normal marine carbonate. The percentage of normal marine carbonate in ACR-3 (VN 945) and ACR-4 (VN 945)

was calculated to become enriched in  $^{13}\text{C}$  with  $\delta^{13}\text{C}$  values of  $-41.63\text{‰}$  and  $-30.11\text{‰}$ , respectively.

For the purpose of a mass balance calculation,  $\delta^{13}\text{C}$  of microbial methane is used to calculate the percentage of normal marine carbonate added to ACR as follows, using a  $\delta^{13}\text{C}$  of  $-80\text{‰}$  for the methane and  $\delta^{13}\text{C}$  of  $-41.63\text{‰}$  for ACR-3 (VN 945):  $X(-80\text{‰}) + (1 - X)(0\text{‰}) = -41.63\text{‰}$ , where  $X$  is the fraction of methane produced by methane oxidation. Here  $X = 0.52$ , or 52%. Thus, as calculated, 52% methane oxidation and 48% normal marine carbonate have contributed to ACR-3 (VN 945). From these calculations, 38% methane oxidation and 62% normal marine carbonate carbon have contributed to ACR-4 (VN 945).

To examine and quantify carbon sources for ACR, a point count technique was used in the thin section images for each ACR sample in Fig. (4.9).

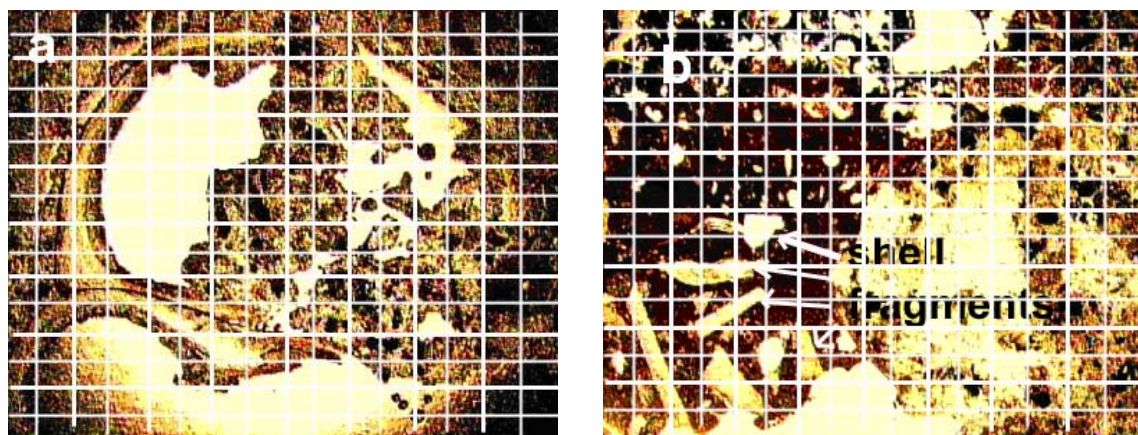


Fig. 4.9. Point count analyses of thin sections of (a) ACR-3 (VN 945) and (b) ACR-4 (VN 945). Each image is  $\sim 6$  mm across. Note that the thin section image of (a) is classified as the features of normal marine carbonates (61 grids) and pore spaces (124 grids) out of the total 256 grids. Therefore, 46% of normal marine carbonate has contributed to ACR-3 (VN 945). Also, the thin section image of (b) is classified as the features of normal marine carbonates (55 grids) and pore spaces (107 grids) out of the total 256 grids. Therefore, 37% of normal marine carbonates have contributed to ACR-4 (VN 945).

For the ACR-3 (VN 945), the point count analysis shows that the 46% normal marine carbonates have contributed to ACR. This is closely consistent with the calculation result of 48%. However, the 46% marine carbonate in ACR-4 (VN 945) through the point count analysis does not correspond to the 62% marine carbonate calculated by the mass balance. Thus, for ACR-4 (VN 945) the  $\delta^{13}\text{C}$  value of  $-30.11\text{‰}$  reflects microbial oxidation of degraded crude oil. This is because the  $\delta^{13}\text{C}$  values of biodegraded crude oil are in the range of  $-30.2$  to  $-32.0\text{‰}$  (Sassen, 2004). However, the point count analysis shows that ACR may have 37% normal marine carbonate, which means the explanation for ACR-4 (VN 945) may be reasonable. The most likely explanation of the  $\delta^{13}\text{C}$  of ACR-4 (VN 945) may involve a physical mixture of isotopically light carbon from microbial methane oxidation and degraded crude oil oxidation. The  $\delta^{18}\text{O}$  values have  $+3.04\text{‰}$  of ACR-3 (VN 945) and  $+3.59\text{‰}$  of ACR-4 (VN 945) from the VN 945 site (Table 4.3). No seafloor temperature data were reported at this site.

### **The Elbow (EL) 711**

The EL 711 site is located at  $27^{\circ} 14.0' \text{N}$  and  $85^{\circ} 36.7' \text{W}$  (Fig. 2.2) at a water depth of 3,220 meters. Seafloor temperature is  $\sim 4^{\circ}\text{C}$ . A chemosynthetic community with well-developed tube worms was discovered during the 2003 ALVIN dive to the deep seafloor. One sample of ACR-5 (EL 711) was collected from the chemosynthetic community seafloor. Microbial methane highly depleted in  $^{13}\text{C}$  with  $\delta^{13}\text{C}$  of  $\sim -80.0\text{‰}$  occurs in high concentration in sediment samples from the site. There was no evidence from  $\text{C}_{15+}$  gas chromatography of any crude oil in extracts of sediment samples. ACR is abundant at the EL 711 site. Gas hydrate has not been found at the site (Sassen et al., 2004b).

An unusual texture of ACR-5 (EL 711) was recovered as a large ( $\sim 40 \text{ cm}^3$ ) nodular cobble. ACR recovered from chemosynthetic communities usually appears

densely cemented, whereas ACR-5 (EL 711) is friable and exhibits extremely high microporosity and concomitant low density (Fig. 4.10).

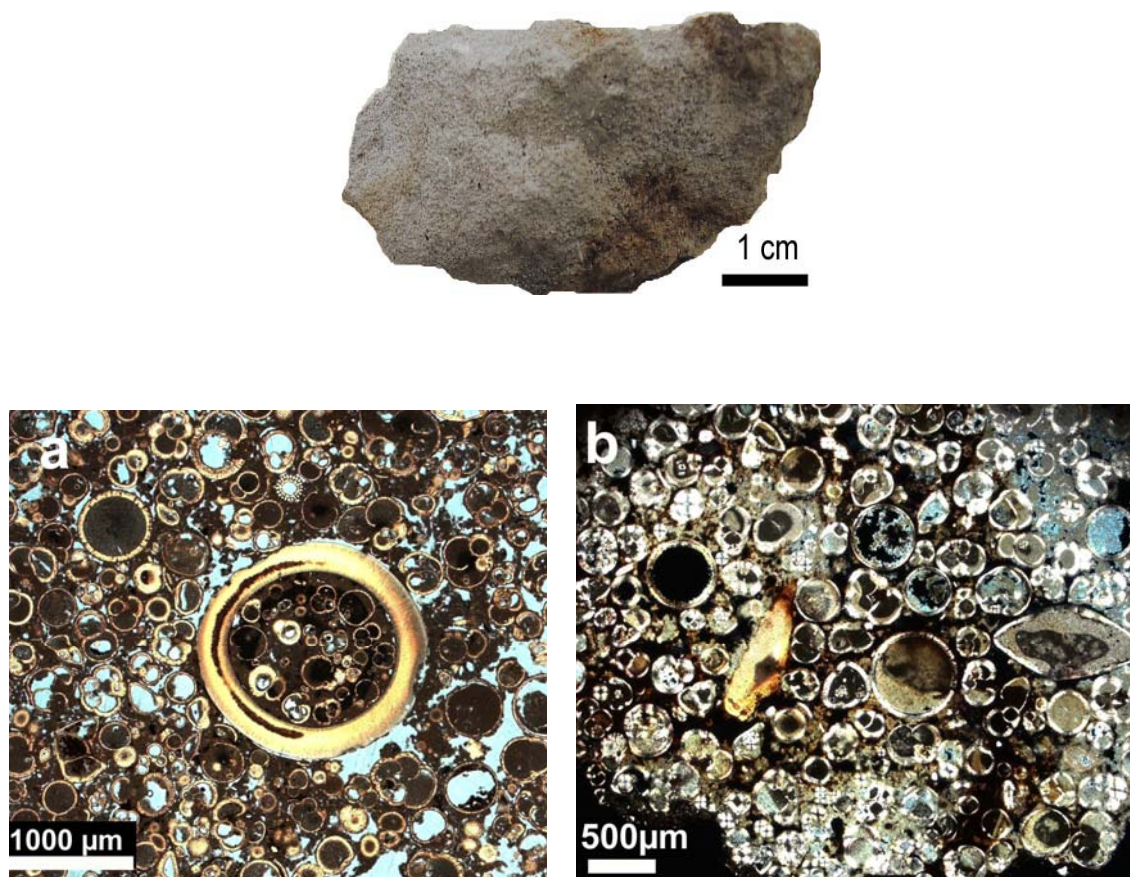


Fig. 4.10. Authigenic carbonate rock and thin section images from the Elbow (EL) 711 site. Circular and chambered features are sections of foraminifera and other planktonic organisms with skeletal carbonate with isotopic properties of normal marine carbonate. Note that image (a) is under plain light and (b) is under polarized light.

Table 4.4

Isotopic composition of authigenic carbonate rock from the EL 711 site  
(Sassen et al., 2004b)

	ACR sample# from Table 3.1	Sample depth (mbsf)	Dive#	$\delta^{13}\text{C}$ (‰, PDB)	$\delta^{18}\text{O}$ (‰, PDB)
EL 711	ACR-5	0-0.3	3918	-34.78	+2.43

With the unusual texture of authigenic carbonate rock rich in cemented foraminifera, highly polished thin sections of ACR using a CAMECA SX50 Electron Microprobe were used. Back Scattered Electron (BSE) images (Figs. 4.11, 4.12, and 4.13) and chemical element distributions from Energy Dispersive Spectroscopy (EDS) (Fig. 4.14) of thin sections of ACR were analyzed.

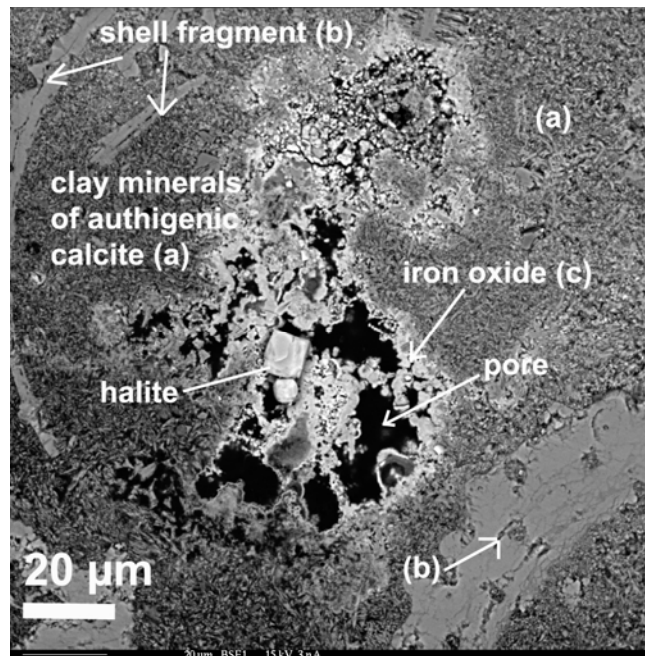


Fig. 4.11. Back Scattered Electron images (600X) of ACR from the EL 711 site. The bulk of the sample contains calcite and fine-grained clay minerals of authigenic calcite. Fragments of calcareous shell material are also present. A visible square section of a halite crystal indicates a drying process.

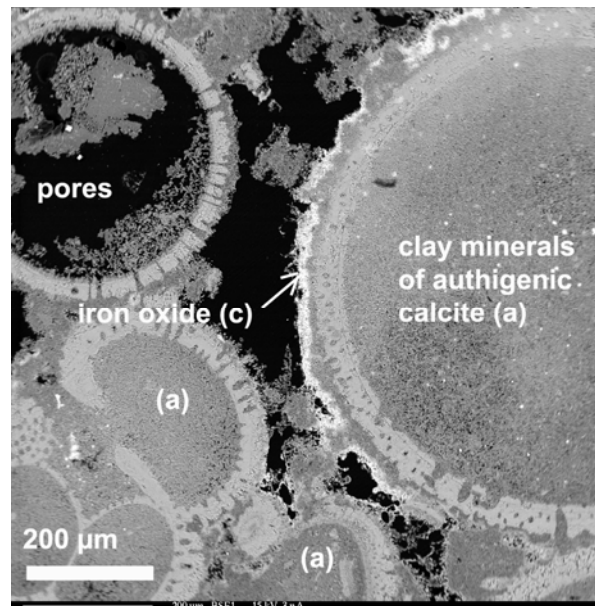


Fig. 4.12. Back Scattered Electron image (100X) of ACR from the EL 711 site. The bright zone surrounding the sections through a subspherical foraminifera test marked “c” is iron oxide. Fine grained clay minerals occur in association with calcite and iron oxide.

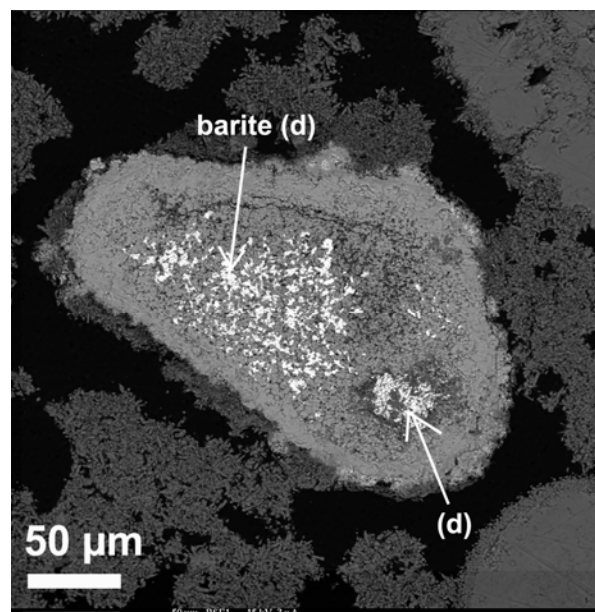


Fig. 4.13. Back Scattered Electron image (300X) of ACR from the EL 711 site. A small carbonate feature contains abundant barite. BSE suggests that the exterior of the feature is relatively rich in iron oxide.



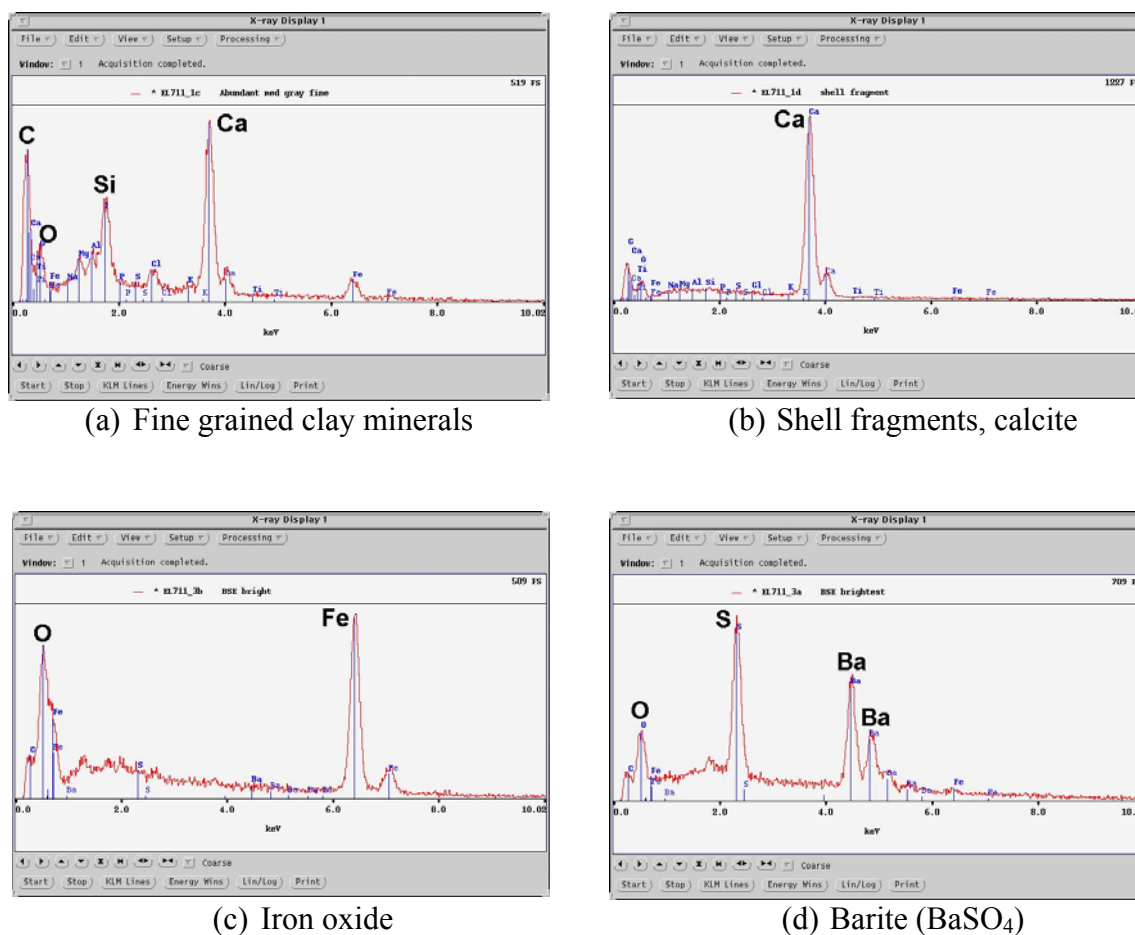


Fig. 4.14. Energy dispersive X-ray spectroscopy (EDS) images of ACR from the EL 711 site. Note that EDS images of mark a, b, c, and d are in Figs. 4.11, 4.12, and 4.13.

Petrographic thin sections show that ACR-5 (EL 711) contains many circular and chambered features. They include sections of foraminifera and planktonic organisms with the inclusions of very few carbonate skeletal materials. Foraminifera and other planktonic organisms with skeletal carbonate are bound together during deposition as shown by intergrown skeletal carbonate. The foraminifera are also cemented by fine-grained authigenic calcite.

Sen Gupta and Aharon (1994) reported isotope data of benthic foraminifera collected from hydrocarbon vent sites of the Mississippi Canyon, Green Canyon, and Garden Banks in the Gulf of Mexico. The sampling was by means of a coring tube 6 cm

in diameter, a grab, or a suction device for seafloor sediment during the submersible Johnson Sea-Link (JSL) dives in 1989, 1991, and 1993. Water depth is in the range of 216 to 694 meters. The  $\delta^{13}\text{C}$  and  $\delta^{18}\text{O}$  values of benthic foraminifera are in a range from  $-3.6$  to  $+0.4\text{‰}$  and  $+0.8$  to  $+1.8\text{‰}$ , respectively. In addition, in that study,  $\delta^{13}\text{C}$  values of benthic foraminifera were independent of water depth.

Bulk  $\delta^{13}\text{C}$  and  $\delta^{18}\text{O}$  isotopes of the ACR-5 (EL 711) from the EL 711 site were measured (Table 4.4). ACR-5 (EL 711) has  $\delta^{13}\text{C}$  value of  $-34.78\text{‰}$ . This site is characterized by microbial methane highly depleted in  $^{13}\text{C}$  ( $\delta^{13}\text{C} = -80\text{‰}$ , Sassen et al., 2004b). Thus, if the methane was the primary source of carbon to ACR, one would expect it to be also highly depleted in  $^{13}\text{C}$ . However, ACR is enriched in  $^{13}\text{C}$  when compared to the microbial methane. The enrichment in  $^{13}\text{C}$  can be explained by petrographic thin sections (Fig. 4.10). They show that ACR-5 (EL 711) contains some carbonate skeletons of microscopic foraminifera that are cemented by lesser authigenic carbonate.

Therefore, foraminifera and other planktonic organisms with skeletal carbonate may affect the bulk carbon isotopes of ACR-5 (EL 711). The percentage of methane oxidation that contributed to ACR was calculated with the foraminifera  $\delta^{13}\text{C}$  value of  $-1.6\text{‰}$  PDB (Sen Gupta and Aharon, 1994).

Using  $\delta^{13}\text{C}$  of  $-80\text{‰}$  for the methane and  $\delta^{13}\text{C}$  of  $-34.78\text{‰}$  for ACR-5 (EL 711):  $X(-80\text{‰}) + (1 - X)(-1.6\text{‰}, \text{mean } \delta^{13}\text{C} \text{ of foraminifera}) = -34.78\text{‰}$ , where  $X$  is the percentage of methane oxidation. Here  $X = 0.42$ , or 42%. Thus, as calculated, 42% methane oxidation and 58% marine foraminifera have contributed to ACR-5 (EL 711).

To examine carbon sources to ACR, the percentage of methane oxidation and normal marine carbonate that contributed to ACR through petrographic thin section images in Fig. (4.10) visually was quantified. It appears to be consistent with the calculations.

The bulk  $\delta^{18}\text{O}$  of ACR-5 (EL 711) is  $+2.43\text{‰}$  at the seafloor temperature of  $\sim 4.0^\circ\text{C}$ . Isotopically heavy  $\delta^{18}\text{O}$  values of ACR-5 (EL 711) may reflect the temperature of initial formation of ACR. The calculated temperature of  $+4.4^\circ\text{C}$  is consistent with the

measured temperature of +4.0°C at the site. For the calculations,  $\delta^{18}\text{O}$  value of +0.3‰ SMOW was used for seawater in the GOM (<http://data.giss.nasa.gov/o18data>; GEOSECS Grossman and Ku, 1986) at a nearest location (latitude: 26.71°N and longitude: 95.00°E, water depth: 1,570 m) to the study site of EL 711 (latitude: 27° 14.0'N and longitude: 85° 36.7'W, water depth: 3,220 m).

### **Atwater Valley (AT) 425**

The AT 425 site is located at 27° 34.1'N and 88° 29.7'W in the Gulf of Mexico (Fig. 2.2). ACR-6 (AT 425) was collected from the seafloor at a water depth ranging from 1,920 to 1,930 m. Seafloor temperature is 6°C. At the AT 425 site, fluids from depth pierce a wide and thick apron of gently dipping sediment transported from the mouth of the Mississippi Fan Channel during the Pleistocene (Sassen et al., 2001a; Sassen, 2004). In 2003, ALVIN visited the AT 425 site and revealed that the site includes hydrocarbon seeps of thermogenic gas, complex chemosynthetic communities (lower slope species of tube worms, mussels, etc.), abundant authigenic carbonate rock, gas hydrate, and high concentrations of crude oil-stained sediment. Total Extractable Organic Matter (EOM) of one 30 cm push core sample from AT 425 site was in the range of 43,478 to 116,053 ppm (Sassen, 2004).

Sassen et al. (2001a) obtained H<sub>2</sub>S-rich water and sediment pressured by free thermogenic gas from three 30 cm push cores from the AT 425 site. The sediment samples also contain between ~4 and ~12% oil by weight. They also recovered Structure II hydrates, methane-ethane hydrates, and hydrate-included crude oil from the AT 425 site. The molecular and isotopic compositions of gas hydrate samples are given in Table 4.5.

Methane is the main component of the gas hydrate from the AT 425 site with a mean C<sub>1</sub> of 90.4%. The relative abundance of other hydrocarbons is propane (mean = 4.7%), ethane (mean = 2.6%), isobutene (mean = 1.1%), normal butane (mean = 0.8%),



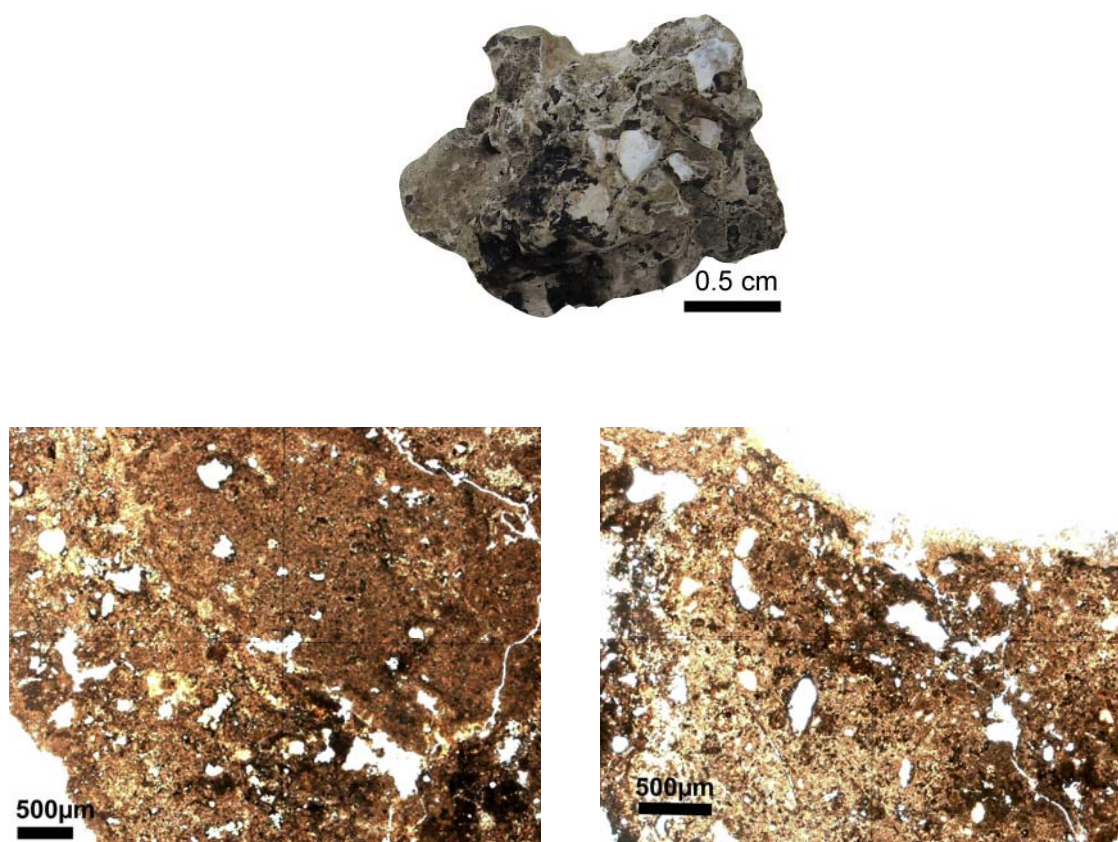


Fig. 4.15. Authigenic carbonate rock and thin section images from the AT 425 site. The rock contains almost totally fine-grained calcite from hydrocarbon oxidation with few inclusions of carbonate skeletal material. Small black areas in thin sections are crude oil.

Table 4.6

Isotopic composition of authigenic carbonate rock of ACR-6 from the AT 425 site (Sassen, 2004)

Sample Location	Sample depth (mbsf)	GERG ID	Dive#	$\delta^{13}\text{C}$ (‰, PDB)	$\delta^{18}\text{O}$ (‰, PDB)
AT 425	0–0.3	ALVIN-18	3918	–24.34	+3.85
AT 425	0–0.3	ALVIN-19	3918	–28.62	+3.86
AT 425	0–0.3	ALVIN-20	3918	–26.31	+3.84
AT 425	0–0.3	ALVIN-20	3918	–27.35	+4.14
AT 425	0–0.3	ALVIN-21	3918	–27.43	+3.93
AT 425	0–0.3	ALVIN-22	3918	–26.60	+3.95
AT 425	0–0.3	ALVIN-23	3918	–24.13	+4.02
AT 425	0–0.3	ALVIN-24	3918	–23.88	+3.94
AT 425	0–0.3	ALVIN-25	3918	–22.55	+4.12
AT 425	0–0.3	ALVIN-25	3918	–24.93	+4.00

One large ( $\sim 20 \text{ cm}^3$ ) oil-stained cobble of ACR-6 (AT 425) was recovered from the AT 425 site during ALVIN dive 3918 in 2003 (Fig. 4.15). ACR-6 (AT 425) is densely cemented. Bulk  $\delta^{13}\text{C}$  values of ACR are in the range of  $-22.6$  to  $-28.6\text{‰}$  (Table 4.6). The mean  $\delta^{13}\text{C}$  value is  $-25.6\text{‰}$ .

If thermogenic methane (mean  $\delta^{13}\text{C} = -48.8\text{‰}$  from gas hydrate, Sassen et al., 2001c) was the primary source of carbon to ACR, then one would expect it to be also highly depleted in  $^{13}\text{C}$ . However, the rock is instead enriched in  $^{13}\text{C}$ . Why is the ACR sample so enriched in  $^{13}\text{C}$  when compared to the thermogenic methane, which is highly depleted in  $^{13}\text{C}$ ?

Two likely hypotheses might explain why ACR-6 (AT 425) is depleted in  $^{13}\text{C}$ : (1) if methane from the AT 425 site was the primary source of carbon to ACR, one would expect it to be also highly depleted in  $^{13}\text{C}$  or (2) the  $\delta^{13}\text{C}$  reflects the oxidation of biodegraded crude oil with the range of  $-22.6$  to  $-28.6\text{‰}$  (mean =  $-25.6\text{‰}$ ).

Bulk  $\delta^{13}\text{C}$  values (mean =  $-25.6\text{‰}$ ) of ACR do not closely correspond to that of the methane ( $\delta^{13}\text{C} = -48.8\text{‰}$ ). Petrographic thin section images (Fig. 4.15) were analyzed. Petrographic thin section images show that ACR-6 (AT 425) contains almost totally fine-grained calcite with few inclusion of carbonate skeletal material. Therefore, the first hypothesis may be eliminated because of lack of normal marine carbonates in ACR.

The second hypothesis, then suggests that the  $\delta^{13}\text{C}$  reflects the oxidation of biodegraded crude oil. For the best explanation of the hypothesis, biodegradation of crude oil will be discussed at this site. Biodegradation is a common process in deep subsurface reservoirs of the Gulf of Mexico (Philippi, 1977). But, few publications address the biodegradation of oil in the deep sea. Oil can be separated by precipitation in hexane and by column chromatography into four main fractions by a procedure referred to as "SARA." The main geochemical fractions of oil are saturated hydrocarbons (SAT), aromatic hydrocarbons (AROM), nitrogen, sulfur, and oxygen (NSO) compounds also known as resins, and asphaltenes (ASPH). SAT and AROM consist of the majority of most unaltered crude oils from reservoirs (Sassen, 2004).

The saturated hydrocarbon fraction of oil is the most rapidly biodegraded component in reservoirs and in natural oil seeps. The process occurs step-wise, starting with the lower molecular weight *n*-alkanes ( $< C_{20}$ ) and quickly progresses to high molecular weight *n*-alkanes ( $> C_{20}$ ). As the *n*-alkanes are biodegraded, a class of branched-chain saturated hydrocarbons remains stable. The branched-chain hydrocarbons are called “isoprenoids,” and two compounds called “pristane (*ip*- $C_{19}$ )” and “phytane (*ip*- $C_{20}$ )” are used by petroleum geochemists to assess degree of biodegradation. The ratio of the fast-biodegrading *n*- $C_{17}$  alkanes is compared to the stable pristane by a ratio (e.g. *n*- $C_{17}$ /*ip*- $C_{19}$ ). Similarly, the ratio of *n*- $C_{18}$  alkanes to phytane may be compared (e.g. *n*- $C_{18}$ /*ip*- $C_{20}$ ) (Sassen, 2004).

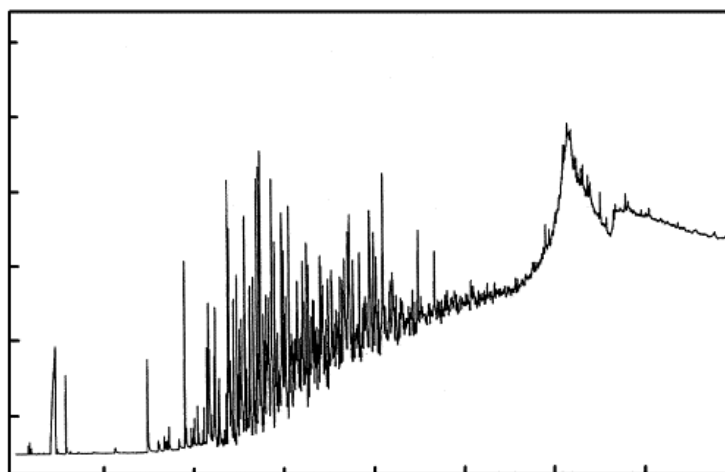


Fig. 4.16. Whole-oil chromatogram of bacterially oxidized crude oil from the AT 425 site showing hydrocarbons in the approximate  $C_9$  to  $C_{20}$  range (Sassen et al., 2001b).

A gas chromatography of highly biodegraded saturated hydrocarbons shows a strongly elevated baseline that is called “humpane” which consists of naphthenes because the other alkanes have been destroyed by microbes, whereas the AROM is more stable than SAT.

Fig. (4.16) shows biodegraded saturated hydrocarbons from carbonate rock from the AT 425 site. This elevated baseline is called the Unresolved Complex Mixture

(UCM). The UCM occurs with some *n*-alkanes and isoprenoids that project above the elevated baseline. The *n*-alkanes and isoprenoids are in the light to medium molecular weight range, approximately C<sub>9</sub> to C<sub>20</sub>. The overall hump-like chromatographic pattern is consistent with bacterial oxidation of oil (Sassen et al., 2001b).

The  $\delta^{13}\text{C}$  of oil from ACR-6 (AT 425) is representative of unaltered source oil from the subsurface. The Total Extractable Organic Matter (EOM) from ACR-6 (AT 425) from the AT 425 site is 42,447 ppm or roughly 4% oil by weight. The  $\delta^{13}\text{C}$  of SAT =  $-27.8\text{‰}$ ; AROM =  $-26.7\text{‰}$ ; NSO =  $-27.0\text{‰}$ ; ASPH =  $-26.6\text{‰}$  (Sassen, 2004). These carbonate isotopic properties of ACR are similar to those of abundant biodegraded crude oil that stains the rock.

As a result, ACR-6 (AT 425) is visibly oil-stained (Fig. 4.15). The  $\delta^{13}\text{C}$  of ACR (n=10) ranges from  $-22.6$  to  $-28.6\text{‰}$  (Table 4.6). The  $\delta^{13}\text{C}$  of oil from ACR is consistent with the  $\delta^{13}\text{C}$  value (mean =  $-25.6\text{‰}$ ) of ACR. Also, petrographic thin sections contain almost totally fine-grained calcite with few inclusions of carbonate skeletal material (Fig. 4.15). Therefore, the third hypothesis appears to be supported by the  $\delta^{13}\text{C}$  values of ACR-6 (AT 425), which reflect the oxidation of biodegraded crude oil.

Measured  $\delta^{18}\text{O}$  values of ACR-6 (AT 425) range from  $+3.85$  to  $+4.14\text{‰}$  (mean  $\delta^{18}\text{O} = +3.97\text{‰}$ ). The  $\delta^{18}\text{O}$  range is isotopically heavier than those of previous data from normal marine calcite (Mozley and Burns, 1993).

Isotopically heavy  $\delta^{18}\text{O}$  values may reflect the movement of isotopically heavier water than ambient seawater from greater depth. The isotopically heavy water can be explained by numerous geologically young basins. Those young basins formed by salt withdrawal pierce the slope salt thrust (Sassen, 2004). Then the isotopically heavy water migrates upward through the openings in the salt thrust.



## Authigenic carbonate rock from the Krishna-Godawari basin offshore India

### Site 3 (NGHP-01-03, GDGH05-A)

Site 3 is located at 15° 53.90'N and 81° 53.97'E in the Krishna-Godawari (KG) basin offshore India at a water depth of ~1,076 m (Fig. 2.5). Seafloor temperature and geothermal gradient of Site 3 are 6.5°C and 3.9°C per 100 m, respectively.

The bottom simulating reflector (BSR) at Site 3 is at a depth of ~209 mbsf based on seismic data (Fig. 4.17). Stratigraphic layers are characterized by a seafloor parallel to slightly inclined beds to a depth of ~125 mbsf.

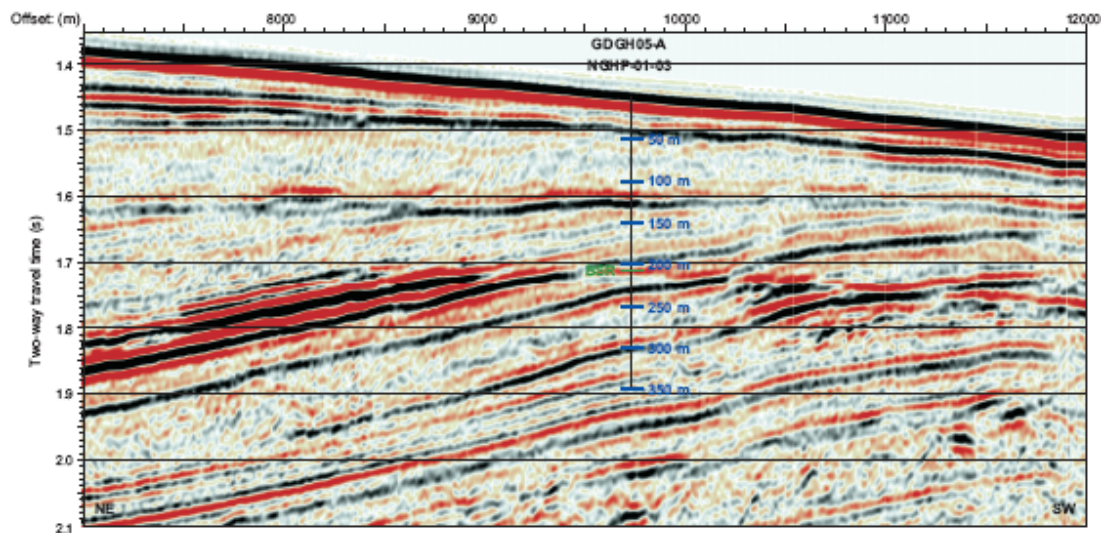


Fig. 4.17. Multichannel seismic reflection line across Site 3 (GDGH05-A) in the Krishna-Godawari basin (Collett et al., 2006). Northwest (NW) is to left. Below the BSR of 209 mbsf a structural unconformity is indicated through a strong seismic reflection, showing the sediments dip toward the NW. Free gas is observed at the dipping layers.

A strong reflection at the base of the inclined beds indicates an unconformity. Below the unconformity the layers dip to the northwest. Free gas trapping is indicated by the strong seismic reflectivity below the BSR (Collett et al., 2006).

At Site 3, sediments range from Quaternary to recent in age. In the depth range of 0 to 198 mbsf, the major lithologies are primarily clay sized sediments with minor amounts of silt sized sediments and absence of sand in general (Fig. 4.18). Minor lithologies include silt-sand beds and iron monosulfide rich zones. The major non biogenic components are feldspar, quartz, and clay and opaque minerals (mostly sulfides and framboidal forms). The total biogenic component of the sediment is dominated by calcareous nannofossils, which comprise 5 to 40% of the total (biogenic and non biogenic) sediment grains. Terrestrial organic matter is observed as trace to 5% throughout the sediments. Shell fragments, visible foraminifera, and gastropods are occasionally observed throughout the section. Authigenic carbonates are abundant throughout the sediments (Fig. 4.19). They precipitate in the form of nodules and bands (Collett et al., 2006).

No gas hydrate was recovered, and gas hydrate bearing sediment was not observed at this site. However, gas hydrate may have been disseminated within the pore spaces or fracture fills and dissociated completely during recovery (Collett et al., 2006).

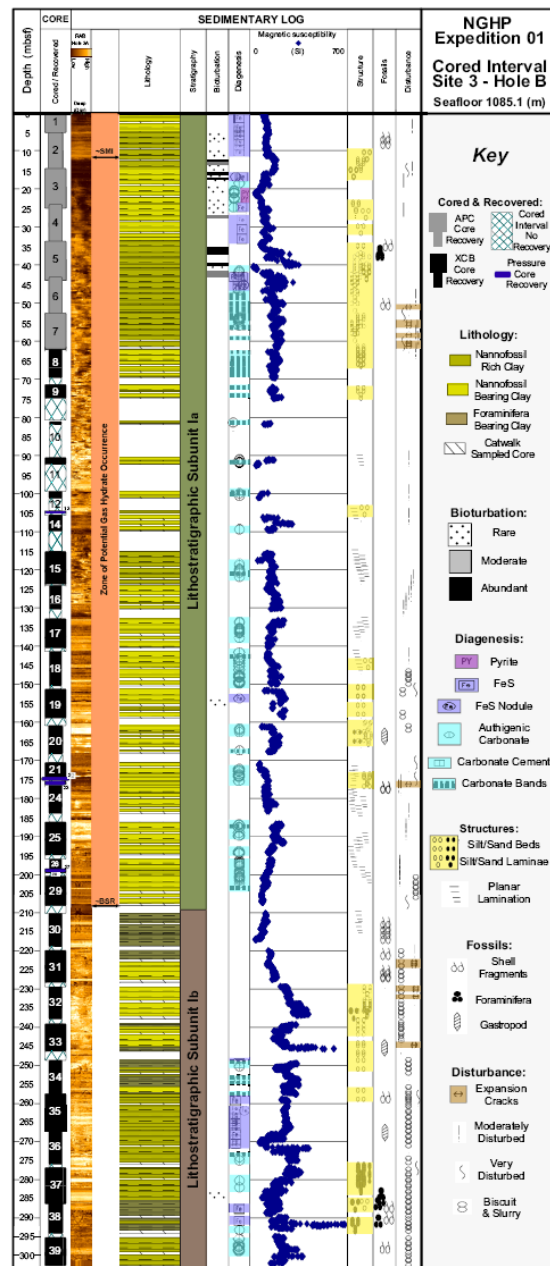


Fig. 4.18. Lithostratigraphic summary of Hole NGHP-01-03B (Collett et al., 2006).

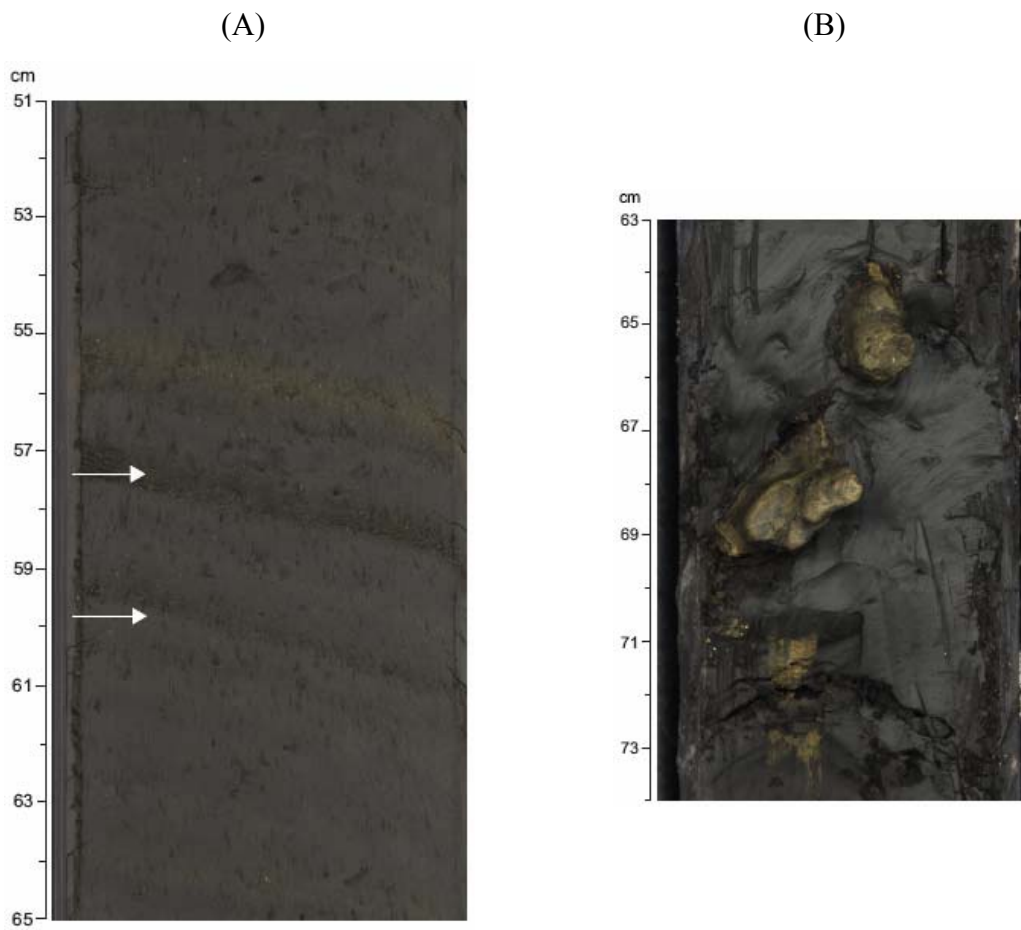


Fig. 4.19. Authigenic carbonate bands and rock typical of those observed in core sections from Site 3 (Collett et al., 2006). (A) Section NGHP-01-03B-07H, 62.4 mbsf: authigenic carbonate bands shown by arrows. (B) Section NGHP-01-03B-03C-09Y-1, 81.3 mbsf: branching shapes imply formation of ACR in burrows. Vertical scale is in centimeters down core section.

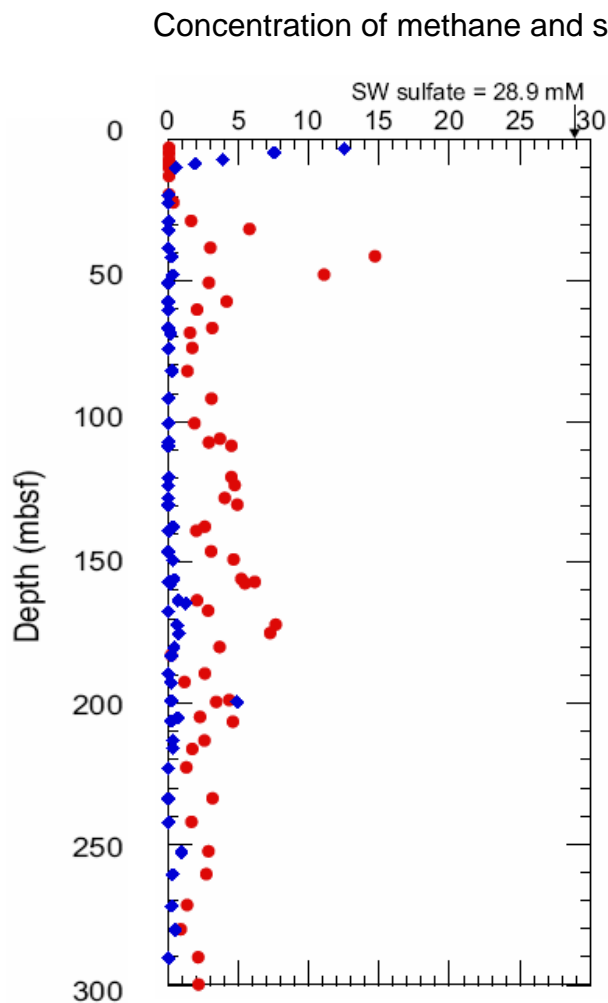


Fig. 4.20. Concentration depth profile of sulfate and methane at Site 3 (Collett et al., 2006). Sulfate/methane interface is located at ~12 mbsf. Sulfate concentration is 12.5 mM at 2.9 mbsf, and is totally depleted by 12 mbsf. Note that blue = methane, red = sulfate.

In Site 3 Hole B, the sulfate/methane interface (SMI) is located at ~12 mbsf (Fig. 4.20). Sulfate concentration is 12.5 mM at 2.9 mbsf, and is totally depleted by 12 mbsf. Headspace methane ( $\text{CH}_4$ ) concentration increases strongly from nondetectable to 3.8 mM at ~12 mbsf, likely denoting the SMI (Fig. 4.21). The slight increase in  $\text{CH}_4$  concentration at ~40 mbsf may be associated with the presence of free gas or gas hydrate.

however, other gas hydrate proxy measurements indicated that gas hydrate was not present. The  $\text{CH}_4$  concentration slightly decreases below the bottom simulating reflector (BSR) and it is generally constant throughout the length of the borehole.

Headspace carbon dioxide ( $\text{CO}_2$ ) concentration ranges from 0.6 to 11 mM.  $\text{CO}_2$  concentration shows no consistency with depth, as indicated throughout the sediment by scatter. The sediment may be dominated by  $\text{CO}_2$ . The high concentration of  $\sim 10$  mM is found at the depths of 45, 95, and 170 mbsf (Fig. 4.22).

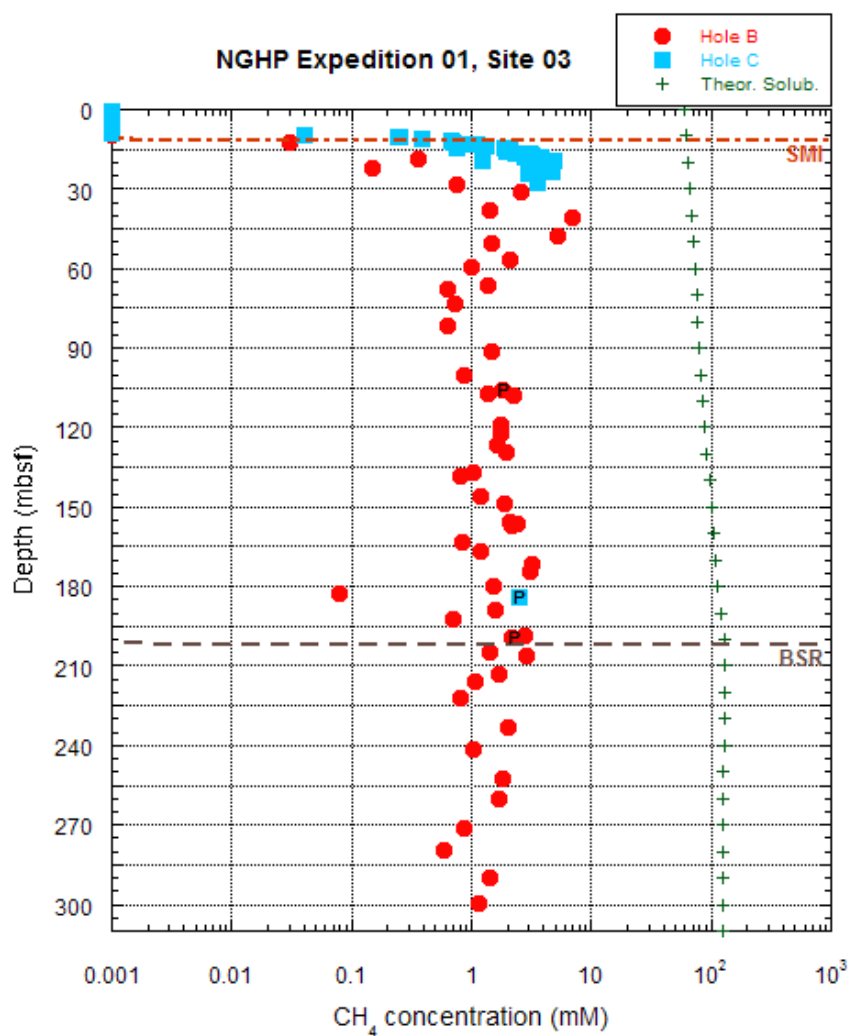


Fig. 4.21. Plot of headspace methane gas concentration with depth at Site 3 (Collett et al., 2006). Methane concentration increases strongly from non detectable to 3.8 mM at  $\sim 12$  mbsf, likely denoting the SMI, and it is generally constant throughout the length of the borehole.

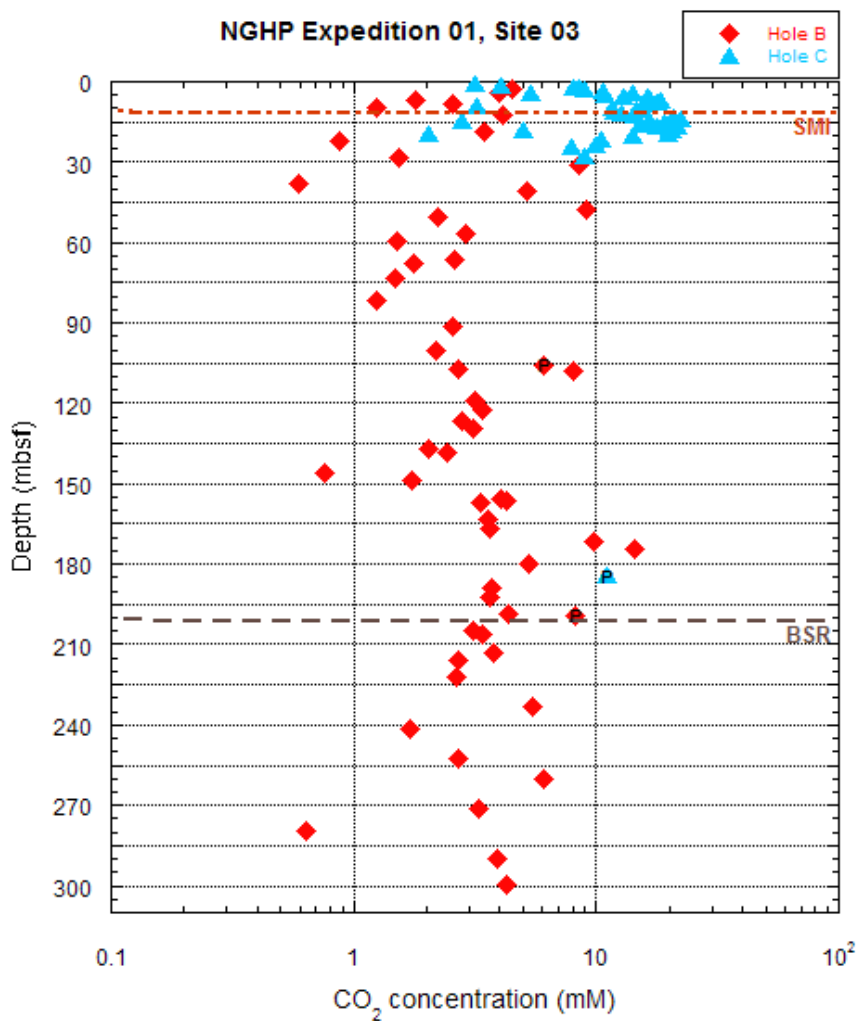


Fig. 4.22. Plot of headspace carbon dioxide gas concentration with depth at Site 3 (Collett et al., 2006). CO<sub>2</sub> concentration ranges from 0.6 to 11 mM in Site 3 Hole B. Scatter in the CO<sub>2</sub> concentration shows no consistency with depth. The sediment may be dominated by CO<sub>2</sub>. The high concentration of ~10 mM is found at the depths of 45, 95, and 170 mbsf.

A smooth nodule of ACR-1 (Site 3) (Fig. 4.23) was collected from Site 3 (core# EXP01-03B-7H3) at a depth of 56.2 mbsf. The nodule contains fine-grained calcite with few inclusions of carbonate skeletal material and fossil wood fragments.

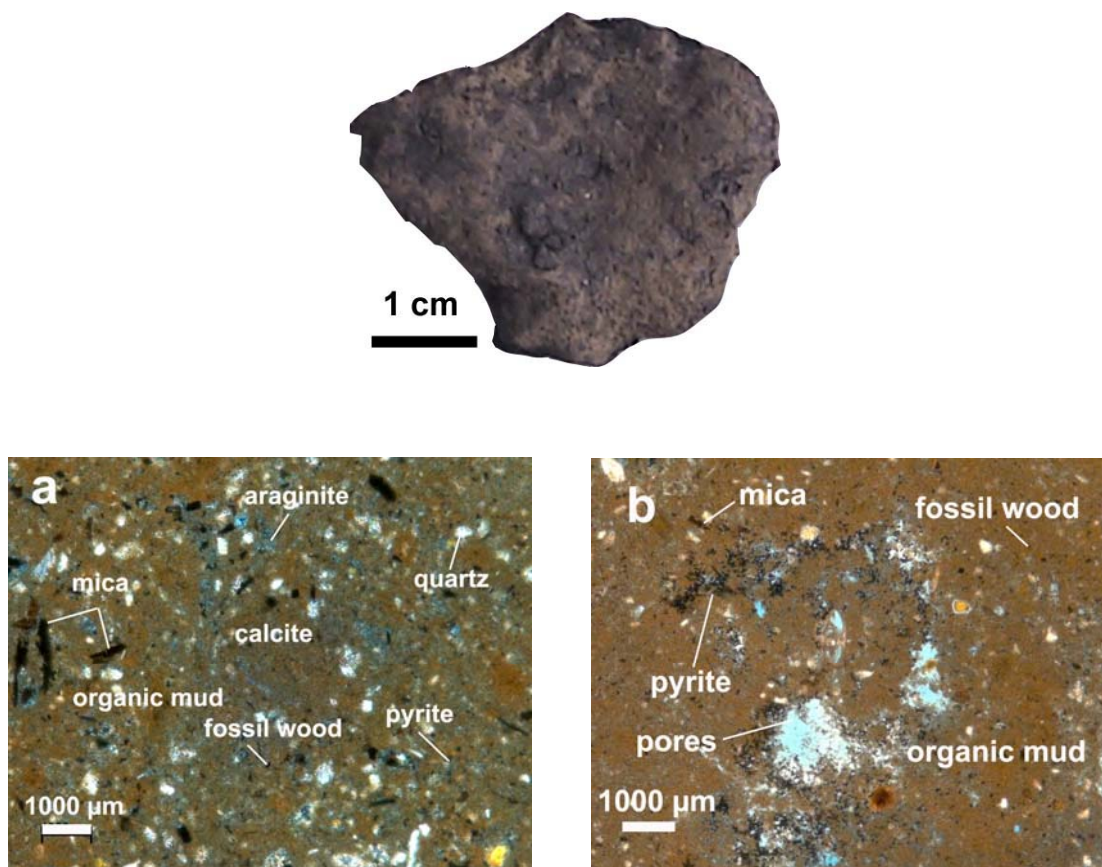


Fig. 4.23. Authigenic carbonate rock and thin section images of ACR-1 (Site 3). ACR contains fine-grained calcite with few inclusions of carbonate skeletal material and fossil wood fragments. Other minerals such as aragonite, quartz, mica, and pyrite are imbedded in the fine-grained mud matrix with pore spaces.



Table 4.7  
Isotopic composition of authigenic carbonate rock from Site 3

Sample#	Site	Hole	Sample depth (mbsf)	$\delta^{13}\text{C}$ (‰, PDB)	$\delta^{18}\text{O}$ (‰, PDB)
ACR-1	Site 3	B	56.2	+10.95	+4.99

Bulk carbon and oxygen ( $\delta^{13}\text{C}$  and  $\delta^{18}\text{O}$ ) isotopes of ACR-1 were measured (Table 4.7). The sample has  $\delta^{13}\text{C}$  of +10.95‰. The  $\delta^{13}\text{C}$  value is isotopically heavier than normal marine carbonate. At this site, microbial methane is highly depleted in  $^{13}\text{C}$  ( $\delta^{13}\text{C} = -69$ ‰, Oil and Natural Gas Corporation India, ONGC). Therefore, if the microbial methane was the primary source of carbon to ACR, one would expect it to be also highly depleted in  $^{13}\text{C}$ . However, the ACR is highly enriched in  $^{13}\text{C}$  with  $\delta^{13}\text{C}$  of +10.95‰. Why is ACR-1 (Site 3) so enriched in  $^{13}\text{C}$  when compared to the microbial methane ( $\delta^{13}\text{C} = -69$ ‰, ONGC), which is highly depleted in  $^{13}\text{C}$ ?

The  $\delta^{13}\text{C}$  of ACR-1 (Site 3) may reflect the oxidation of sedimentary organic matter in the zone of methanogenesis. Two explanations support this proposal: (1) the  $\delta^{13}\text{C}$  reflects high rates of organic carbon oxidation from high sedimentary organic matter; and (2) ACR forms in the zone of methanogenesis. Each explanation will be discussed for a reasonable explanation.

Sedimentary organic matter in marine sediments produces  $\text{CH}_4$  and  $\text{CO}_2$  (Claypool and Kaplan, 1974; Burns, 1998; Paull et al., 2000). During organic carbon remineralization, large fractionations of carbon isotopes occur between carbon reservoirs with depth-related changes in the isotopic composition of dissolved inorganic carbon (DIC) (Fig. 4.24).

The  $\delta^{13}\text{C}$  of DIC decreases from  $\sim 0$ ‰ at the seafloor to  $-20$ ‰ near SMI (Claypool and Kaplan, 1974; Mozley and Burns, 1993). Below the SMI,  $^{12}\text{C}$  from  $\text{CO}_2$  preferentially gets fractionated into methane and hence the DIC becomes enriched in  $^{13}\text{C}$  in the zone of methanogenesis.

At this site, in sediments with relatively high rates of organic carbon oxidation, the zone of methanogenesis is found at a shallow depth of ~12 mbsf (Fig. 4.20). The methanogenesis may be enough to cause isotopically heavy  $\delta^{13}\text{C}$  of +10.95‰.

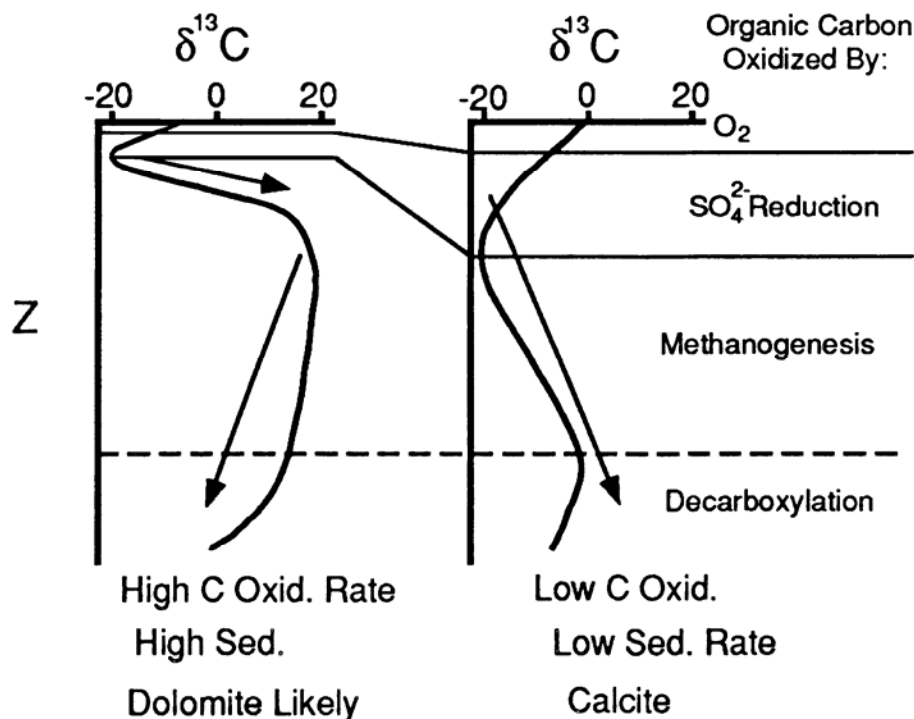


Fig. 4.24. Diagram illustrating effect of varying sedimentation rate and rate of organic-carbon oxidation on  $\delta^{13}\text{C}$  values with depth (Mozley and Burns, 1993, permitted by Peter Mozley).

In addition,  $\text{CH}_4$  and  $\text{CO}_2$  concentrations (Figs. 4.21 and 4.22) were checked for high rates of organic carbon oxidation at the site. The SMI is located at ~12 mbsf (Fig. 4.20). Sulfate is totally depleted by SMI, and then methanogenesis begins into the sediments. Thus,  $\text{CH}_4$  concentration rapidly increases just below the SMI, and it shows the highest value of ~7 mM around the depth of ACR-1 (Site 3) (Fig. 4.21). Concomitantly,  $\text{CO}_2$  occurs in low concentration at that depth (Fig. 4.22).

Bulk  $\delta^{18}\text{O}$  of ACR-1 (Site 3) is +4.99‰. The  $\delta^{18}\text{O}$  value is isotopically heavier than that of normal marine carbonate. Three likely hypotheses account for the isotopically heavy  $\delta^{18}\text{O}$  value from ACR-1(Site 3): (1) it reflects the temperature of initial formation of ACR; (2) it reflects isotopically heavy  $\delta^{18}\text{O}$  values from gas hydrate decomposition; or (3) it reflects the movement of isotopically heavier water than ambient seawater from greater depth.

Each hypothesis will be discussed separately. The first hypothesis is that the measured  $\delta^{18}\text{O}$  value of +4.99‰ reflects the temperature of initial formation of ACR. To calculate the temperature, the measured  $\delta^{18}\text{O}$  of +4.99‰ in PDB to the value of +36.0‰ in SMOW was converted using the relation of  $\delta^{18}\text{O}_{\text{SMOW}} = 1.03086 \delta^{18}\text{O}_{\text{PDB}} + 30.86$  (Friedman and O'Neil, 1977). Then, using an equilibrium oxygen isotope equation (Kim and O'Neil, 1997) of  $1000 \times \ln(\alpha) = 18.03 \times (10^3 \text{ T}^{-1}) - 32.42$ , the temperature of  $-6.6^\circ\text{C}$  was calculated (APPENDIX B).

However, the first hypothesis may be eliminated because the calculated temperature of  $-6.6^\circ\text{C}$  for seawater is unrealistic for environment. Calculating the  $\delta^{18}\text{O}$  water value using the measured  $\delta^{18}\text{O}$  and temperature of ACR-1 (Site 3) and the Kim and O'Neil (1997) equation yielded  $\delta^{18}\text{O}$  water value of +3.83‰ SMOW. The  $\delta^{18}\text{O}$  value of +0.15‰ SMOW was applied for Indian Ocean water (<http://data.giss.nasa.gov/o18data>, GEOSECS Ostlund et al., 1987) at a nearest location (latitude:  $12.53^\circ\text{N}$  and longitude:  $84.51^\circ\text{E}$ , water depth: 1,190 m) to the study site of Site 3 ( $15^\circ 53.90'\text{N}$  and  $81^\circ 53.97'\text{E}$ ).

Although gas hydrate water may cause an isotopically heavy  $\delta^{18}\text{O}$  value, the second hypothesis for isotopically heavy  $\delta^{18}\text{O}$  water resulting from gas hydrate decomposition may also be eliminated. This is because hydrate water would not cause significantly heavy oxygen isotopes from +0.15 to +3.83‰ SMOW (Matsumoto and Borowski, 2000; Greinert et al., 2001; Sassen and Roberts, 2004).

To eliminate the second hypothesis, two examples of isotopically heavy  $\delta^{18}\text{O}$  water values from hydrate water were provided. As discussed in Chapter I, the magnitude of the isotopically heavy oxygen was 0.3 to 0.6‰ SMOW at Blake Ridge

Site 997 (Matsumoto and Borowski, 2000) and 0.86‰ SMOW at Hydrate Ridge (Greinert et al., 2001). Third hypothesis suggests that the  $\delta^{18}\text{O}$  value of +4.99‰ may be affected by the migration and movement of isotopically heavy water from greater depth. The isotopically heavy water from greater depth has  $\delta^{18}\text{O}$  values ranging +3.3 to +5.1‰ (Land and Macpherson, 1992) as produced from Cenozoic hydrocarbon reservoirs in the Gulf of Mexico sedimentary basin. Measured and calculated oxygen isotopic composition of ACR-1 from Site 3 is shown in Table 4.8.

Table 4.8  
Oxygen isotopic properties of ACR-1 (Site 3)

Sample depth (mbsf)	Measured $\delta^{18}\text{O}_{\text{ACR}}$ (‰, PDB)	Calculated temperature (°C)	Temperature at sample depth (°C)	Calculated $\delta^{18}\text{O}_{\text{water}}$ (‰, SMOW)
56.2	+4.99	-6.6	8.69	+3.83

### Site 5 (NGHP-01-05, KGGH02-A)

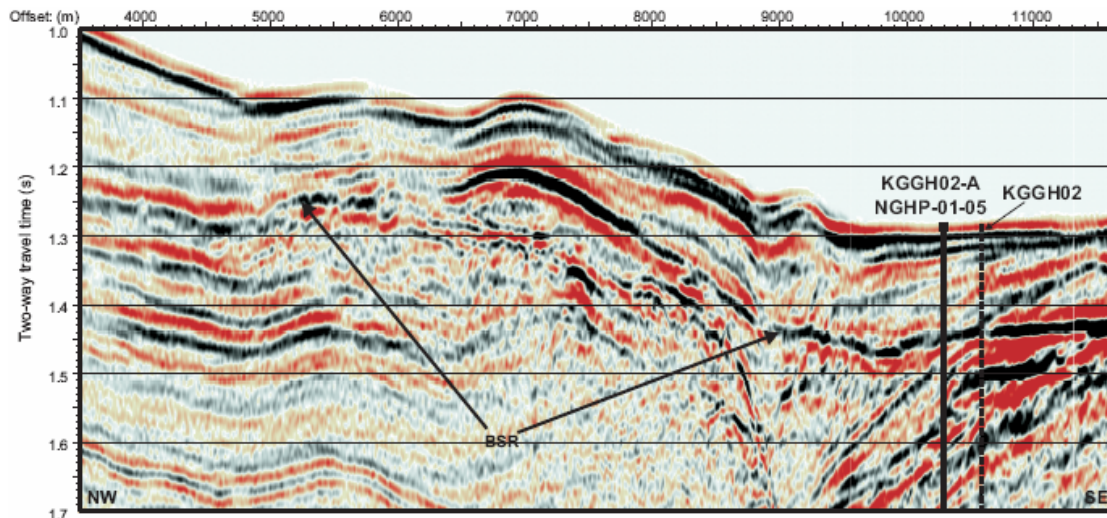


Fig. 4.25. Multichannel seismic reflection line across Site 5 (KGGH02-A) in the Krishna-Godawari basin (Collett et al., 2006). Northwest is to left. Stratigraphic layers indicate a sedimentary section dominated by slopes. Possible faulting is observed through the section. Free gas is observed below BSR depth of 125 mbsf.

Site 5 is located at  $16^{\circ} 01.72'N$  and  $82^{\circ} 02.68'E$  in the KG basin offshore India at a water depth of 945 m (Fig. 2.5). Seafloor temperature and geothermal gradient of Site 5 are  $6.89^{\circ}C$  and  $4.6^{\circ}C$  per 100 m, respectively. Seismic data indicate a distinct BSR at a depth of 125 mbsf for the entire sediment at the site. Stratigraphic layers are characterized by a sedimentary section dominated by slopes. However, the seafloor is relatively flat at around this site. Past slope failures and possible faulting provide evidence of a past slope to the northwest. Below the BSR, the presence of free gas is possible (Fig. 4.25).

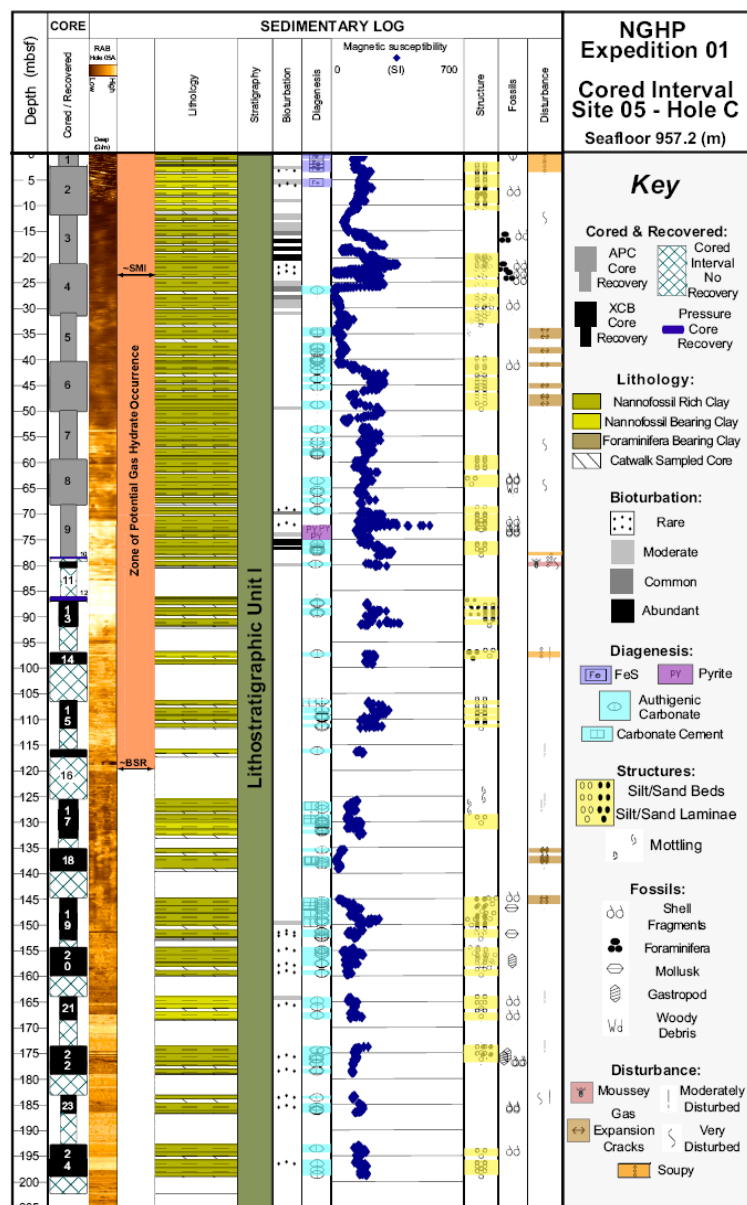


Fig. 4.26. Lithostratigraphic summary of Hole NGHP-01-05C (Collett et al., 2006).

At Site 5, sediments range from Quaternary to recent in age. In the depth range of 0 to 200 mbsf, the major lithologies are primarily clay sized sediments with minor amounts of silt sized sediments absent of sand in general (Fig. 4.26). Minor lithologies include silt beds and authigenic carbonate rich zones. The major nonbiogenic components are feldspar, quartz, and clay and opaque minerals (mostly sulfides). The

total biogenic component of the sediment is dominated by calcareous nannofossils, which comprise 5 to 50% of the total (biogenic and nonbiogenic) sediment grains. Foraminifera are common in sediments. Terrestrial organic matter is also observed throughout section. Nodules and thin horizontal bands (Figs. 4.26 and 4.27) of authigenic carbonates are common below 25 mbsf throughout section (Collett et al., 2006). No gas hydrate was recovered and gas hydrate bearing sediment was not observed at this site. However, gas hydrate may have been disseminated as vein fills in some horizontal bands (Collett et al., 2006).

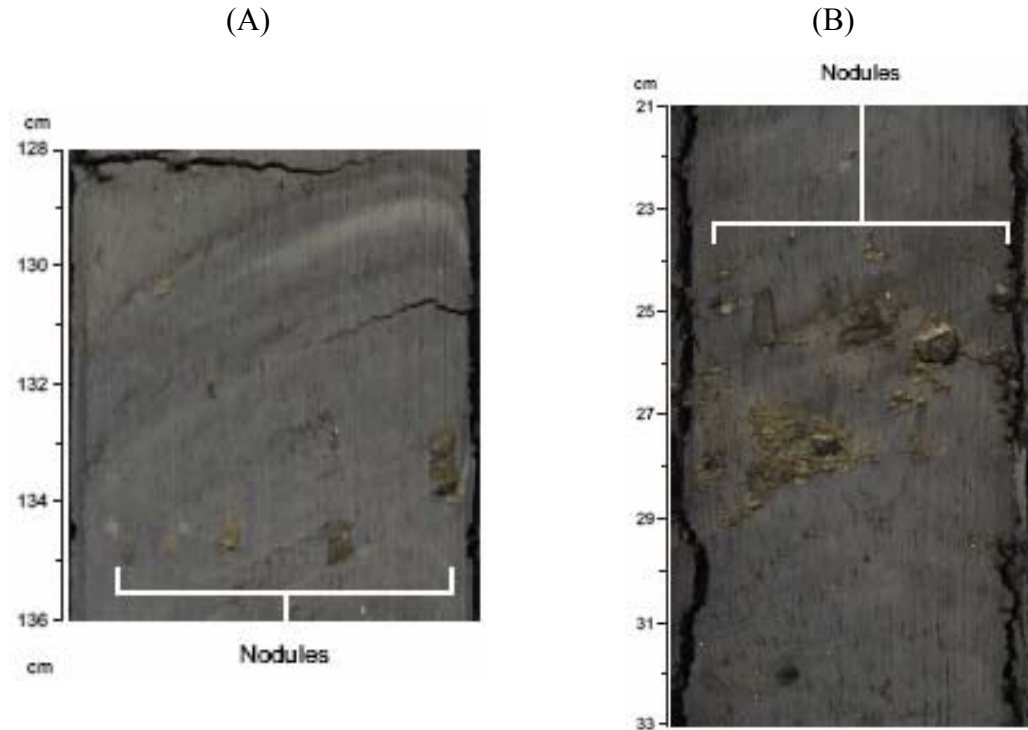


Fig. 4.27. Nodules of authigenic carbonate rock from Site 5 (Collett et al., 2006). (A) Section NGHP-01-05C-05H5, 40.3 mbsf, (B) Section NGHP-01-05C-17X4, 135.1 mbsf.

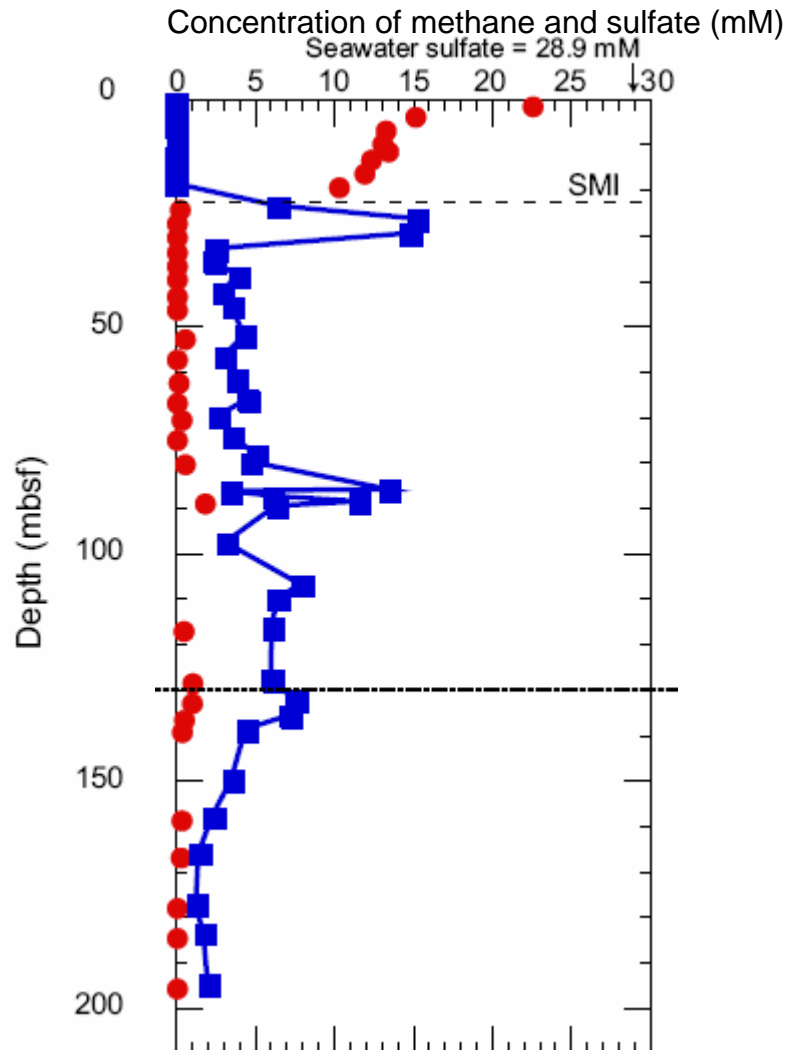


Fig. 4.28. Concentration depth profile of sulfate and methane at Site 5 (Collett et al., 2006). Note that red = sulfate and blue = methane.

In Site 5 Hole C, the SMI is located at ~24 mbsf (Fig. 4.28). Sulfate concentration is 22.5 mM at 1.4 mbsf, and is totally depleted by 24 mbsf.  $\text{CH}_4$  concentration is highest just below ~24 mbsf, likely denoting SMI. A concentration peak is also found at the depth of ~85 mbsf (Figs. 4.28). Headspace  $\text{CH}_4$  concentration is generally at levels between SMI and BSR, and it decreases below BSR. A slight increase



in methane concentration just below the BSR implies that free gas may be trapped just below BSR at depths of ~135 to 140 mbsf (Fig. 4.29).

Headspace  $\text{CO}_2$  concentration ranges from 0.8 to 13 mM in Site 5 Hole C (Fig. 4.30).  $\text{CO}_2$  concentration generally shows scatter, yielding no observable trend in the  $\text{CO}_2$  concentration with depth. Relatively high  $\text{CO}_2$  concentrations are observed below the BSR from 140 to 165 mbsf, whereas low concentrations are found in the interval between SMI and BSR (Fig. 4.30). The lowest concentrations are found at around SMI and in the upper 15 mbsf.

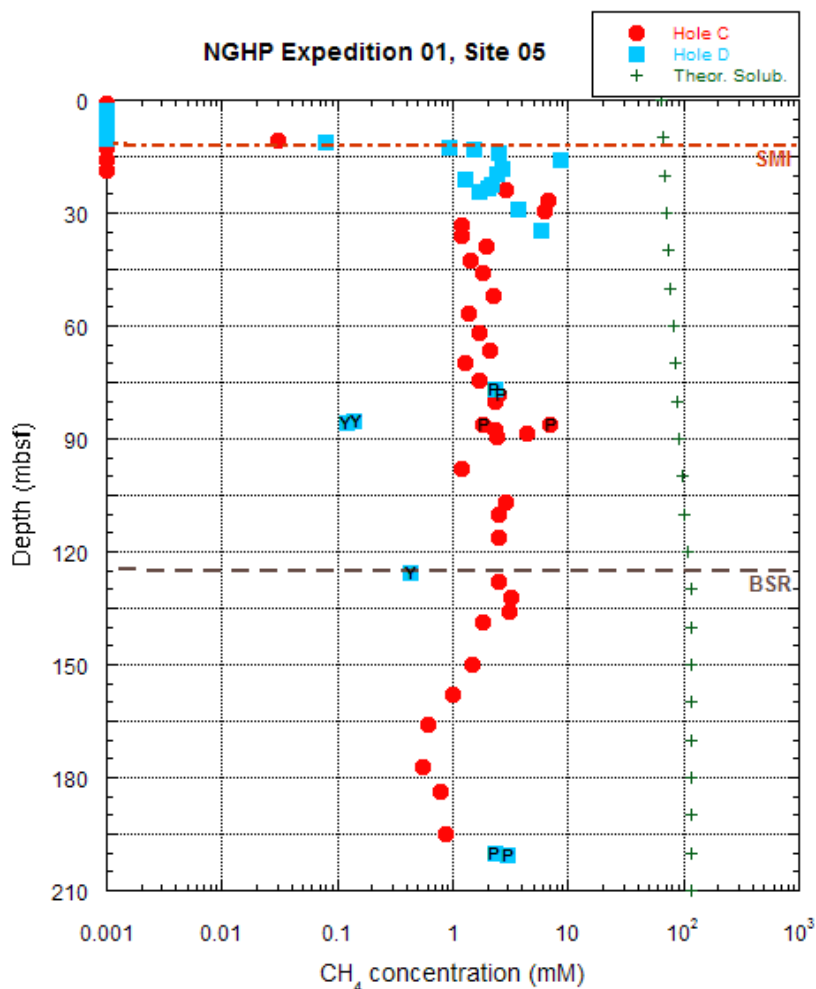


Fig. 4.29. Plot of headspace methane gas concentration with depth at Site 5 (Collett et al., 2006).  $\text{CH}_4$  concentration is generally at levels between SMI and BSR, and it decreases below BSR. A slight increase in methane concentration just below the BSR infers that free gas may be trapped just below BSR at depths of ~135 to 140 mbsf.

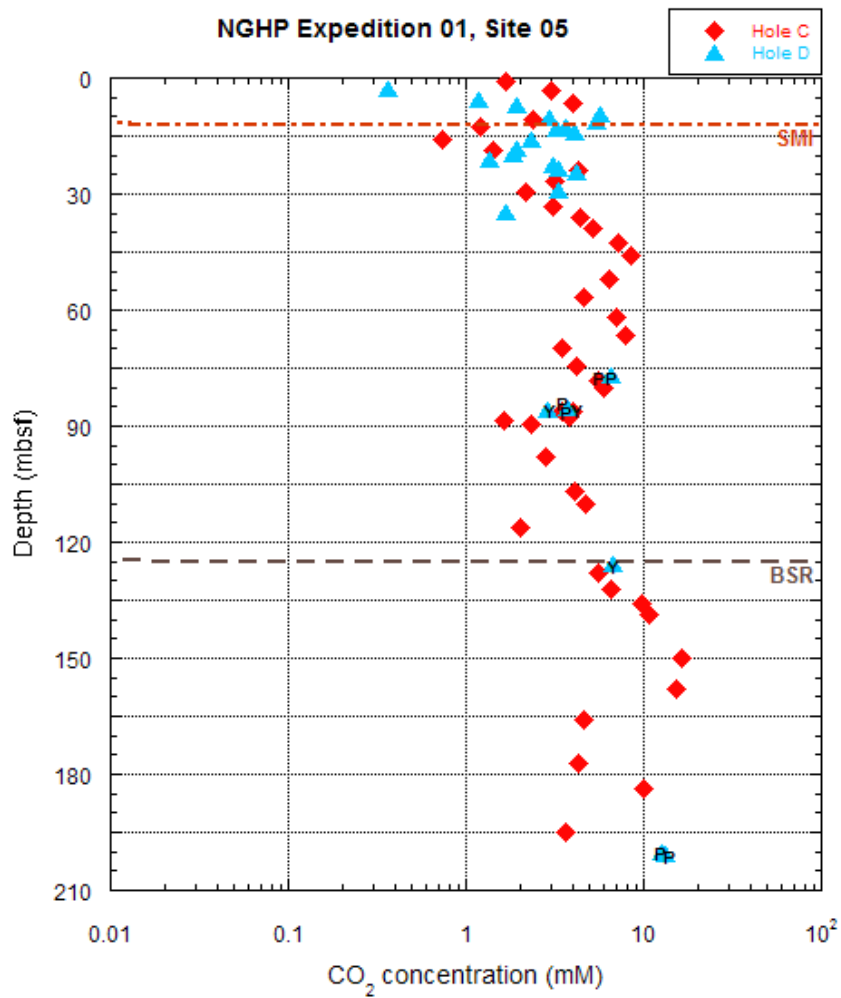


Fig. 4.30. Plot of headspace carbon dioxide gas concentration with depth at Site 5 (Collett et al., 2006). CO<sub>2</sub> concentration ranges from 0.8 to 13 mM in Site 5 Hole C. Relatively high CO<sub>2</sub> concentrations lie below the BSR from 140 to 165 mbsf, whereas low concentrations appear in the interval between SMI and BSR.

Three samples of ACR-2, ACR-3, and ACR-4 (Fig. 4.31) were recovered from Site 5 (core# EXP01-05C-5H7) at depths of 37.1 mbsf (ACR5-1), 40.0 mbsf (ACR5-2), and 110.2 mbsf (ACR5-3) (Table 4.9).



Fig. 4.31. Authigenic carbonate rock from Site 5 in the Krishna-Godawari basin offshore India.

Table 4.9  
Isotopic composition of authigenic carbonate rock from Site 5

Sample#	Site	Hole	Sample depth (mbsf)	$\delta^{13}\text{C}$ (‰, PDB)	$\delta^{18}\text{O}$ (‰, PDB)
ACR-2	Site 5	C	37.1	-24.62	+2.44
ACR-3	Site 5	C	40.0	+14.06	+4.54
ACR-4	Site 5	C	110.2	-2.80	+2.69

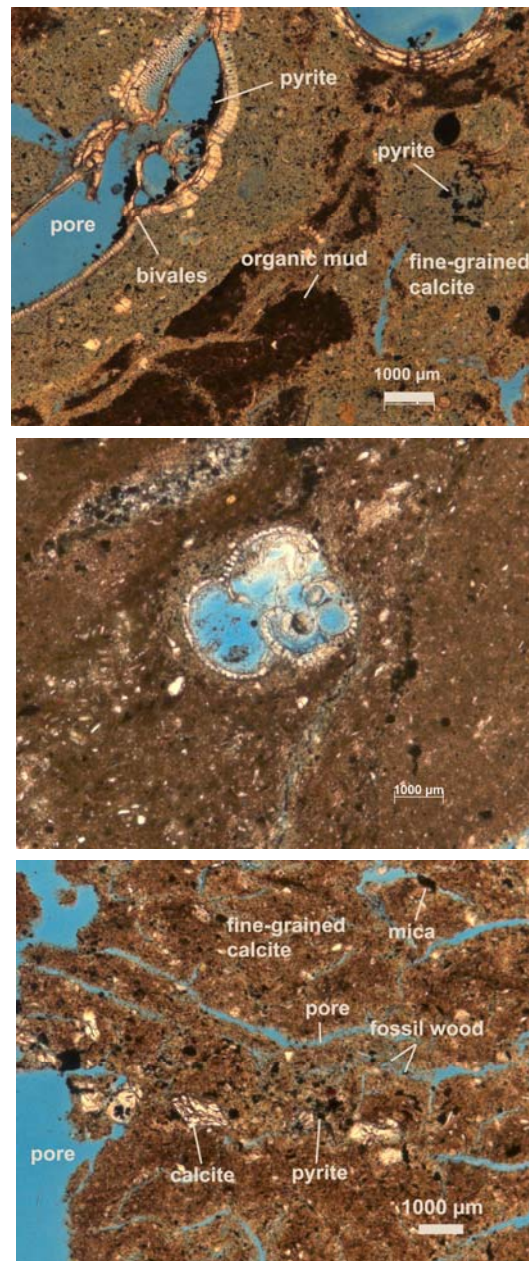


Fig. 4.32. Thin section images of ACR from Site 5 in the Krishna-Godawari basin offshore India. ACR-2 (Site 5) (top) contains fine-grained calcite with inclusions of massive bivalves composed of carbonate and organic mud matrix with pore spaces. ACR-3 (Site 5) (middle) contains fine-grained calcite with inclusions of skeletal material such as foraminifera sections. ACR-4 (Site 5) (bottom) also contains fine-grained calcite with terrigenous organic matter such as fossil wood.

From petrographic thin sections, ACR-2 (Site 5) contains fine-grained calcite with inclusions of massive bivalves composed of carbonate and organic mud matrix within pore spaces. ACR-3 (Site 5) contains fine-grained calcite with inclusions of skeletal material including foraminifera sections. The thin section image from ACR-4 (Site 5) also contains fine-grained calcite with terrigenous organic matter such as fossil wood. Quartz, mica, and pyrite were also identified.

Bulk carbon and oxygen ( $\delta^{13}\text{C}$  and  $\delta^{18}\text{O}$ ) isotopes of ACR recovered from Site 5 were measured (Table 4.9). The samples have  $\delta^{13}\text{C}$  values covering the wide range from  $-24.62\text{‰}$  (ACR-2) to  $-2.80\text{‰}$  (ACR-4) and  $+14.06\text{‰}$  (ACR-3). Based on the wide range of the  $\delta^{13}\text{C}$  values and corresponding carbonate precipitation, Each sample will be discussed separately.

The  $\delta^{13}\text{C}$  of ACR-2 (Site 5) is highly depleted in  $^{13}\text{C}$ . This site is characterized by microbial methane extremely depleted in  $^{13}\text{C}$  ( $\delta^{13}\text{C} = -69\text{‰}$ , ONGC). The SMI is located at  $\sim 24$  mbsf (Fig. 4.28) at the site, which is close to a sample depth of 37.1 mbsf. Although ACR-2 (Site 5) formed in the zone of methanogenesis, which means very rare or no methane oxidation, methane may not be the primary carbon source to ACR-2 (Site 5). Two hypotheses are possible for the  $\delta^{13}\text{C}$  of ACR-2 (Site 5) depleted in  $^{13}\text{C}$ : (1) if methane from Site 5 is the primary source of carbon to the ACR, one would expect it to be also highly depleted in  $^{13}\text{C}$ ; or (2) the  $\delta^{13}\text{C}$  reflects organic carbon oxidation from sedimentary organic matter.

To test the first hypothesis, the percentage of normal marine carbonate in ACR-2 (Site 5) that became enriched in  $^{13}\text{C}$  with  $\delta^{13}\text{C}$  value of  $-24.62\text{‰}$  was calculated. Calculations of mass balance show that ACR-2 (Site 5) may have 65% normal marine carbonate carbon and 35% methane oxidation. However, ACR-2 (Site 5) should include approximately 75% methane oxidation based on petrographic thin sections. This implies that the first hypothesis is unreasonable. Thus, the first hypothesis may be eliminated, because the thin section image of ACR-2 (Site 5) contains lack of normal marine carbonate (Fig. 4.32).

The second hypothesis proposes that the  $\delta^{13}\text{C}$  reflects organic carbon oxidation from sedimentary organic matter in the zone of methanogenesis. As discussed in Section 4.2.1 (Site 3), oxidation of sedimentary organic matter has  $\delta^{13}\text{C}$  value of  $\sim -20\text{‰}$  (Burns, 1998). The  $\delta^{13}\text{C}$  value of DIC decreases with depth from  $\sim 0\text{‰}$  at the seafloor to  $-20\text{‰}$  near SMI (Fig. 4.24) during the oxidation by oxygen or sulfate reduction. Below SMI,  $^{12}\text{C}$  from  $\text{CO}_2$  preferentially gets fractionated into methane, and hence the DIC becomes enriched in  $^{13}\text{C}$  in the zone of methanogenesis.

At Site 5, the SMI is located at  $\sim 24$  mbsf (Fig. 4.28). Although the ACR-2 (Site 5) below SMI is within the zone of methanogenesis,  $\delta^{13}\text{C}$  may not be affected by methanogenesis processes. The reason is that the methanogenesis either may not occur at all or not ever be enough to generate isotopically heavy carbon isotopes in pore waters at the depth of ACR-2 (Site 5) (Mozley and Burns, 1993).

For more explanation for ACR-2 (Site 5), concentration depth profiles of sulfate and methane (Fig. 4.28), headspace  $\text{CH}_4$  concentration (Fig. 4.29), and headspace  $\text{CO}_2$  concentration (Fig. 4.30) was checked. Sulfate is totally depleted by SMI, and then methanogenesis begins into the sediments.  $\text{CH}_4$  concentration rapidly increases and shows a highest peak just below SMI, whereas  $\text{CH}_4$  shows low concentration at the depth of ACR-2 (Site 5) (Fig. 4.28). In addition, headspace  $\text{CO}_2$  concentration ranges from 0.4 to  $\sim 8$  mM above BSR. Concomitantly,  $\text{CO}_2$  shows high concentration around the depth of ACR-2 (Site 5) (Fig. 4.30).

Whereas the  $\delta^{13}\text{C}$  of ACR-2 (Site 5) may not be affected by methanogenesis processes, the methanogenesis occurs enough to cause isotopically heavy  $\delta^{13}\text{C}$  value of  $+14.06\text{‰}$  of ACR-3 (Site 5) (Fig. 4.24). Consequently, at this site ACR samples may form in sediments with relatively high rates of organic carbon oxidation. Based on the observation for ACR-2 (Site 5) and ACR-3 (Site 5), the  $\delta^{13}\text{C}$  ( $-2.8\text{‰}$ ) of ACR-4 (Site 5) may reflect the carbon isotopic composition of pore waters below methanogenesis (i.g., decarboxylation process) (Fig. 4.24).

Bulk  $\delta^{18}\text{O}$  of ACR samples from Site 5 were measured. The samples have  $\delta^{18}\text{O}$  values of +2.44‰ (ACR-2), +4.54‰ (ACR-3), and +2.69‰ (ACR-4). Samples of ACR5-2, 5-3 and 5-4 (Site 5) will be discussed.

Calculated temperatures of initial formation of ACR are +3.8°C for ACR-2, -4.8°C for ACR-3, and +2.7°C for ACR-4. However, the calculated temperatures are much different from measured temperatures (Table 4.10). The  $\delta^{18}\text{O}$  water values of +1.26‰ SMOW for ACR-2, +3.39‰ SMOW for ACR-3, and +2.26‰ SMOW for ACR-4 were calculated with  $\delta^{18}\text{O}$  of +0.15‰ SMOW for Indian Ocean water. The initial  $\delta^{18}\text{O}$  water values are in the range of +1.26 to +3.39‰ SMOW. Thus, the  $\delta^{18}\text{O}$  values of ACR samples at the site may reflect the movement of isotopically heavier water than ambient seawater from greater depth.

Table 4.10  
Oxygen isotopic properties of authigenic carbonate rock from Site 5

Sample#	Sample depth (mbsf)	Measured $\delta^{18}\text{O}_{\text{ACR}}$ (‰, PDB)	Calculated temperature (°C)	Temperature at sample depth (°C)	Calculated $\delta^{18}\text{O}_{\text{water}}$ (‰, SMOW)
ACR-2	37.1	+2.44	+3.8	8.60	+1.26
ACR-3	40.0	+4.54	-4.8	8.73	+3.39
ACR-4	110.2	+2.69	+2.7	11.96	+2.26

### Site 10 (NGHP-01-10, GD-3-1)

Site 10 is located at 15° 51.86'N and 81° 50.07'E in the KG basin offshore India at a water depth of 1,030 m (Fig. 2.5). The seafloor temperature and geothermal gradient of Site 10 are 6.5°C and 4.5°C per 100 m, respectively. A distinct BSR at Site 10 is observed at a depth of 125 mbsf for the entire seismic profile (Fig. 4.33). Stratigraphic layers are characterized by highly concentrated gas hydrates. Overall, the area is dominated by strong reflectivity of free gas below the seafloor. A large-scale fault is also identified. A distinct seafloor expression of ~350 m in length and ~30 m height is indicated. This feature, located at the crest of the underlying free-gas anticline structure, may be associated with cold vent activity, mud-volcanism, and chemosynthetic communities at the seafloor (Collett et al., 2006).

Gas hydrates from Site 10 (NGHP-01-10) in the KG basin offshore India were collected from drilled cores during the NGHP. Molecular compositions and isotopes of gas hydrates were measured by Oil and Natural Gas Corporation India (ONGC). C<sub>1</sub> is the main component of gas hydrates. The mean concentration of C<sub>1</sub> and C<sub>2</sub> was 99.6% and 0.2%, respectively, whereas CO<sub>2</sub> is a relatively minor component. In relative terms, the concentration of CO<sub>2</sub> is ~0.1%. Gas from gas hydrate is of microbial origin having  $\delta^{13}\text{C}$  values of -69.0‰ for C<sub>1</sub> and -50.8‰ for C<sub>2</sub> (Table 4.11).

Table 4.11

Molecular and isotopic composition of gas hydrates from Site 10

Note that data are from Oil and Natural Gas Corporation India (ONGC)

Gas hydrate sample#	C <sub>1</sub> (%)	$\delta^{13}\text{C}_1$ (‰)	C <sub>2</sub> (%)	$\delta^{13}\text{C}_2$ (‰)	C <sub>3</sub> (%)	$\delta^{13}\text{C}_3$ (‰)	CO <sub>2</sub> (%)
10D-7X2-63-68	99.88	-70.2	0.02	-51.2	-	-	0.10
10D-8X1-140-150	99.87	-68.2	0.02	-50.9	-	-	0.12
10D-10X4-75-80	99.06	-68.6	0.01	-50.4	-	-	0.11



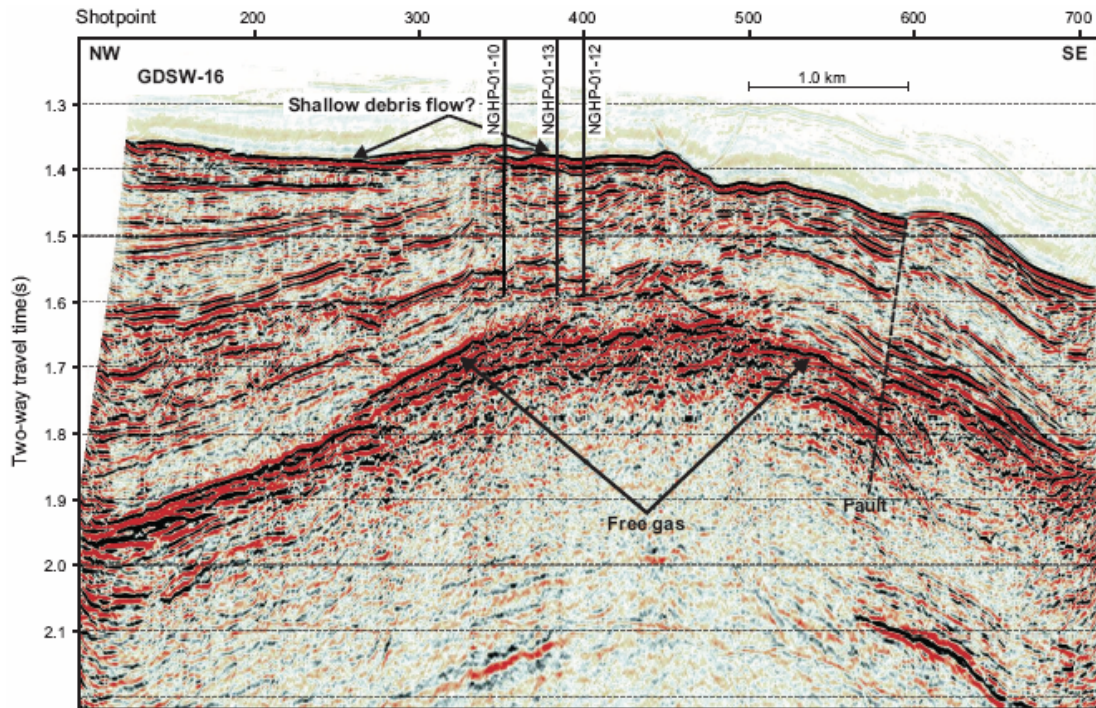


Fig. 4.33. Multichannel seismic reflection line across Site 10 (NGHP-01-10) in the Krishna-Godawari basin. Northwest is to left. Bottom Simulating Reflector (BSR) is observed at a depth of ~160 mbsf. Strong reflectivity indicates the well-developed trapping of free gas under BSR. A distinct seafloor expression of ~350 m in length and ~30 m height is indicated. This feature, located at the crest of the underlying free-gas anticline structure, may be associated with cold vent activity, mud-volcanism, and chemosynthetic communities at the seafloor. A large-scale fault is also identified (Collett et al., 2006).

At Site 10, sediments range from Quaternary to recent in age. In the depth range of 0 to ~204 mbsf, the major lithologies are primarily clay sized sediments with minor amounts of silt sized sediments and absence of sand generally (Figs. 4.34 and 4.35). Minor lithologies include silt beds and authigenic carbonates (Fig. 4.36). Biogenic components of the sediment are dominated by calcareous nannofossils, whereas major nonbiogenic components are feldspar, quartz, clay, and opaque minerals. Foraminifera are common in the sediments, where they are the dominant biogenic component. Terrestrial organic matter is also observed as trace throughout the sediments (Collett et al., 2006).

Gas hydrates were recovered from several drilled cores. The recovered gas hydrates include solid nodules and subhorizontal veins, or are disseminated throughout the cores (Collett et al., 2006).

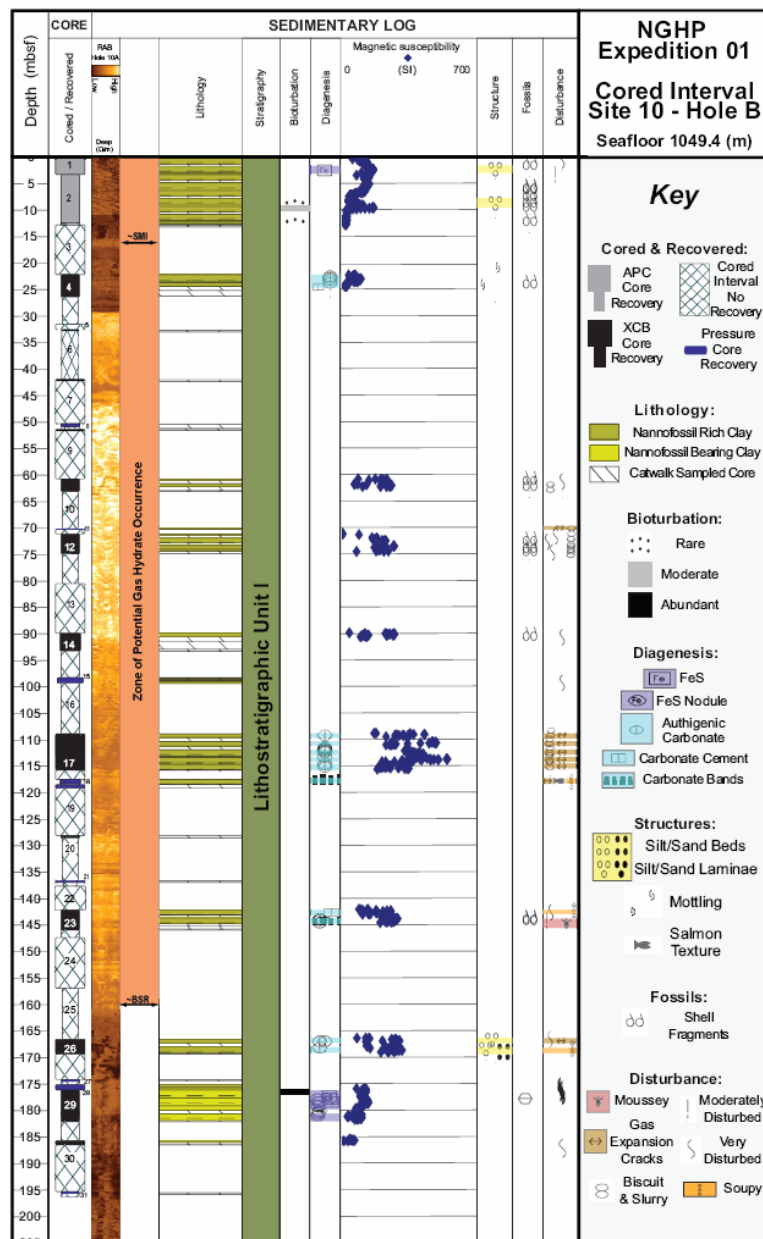


Fig. 4.34. Lithostratigraphic summary of Hole NGHP-01-10B (Collett et al., 2006).

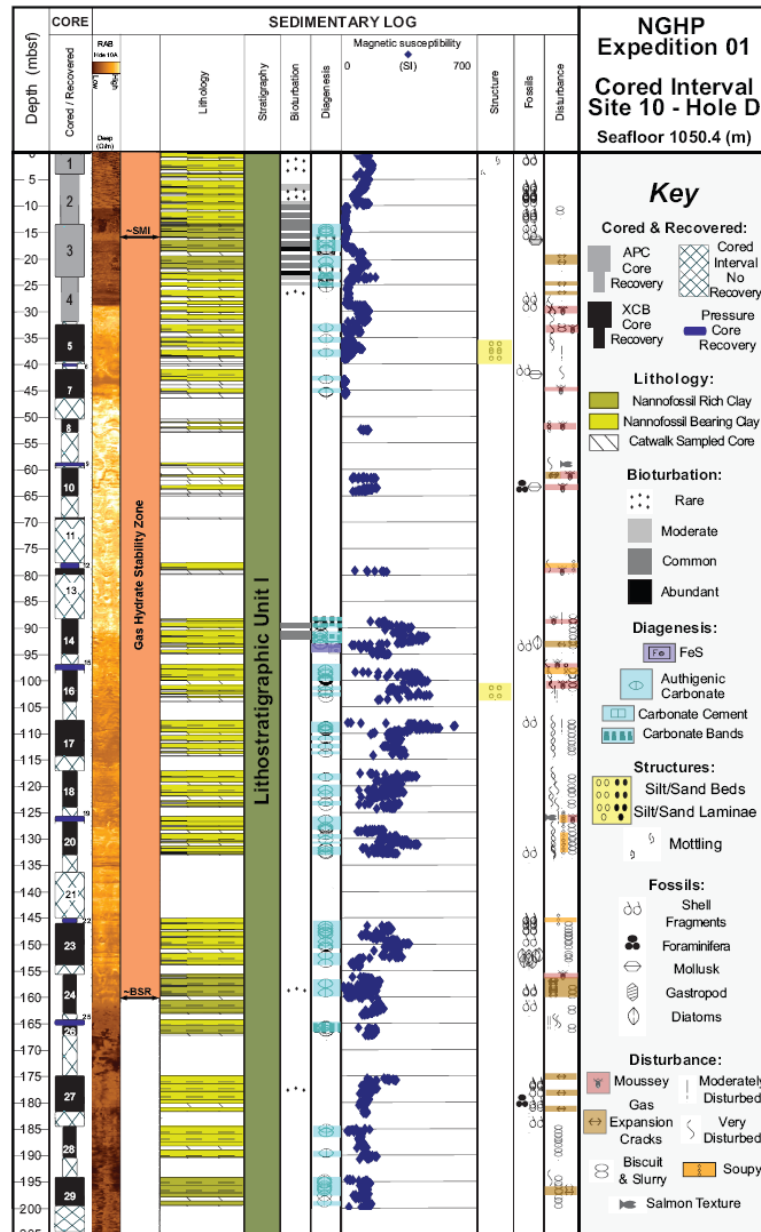


Fig. 4.35. Lithostratigraphic summary of NGHP-01-10D (Collett et al., 2006).

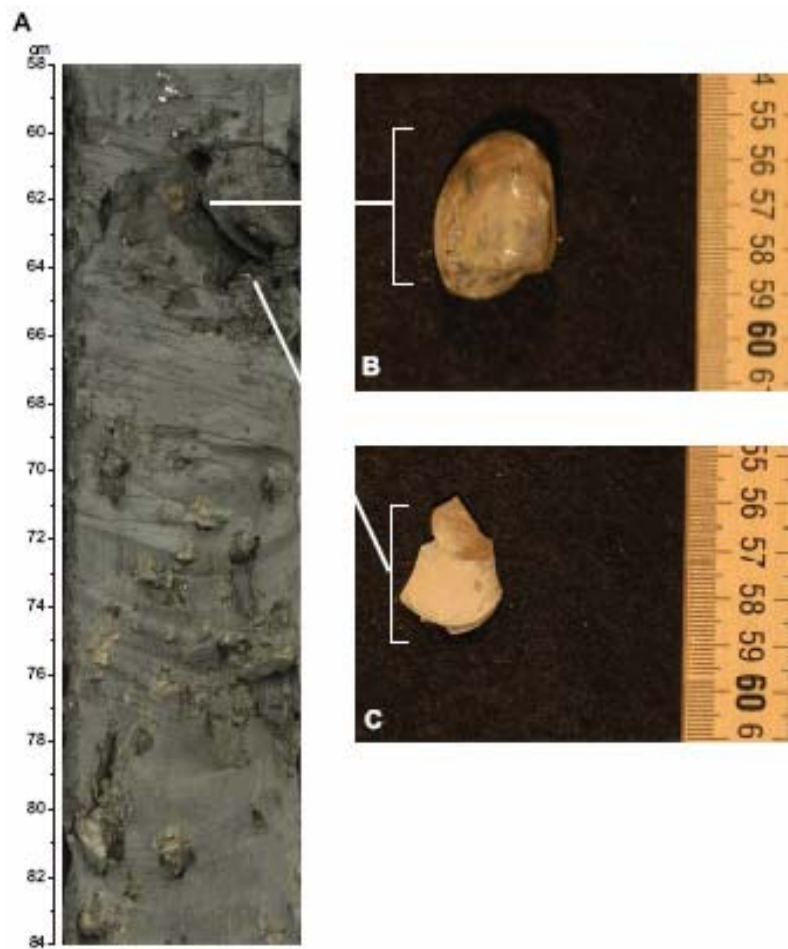


Fig. 4.36. Authigenic carbonate rock and possible fossil chemosynthetic communities at Site 10 (Collett et al., 2006). (A) Section NGHP-01-10D-03H2, 23.1 mbsf. Core section includes corals and many shells (B and C) that may indicate chemosynthetic communities. Vertical scale is in centimeters down core section.

At Site 10, SMI is located at ~17.2 mbsf (Fig. 4.37). Sulfate concentration from interstitial water decreases from near the seawater value of ~28.9 mM to approximately 10 mM at 16.5 mbsf. Concentration gradients increase below this depth. The change in the concentration gradient may be the result of high sedimentation rate or nonsteady-state conditions. An abrupt increase in methane concentration concomitantly with depletion in sulfate occurs from below the detection limit of 0.1 to ~35 mM (Fig. 4.37). Below SMI, the values appear below the detection limit while others scatter to higher values. The higher values may reflect contamination from drilling fluid.

Headspace methane concentration abruptly increases from nondetectable near the surface to ~10 mM at ~18 mbsf, concomitant with an abrupt decrease in sulfate from 10 mM at 16.5 mbsf to 0.1 mM at 17.2 mbsf, thus likely denoting the SMI. Methane concentration below the SMI ranges from 0.1 to 47 mM with two relatively high concentrations at the depths of ~50 and ~110 mbsf (Fig. 4.38). Both of these methane concentration peaks occur within the zone of potential gas hydrate (Collett et al., 2006).

Headspace CO<sub>2</sub> concentration ranges from ~0.05 to 10 mM (Fig. 4.39). CO<sub>2</sub> concentration throughout the sediment shows much scatter. The lowest concentrations are found above the SMI.

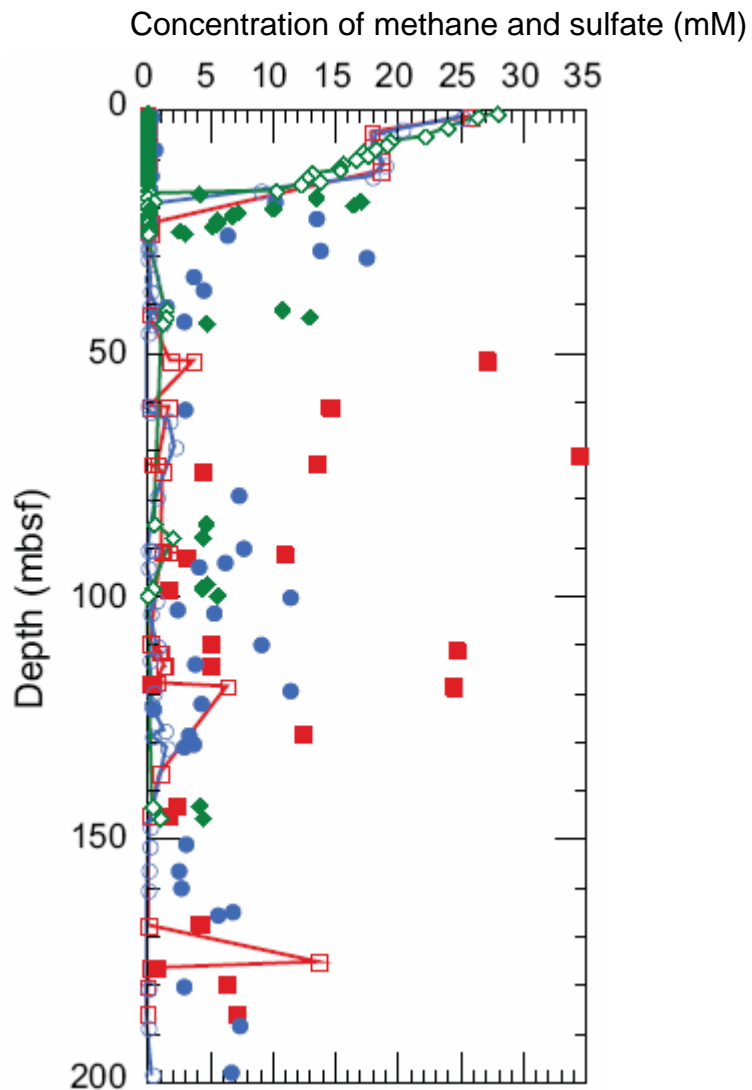


Fig. 4.37. Concentration depth profile of sulfate and methane at Site 10 (Collett et al., 2006). Note that red = Hole NGHP-01-10B, sulfate = empty rectangle in red and connected by line, methane = solid rectangle in red. Blue = Hole NGHP-01-10D, sulfate = empty rectangle in blue and connected by line, methane = solid rectangle in blue. Green = Site 14 (for reference).

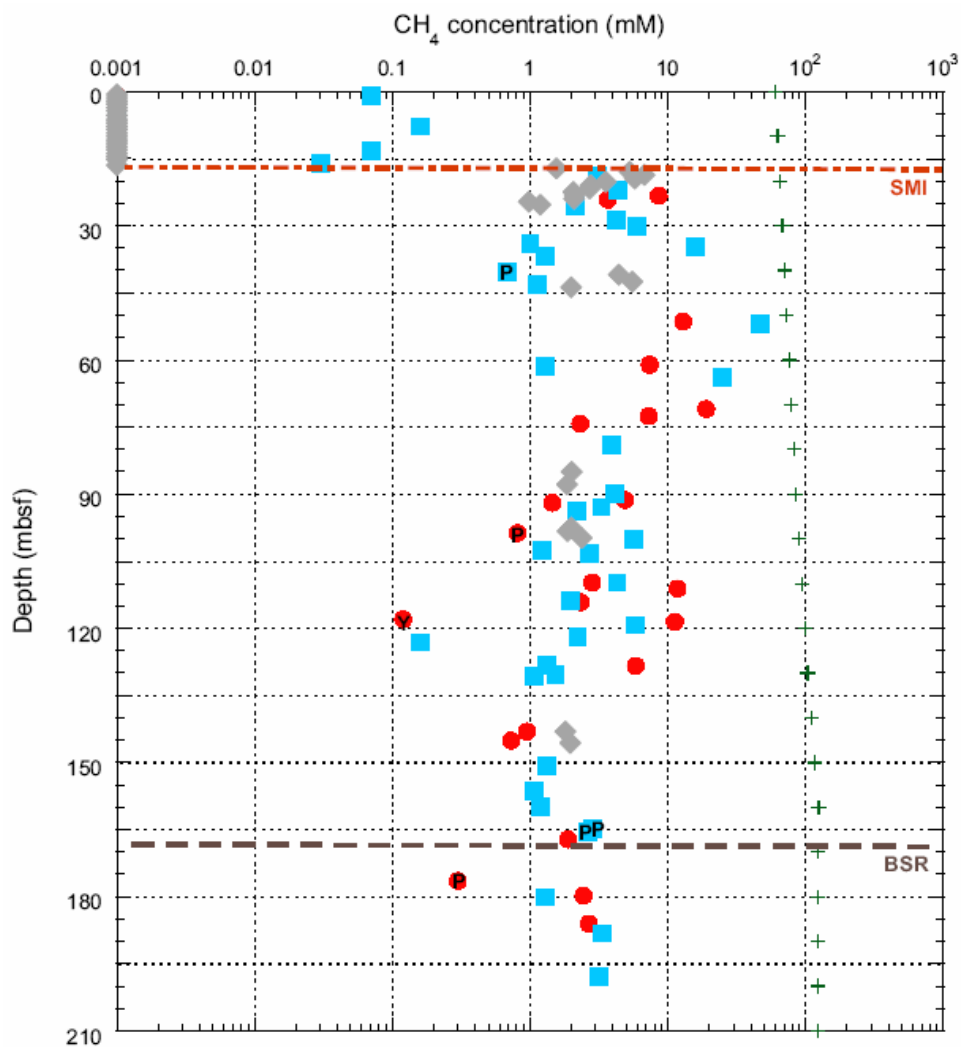


Fig. 4.38. Plot of headspace methane gas concentration with depth at Site 10 (Collett et al., 2006). Note that Holes B = red; Hole D = blue. A rapid decrease in  $\text{CH}_4$  concentration is shown in the upper  $\sim 16$  mbsf at SMI. Below this SMI,  $\text{CH}_4$  concentration increases from  $\sim 0.03$  to  $\sim 40$  mM.  $\text{CH}_4$  concentration throughout the sediment shows scatter. Gray = Site 12 (for reference).

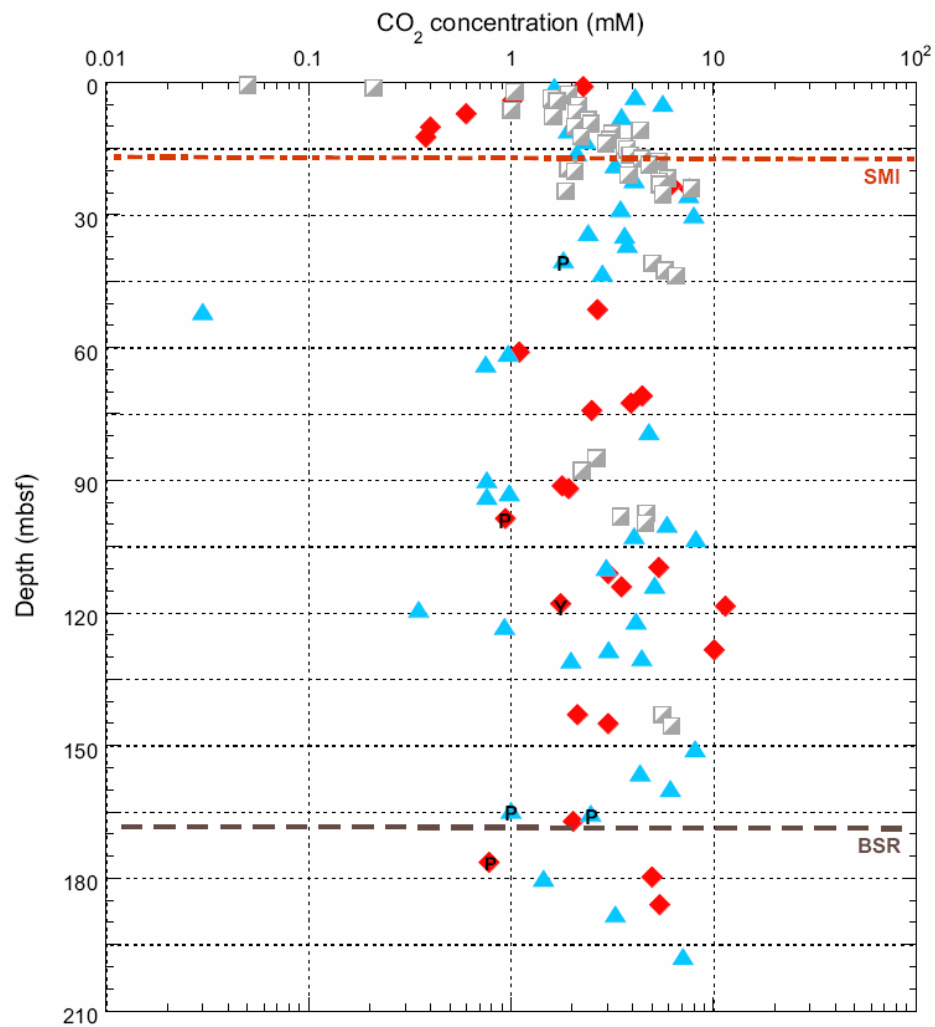


Fig. 4.39. Plot of headspace carbon dioxide gas concentration with depth at Site 10 (Collett et al., 2006). Note that Hole B = red; Hole D = blue. CO<sub>2</sub> concentration ranges from ~0.05 to 10 mM. CO<sub>2</sub> concentration throughout the sediment shows much scatter. Note that Gray = Site 12.



Five samples of ACR were recovered from Site 10 (Table 4.12). A piece of highly-cemented ACR-5 (Site 10) of 50 cm<sup>3</sup> in volume was collected from core# EXP01-10B-4X1 at a depth of 22.3 mbsf (Fig. 4.40a). The rock contains fine-grained calcite with few inclusions of organisms comprising the mud matrix (Fig. 4.41a).

Rocky nodules of ACR-6 (Site 10) were collected from core# EXP01-10B-6XCC at a depth of 31.4 mbsf (Fig. 4.40b). The rock contains coarse-grained calcite and aragonite with much pore space (Fig. 4.41b).

Smooth nodule carbonates of ACR-7 (Site 10) were collected from core# EXP01-10D-3H2 at a depth of 16 mbsf (Fig. 4.40c). The rock contains fine-grained calcite with a few inclusions of organisms and pyrite comprising the mud matrix (Fig. 4.41c).

Fine-grained (mud or clay sized) nodules of ACR-8 (Site 10) were collected from core# EXP01-10D-3H2 at a depth of 16.5 mbsf (Fig. 4.40d). The rock contains muddy calcite carbonate with inclusions of foraminifera and pyrite. Circular and chambered features are the sections of foraminifera (Fig. 4.41d).

A fine-grained (mud or clay size) nodule of ACR-9 (Site 10) was collected from core# EXP01-10D-7X2 at a depth of 43.2 mbsf (Fig. 4.40e). The rock contains only muddy calcite carbonate (Fig. 4.41e).

Table 4.12  
Isotopic composition of authigenic carbonate rock from Site 10

Sample#	Site	Hole	Sample depth (mbsf)	$\delta^{13}\text{C}$ (‰, PDB)	$\delta^{18}\text{O}$ (‰, PDB)
ACR-5	Site 10	B	22.3	-44.90	+2.77
ACR-6	Site 10	B	31.4	-44.30	+3.94
ACR-7	Site 10	D	16.2	-47.16	+4.00
ACR-8	Site 10	D	16.5	-49.12	+4.36
ACR-9	Site 10	D	43.2	-49.06	+3.13

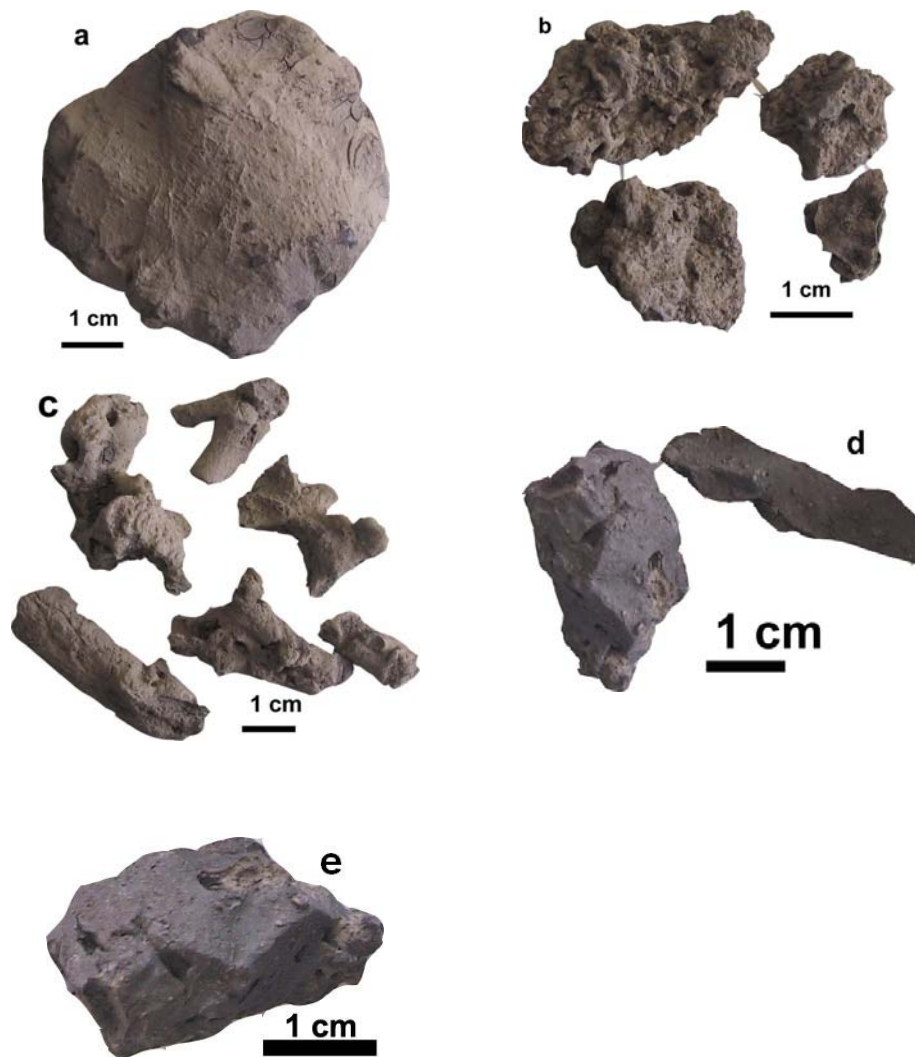


Fig. 4.40. Authigenic carbonate rock from Site 10 in the Krishna-Godawari basin offshore India. Note that (a) (ACR-5) is a piece of highly-cemented carbonate at a depth of 22.3 mbsf. (b) (ACR-6) is rocky nodules at a depth of 31.4 mbsf. (c) (ACR-7) is smooth nodule carbonates at a depth of 16.2 mbsf. (d) (ACR-8) is fine-grained (mud or clay sized) nodule carbonates at a depth of 16.5 mbsf. (e) (ACR-9) is a fine-grained (mud or clay size) nodule carbonate at a depth of 43.2 mbsf.

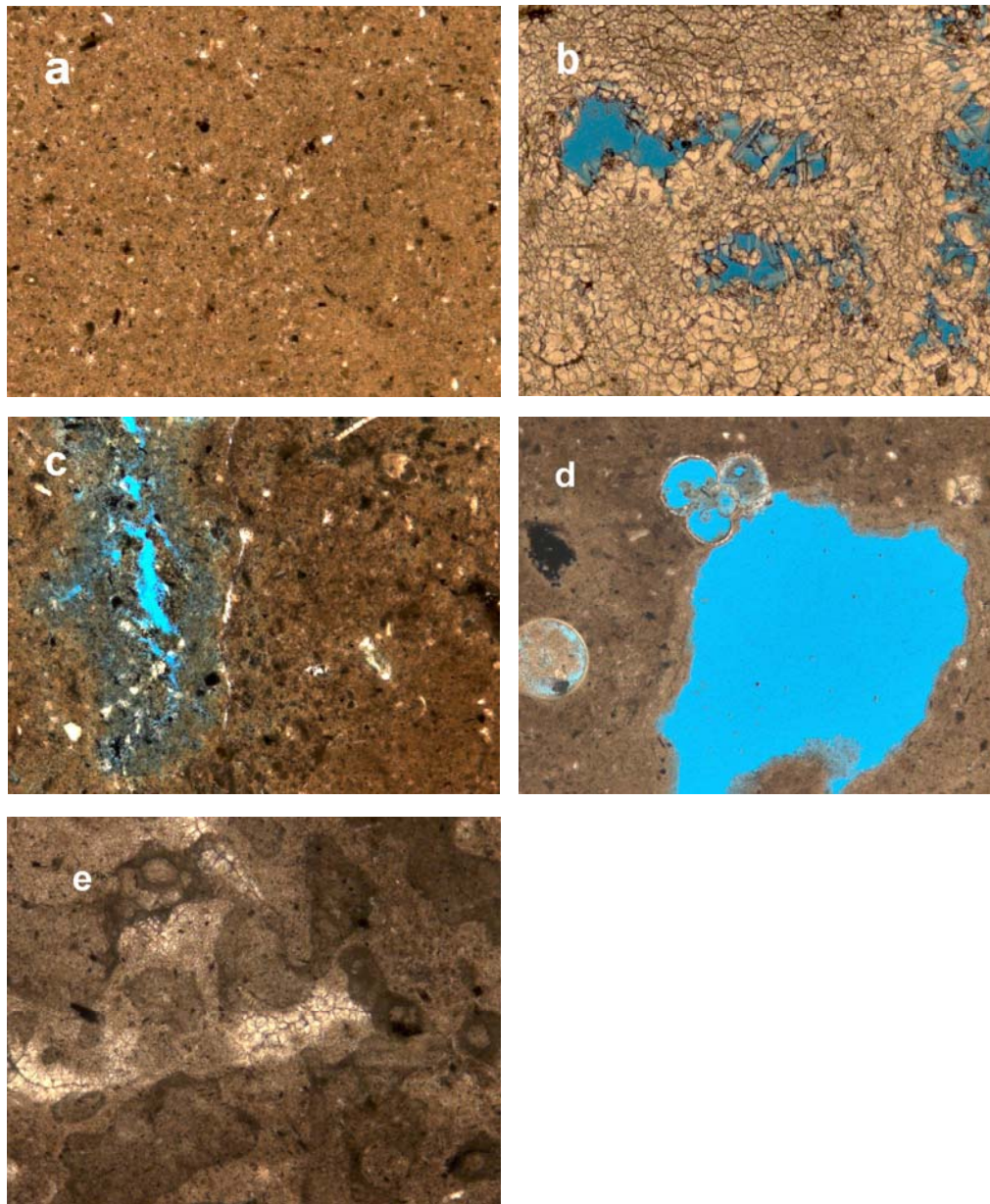


Fig. 4.41. Thin section images of ACR from Site 10 in Krishna-Godawari basin offshore India. Note that (a) (ACR-5) contains fine-grained calcite with few inclusions of organisms comprising the mud matrix. (b) (ACR-6) contains coarse-grained calcite and aragonite with pore spaces. (c) (ACR-7) contains fine-grained calcite with a few inclusions of organisms and pyrite comprising the mud matrix. (d) (ACR-8) contains muddy calcite carbonate with inclusions of foraminifera and pyrite. Circular and chambered features are the sections of foraminifera. (e) (ACR-9) contains only muddy calcite carbonate. Each image is ~8 mm across.

Bulk carbon and oxygen ( $\delta^{13}\text{C}$  and  $\delta^{18}\text{O}$ ) isotopes of five ACR samples from Site 10 were measured (Table 4.12). Five ACR samples are highly depleted in  $^{13}\text{C}$  with a range of  $-44.30$  to  $-49.12\text{‰}$  (mean  $\delta^{13}\text{C} = -46.9\text{‰}$ ).  $\delta^{18}\text{O}$  values are in a range of  $+2.77$  to  $+4.36\text{‰}$  (mean  $\delta^{18}\text{O} = +3.6\text{‰}$ ).

Based on petrographic thin section examination (Fig. 4.41), with  $\delta^{13}\text{C}$  values ranging  $-44.30$  to  $-49.12\text{‰}$ , carbonates are typical of methane ( $\delta^{13}\text{C} = -69\text{‰}$ , ONGC) derived authigenic carbonate rock. To examine and to quantify carbon sources to ACR, the percentage of methane oxidation in ACR was calculated to become depleted in  $^{13}\text{C}$  with a mean  $\delta^{13}\text{C}$  value of  $-46.9\text{‰}$ . Calculations of mass balance with water  $\delta^{13}\text{C}$  value of  $0\text{‰}$  SMOW show that ACR may have 68% methane oxidation and 32% normal marine carbonate carbon. The ACR samples contain tiny organisms (Figs. 4.41a and 4.41c), diagenetic calcite (Figs. 4.41b and 4.41e), and foraminifera (Fig. 4.41d). Petrographic thin sections suggest that approximately 70% methane oxidation likely contributed to ACR. Theoretically, some samples (ACR-5, ACR-6, and ACR-9) might have formed in the zone of methanogenesis because their sample depths are below the SMI, which is located at  $\sim 17.2$  mbsf at Site 10 (Fig. 4.37). However, oxidation of sedimentary organic matter has  $\delta^{13}\text{C}$  of  $\sim -20\text{‰}$  (Burns, 1998). The  $\delta^{13}\text{C}$  of DIC decreases from  $\sim 0\text{‰}$  at the seafloor to  $-20\text{‰}$  near SMI (Claypool and Kaplan, 1974; Mozley and Burns, 1993). Below SMI,  $^{12}\text{C}$  from  $\text{CO}_2$  preferentially gets fractionated into methane, and hence the DIC becomes enriched in  $^{13}\text{C}$  in the zone of methanogenesis. In addition,  $\text{CH}_4$  and  $\text{CO}_2$  concentrations throughout the sediment show much scatter (Figs. 4.37, 4.38 and 4.39). Therefore, ACR samples from Site 10 may be affected by mostly microbial methane oxidation instead of methanogenesis processes.

Bulk oxygen isotopes ( $\delta^{18}\text{O}$ ) of ACR samples recovered from Site 10 were also measured. ACR samples have  $\delta^{18}\text{O}$  values in a range of  $+2.77$  to  $+4.36\text{‰}$  (Table 4.12). The values are isotopically heavier than those of normal marine carbonate. The calculated temperatures of initial formation of ACR are in a range of  $-2.4$  to  $+2.4^\circ\text{C}$ , whereas measured temperatures at depths of ACR are in a range of  $+7.23$  to  $+8.44^\circ\text{C}$ . The wide difference of temperature range may be explained by the initial  $\delta^{18}\text{O}$  water of

ACR. Thus, the initial  $\delta^{18}\text{O}$  water values of ACR formation are in a range of +1.34 to +2.86‰ (Table 4.13). They were calculated with  $\delta^{18}\text{O}$  of +0.15‰ SMOW for Indian Ocean water.

At this site, several possibilities for isotopically heavy  $^{18}\text{O}$  include decomposition of gas hydrate (Hesse and Harrison, 1981; Ussler and Paull, 1995; Matsumoto and Borowski, 2000), mixing of isotopically heavy water migrated and moved from greater depth to seafloor venting (Fig. 4.33) (Morton et al., 1983; Morton and Land, 1987; Land and Macpherson, 1992), mixing of low temperature water invaded through a large scale faulting (Fig. 4.33), or mineral water interactions such as dissolution of  $^{18}\text{O}$  enriched minerals. The most likely explanation for isotopically heavy  $\delta^{18}\text{O}$  values is that the  $\delta^{18}\text{O}$  values may reflect the movement of isotopically heavier water than ambient seawater from greater depth.

Table 4.13  
Oxygen isotopic properties of authigenic carbonate rock from Site 10

Sample#	Sample depth (mbsf)	Measured $\delta^{18}\text{O}_{\text{ACR}}$ (‰, PDB)	Calculated temperature (°C)	Temperature at sample depth (°C)	Calculated $\delta^{18}\text{O}_{\text{water}}$ (‰, SMOW)
ACR-5	22.3	+2.77	+2.4	7.50	+1.34
ACR-6	31.4	+3.94	-2.4	7.91	+2.60
ACR-7	16.2	+4.00	-2.7	7.23	+2.50
ACR-8	16.5	+4.36	-4.1	7.24	+2.86
ACR-9	43.2	+3.13	+0.9	8.44	+1.91

#### Site 14 (NGHP-01-14, GDGH14-A)

Site 14 is located at 16° 31.28'N and 82° 40.86'E in the KG basin offshore India at a water depth of 896 m (Fig. 2.5). Seafloor temperature and geothermal gradient of Site 14 are 7.92°C and 3.9°C per 100 m, respectively. A BSR is observed at a depth of

~109 mbsf (Fig. 4.42). Stratigraphic layers are characterized by the typical sediment sequence of basin and ridge. Each ridge appears to be associated with a deep-rooted fault, with the basin sequence developed on the downthrown side of the fault toward the southeast. The basins are characterized by seafloor-parallel to subparallel sedimentary sequences, whereas the ridge flanks dip toward the northwest. Free gas is indicated below the BSR.

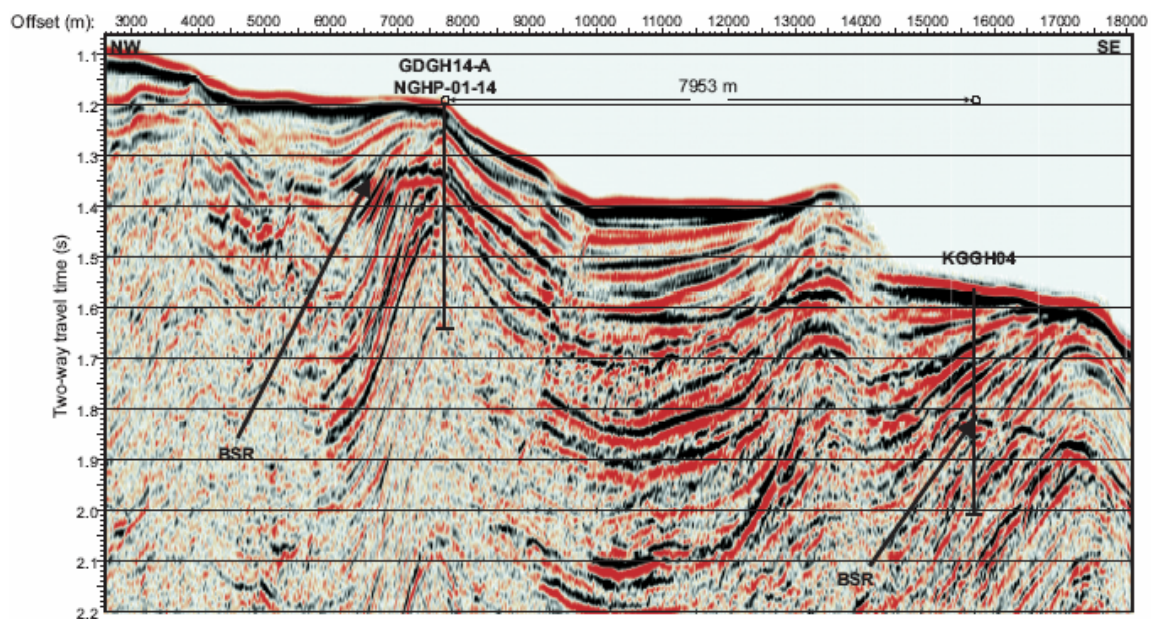


Fig. 4.42. Multichannel seismic reflection line across Site 14 (GDGH14-A) in the Krishna-Godawari basin (Collett et al., 2006). BSR is observed at a depth of ~109 mbsf. Stratigraphic layers are characterized by the typical sediment sequences of basin and ridge. Northwest is to left.

At Site 14, sediments range from Quaternary to recent in age. In the depth range of 0 to 180 mbsf, the major lithologies primarily comprise clay sized sediments with minor amounts of silt sized sediments and sand. Minor lithologies include silt-sand beds, authigenic carbonates, and iron sulfide rich sediments. The biogenic component of the sediment is dominated by calcareous nannofossils, whereas the nonbiogenic component

includes quartz, feldspar, mica, and clay. Foraminifera are common throughout the sediment. Terrestrial organic matter (Fig. 4.43) was observed throughout the sediment. Authigenic carbonate precipitates and woody debris were observed (Fig. 4.43). Dissociated gas hydrate was also observed in the sediment samples (Collett et al., 2006).

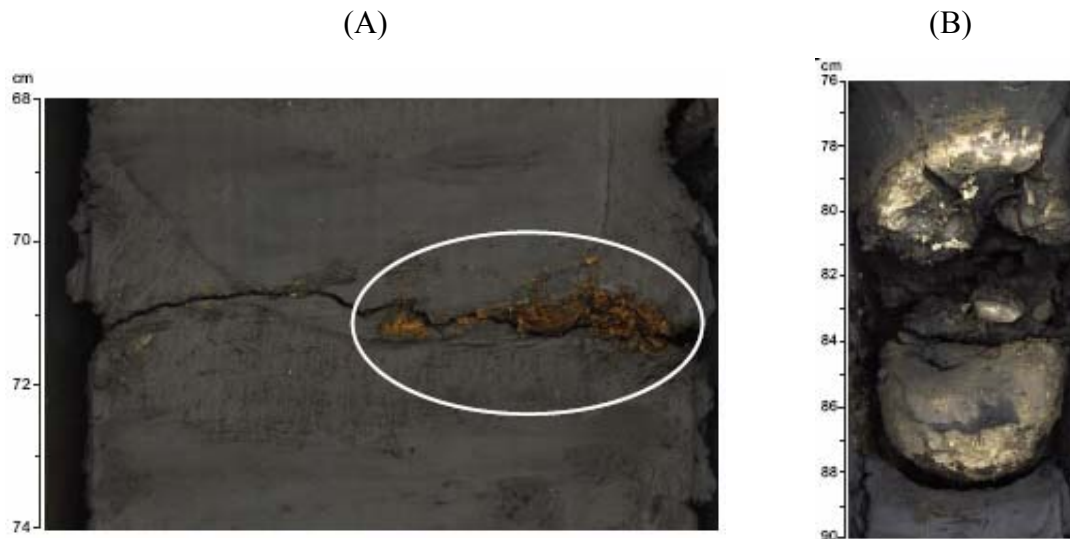


Fig. 4.43. Terrestrial organic matter (circled) and large broken authigenic carbonate rock from Site 14 (Collett et al., 2006). (A) Section NGHP-01-14A-04H6, 33 mbsf. (B) Section NGHP-01-14A-19X1, 140.4 mbsf. Vertical scale is in centimeters down core section.

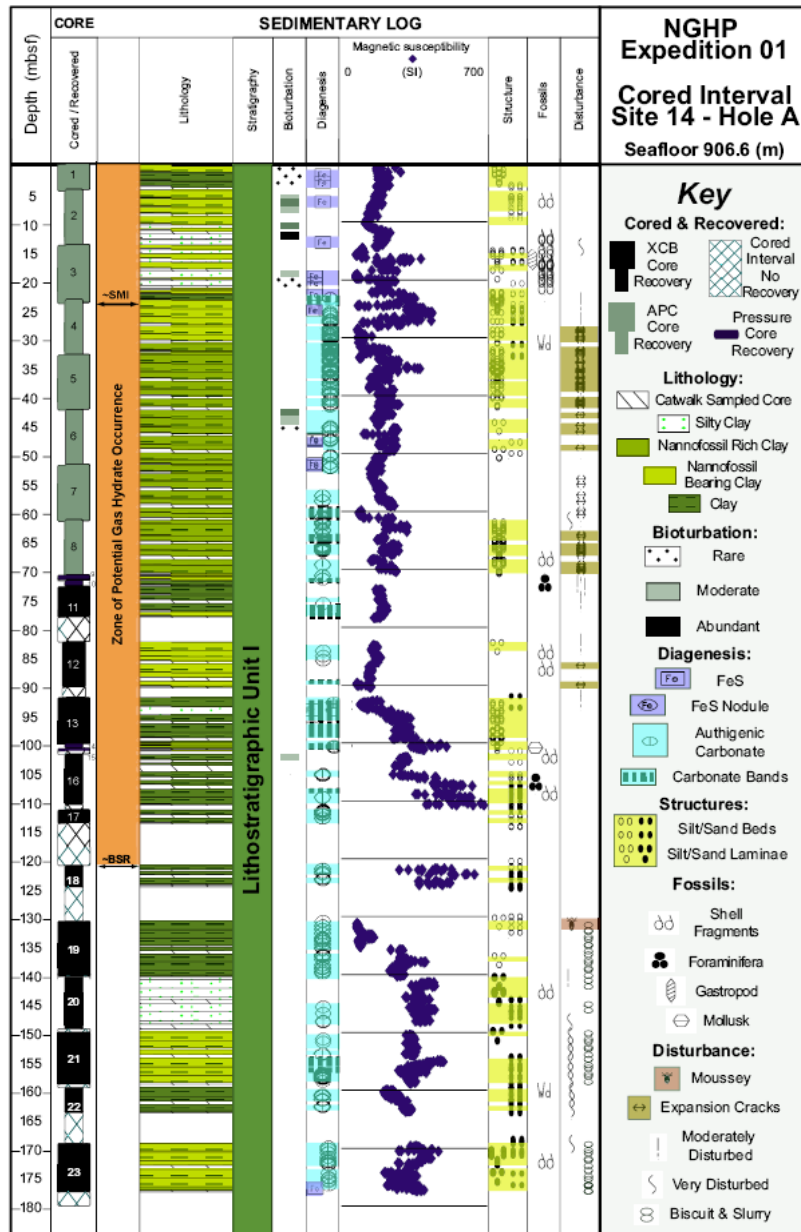


Fig. 4.44. Lithostratigraphic summary of Hole NGHP-01-14A (Collett et al., 2006).



The SMI is located at 23.4 mbsf (Fig. 4.45) at Site 14. Above the SMI, sulfate concentration decreases from the seafloor to 6 mbsf with a corresponding increase in alkalinity, reflecting sulfate reduction.

In the depth interval of 6 to 15.4 mbsf, sulfate concentration decreases with a coincident decrease in alkalinity, reflecting either authigenic carbonate precipitation or a change in the sedimentation rate within this interval. In the depth interval of ~15 to 23.4 mbsf, sulfate concentration also decreases with a concomitant linear increase in alkalinity to ~20 mM by the SMI. The decrease in sulfate and increase in alkalinity reflect anaerobic methane oxidation coupled to sulfate reduction. If authigenic carbonates precipitated, alkalinity would decrease within this interval, indicating the carbonate precipitation. Below the SMI, typically alkalinity concentration becomes progressively depleted to the depth of the BSR, whereas at this site it remains in relatively constant concentration (~25 mM) at the SMI to around the base of ~150 mbsf. This implies that the alkalinity is not depleted by the precipitation of carbonates at this site (Fig. 4.45).

Headspace CH<sub>4</sub> concentration increases step-wise from nondetectable to 0.4 mM at 23.4 mbsf, then to 5.2 mM at 27.6 mbsf, corresponding to SMI (Fig. 4.46). Below the SMI, CH<sub>4</sub> concentration gradually decreases to nearly 1 mM just below the BSR. CH<sub>4</sub> concentration increases 1 to 2 mM at ~40 mbsf below the SMI, which is likely to be associated with the presence of free gas in this interval.

Headspace CO<sub>2</sub> concentration ranges from 0.2 to 11.5 mM (Fig. 4.47). It also shows an increase from the seafloor through the SMI to ~60 mbsf, and gradually decreases with depth. Low concentrations are found above the SMI at depths ranging from 0 to 15 mbsf. Below the BSR, CO<sub>2</sub> concentration generally declines to less than 3 mM (Fig. 4.47).

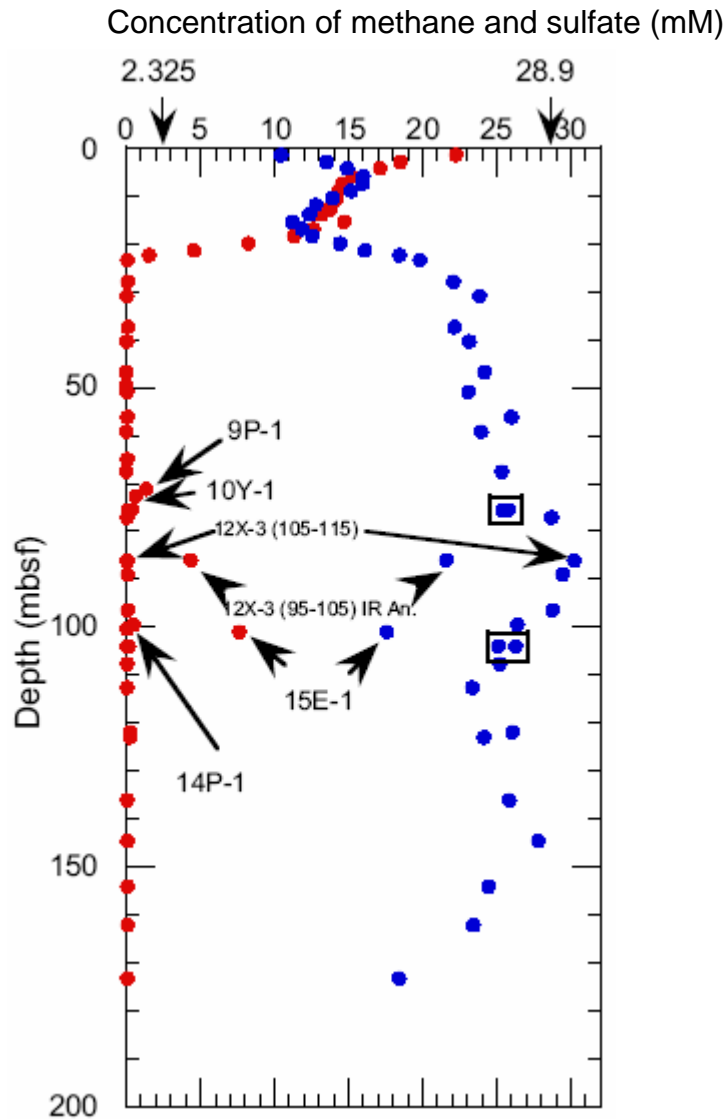


Fig. 4.45. Sulfate and alkalinity concentrations from Hole NGHP-01-14A (Collett et al., 2006). SMI is located at 23.4 mbsf. Above the SMI, sulfate concentration decreases from the seafloor to 6 mbsf with a corresponding increase in alkalinity concentration, reflecting sulfate reduction and alkalinity production in the zone of sedimentary organic matter oxidation. Below the SMI, typically alkalinity concentration becomes progressively depleted to the depth of the BSR, whereas at this site it remains relatively constant in concentration ( $\sim 25$  mM) at the SMI to around base of  $\sim 150$  mbsf. Note that solid red in circles represent sulfate concentrations and blue in circles represent alkalinity.

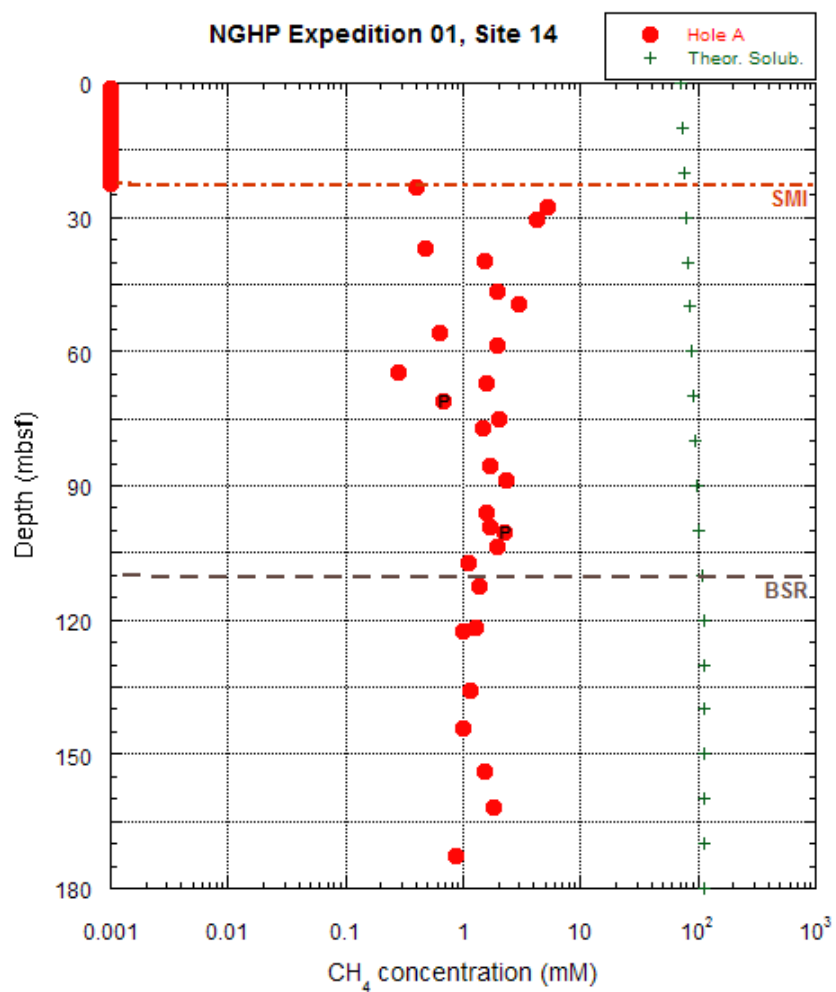


Fig. 4.46. Plot of headspace methane gas concentration with depth at Site 14, Hole A (Collett et al., 2006). CH<sub>4</sub> concentration increases step-wise from nondetectable to 0.4 mM at 23.4 mbsf, then to 5.2 mM at 27.6 mbsf, corresponding to SMI. Below the SMI, CH<sub>4</sub> concentration gradually decreases to nearly 1 mM just below the BSR. CH<sub>4</sub> concentration increases 1 to 2 mM at ~40 mbsf below the SMI, which is likely to be associated with the presence of free gas in this interval.

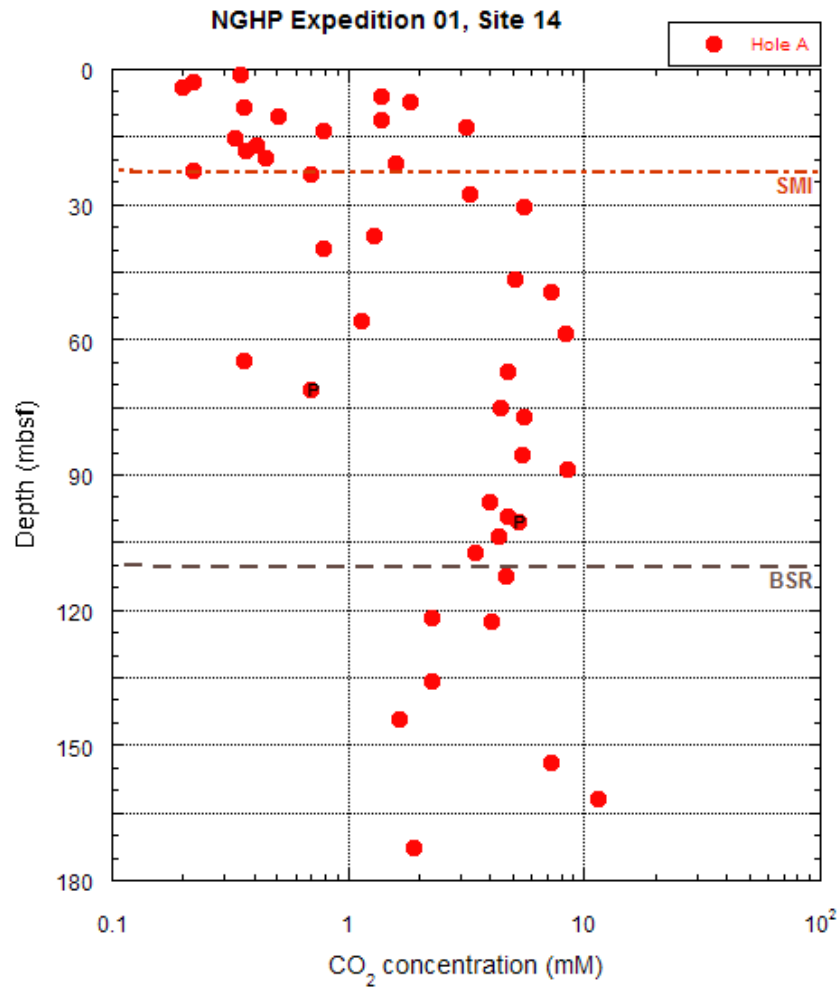


Fig. 4.47. Plot of headspace carbon dioxide gas concentration with depth at Site 14, Hole A (Collett et al., 2006). CO<sub>2</sub> concentration ranges from 0.2 to 11.5 mM. It also shows an increase from seafloor through the SMI to ~60 mbsf, and gradually decreases with depth. Low concentrations are found above the SMI at depths ranging from 0 to 15 mbsf. Below the BSR, CO<sub>2</sub> concentration generally declines to less than 3 mM.

A nodule of ACR-10 (Site 14) (Fig. 4.48) was collected from core# EXP01-16X6 at the depth of 109.5 mbsf (Table 4.14). The major lithologies primarily comprise of clay sized sediments with minor amounts of silt sized sediments and sand. ACR sample from Site 14 also contains sand.

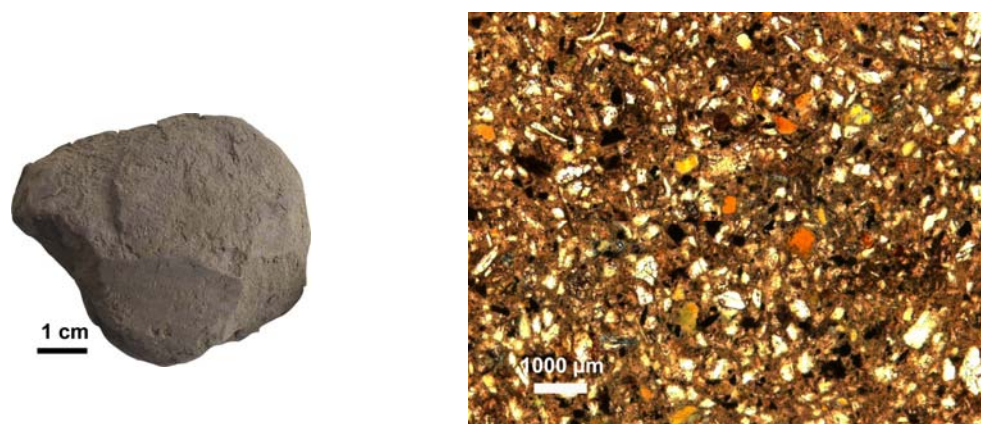


Fig. 4.48. Authigenic carbonate rock and thin section image of ACR-10 (Site 14) in Krishna-Godawari basin offshore India. The nodule was collected from sand-filled burrows. The thin section image includes fine-grained calcite mixed with fragments of carbonate skeletal material, woody debris, and sand.

Table 4.14  
Isotopic composition of ACR-10 (Site 14)

Sample#	Site	Hole	Sample depth (mbsf)	$\delta^{13}\text{C}$ (‰, PDB)	$\delta^{18}\text{O}$ (‰, PDB)
ACR-10	Site 14	A	109.5	-0.36	+1.27

Bulk carbon and oxygen ( $\delta^{13}\text{C}$  and  $\delta^{18}\text{O}$ ) isotopes of ACR-10 (Site 14) were measured. The  $\delta^{13}\text{C}$  and  $\delta^{18}\text{O}$  values are  $-0.36\text{‰}$  and  $+1.27\text{‰}$ , respectively (Table 4.14). ACR-10 (Site 14) may form in sediments with relatively low rates of organic carbon oxidation (Fig. 4.24). Possible explanations for low rates of organic carbon oxidation at

this site include that: (1) stratigraphic layers are characterized by the typical sediment sequences of the basin (Fig. 4.42), (2) the major lithologies include sand (Fig. 4.44), (3) the zone of sulfate reduction is relatively deeper, (4) alkalinity concentration gradually increases from the seafloor with a corresponding decrease in sulfate concentration in general (Fig. 4.45), (5) below the SMI, headspace CH<sub>4</sub> concentration gradually decreases to nearly 1 mM just below the BSR (Fig. 4.46), and (6) headspace CO<sub>2</sub> concentration gradually decreases with depth below SMI (Fig. 4.47). Therefore, based on earlier observations, the  $\delta^{13}\text{C}$  of  $-0.36\text{‰}$  of ACR-10 (Site 14) may reflect low rates of organic carbon oxidation in the zone of methanogenesis. The methanogenesis may not be enough to generate isotopically heavy  $\delta^{13}\text{C}$  in the pore waters (Fig. 4.24).

The bulk oxygen isotope ( $\delta^{18}\text{O}$ ) of ACR-10 (Site 14) is  $+1.27\text{‰}$  (Table 4.14), which allowed calculation of the initial temperature ( $+8.9^\circ\text{C}$ ) of the carbonate formation. However, that does not correspond to the measured temperature ( $+11.97^\circ\text{C}$ ) at the depth of ACR-10 (Site 14). Thus, ACR-10 (Site 14) formed in the isotopically heavy water. To examine the hypothesis, initial formation  $\delta^{18}\text{O}$  value of ACR-10 (Site 14) was calculated. Calculations of the initial formation  $\delta^{18}\text{O}$  value in water with  $+0.15\text{‰}$  SMOW for Indian Ocean water resulted in  $+0.85\text{‰}$  SMOW (Table 4.15). The initial formation  $\delta^{18}\text{O}$  of ACR-10 (Site 14) is close to  $\delta^{18}\text{O}$  of ambient seawater. Therefore, the dissolution of marine carbonate primarily may affect  $\delta^{18}\text{O}$  value of ACR-10 (Site 14).

Table 4.15  
Oxygen isotopic properties of carbonate rock from Site 14

Sample depth (mbsf)	Measured $\delta^{18}\text{O}_{\text{ACR}}$ (‰, PDB)	Calculated temperature ( $^\circ\text{C}$ )	Temperature at sample depth ( $^\circ\text{C}$ )	Calculated $\delta^{18}\text{O}_{\text{water}}$ (‰, SMOW)
109.5	+1.27	8.9	11.97	+0.85

## CHAPTER V

## DISCUSSION

## Gulf of Mexico

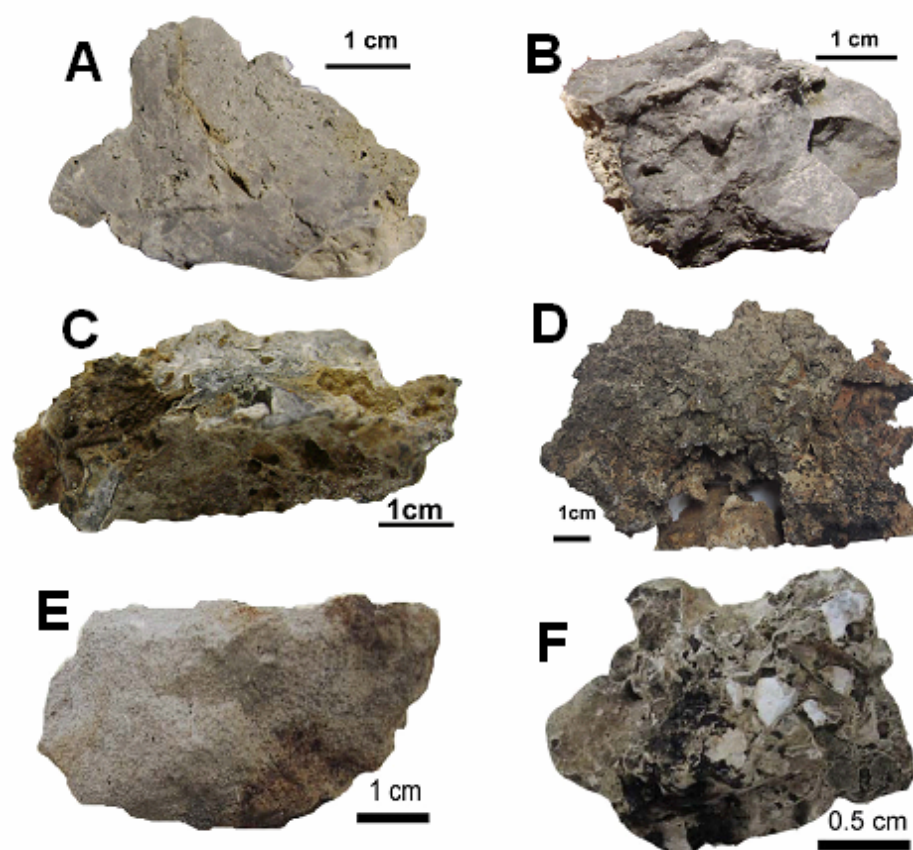


Fig. 5.1. Authigenic carbonate rock from the Gulf of Mexico. Note that A = ACR-1 and B = ACR-2 from MC 118, C = ACR-3 and D = ACR-4 from VN 945, E = ACR-5 from EL 711, and F = ACR-6 from AT 425.

Six samples (Fig. 5.1) of authigenic carbonate rock (ACR) collected from 30 cm push cores at the seafloor in the Gulf of Mexico (GOM) were characterized petrographically, mineralogically, and geochemically. The samples are gray to light brown in color but often coated by dark brown, exhibiting extremely irregular shapes. ACR collected from the seafloor in the GOM are generally densely cemented (A, B, C, D, and F in Fig. 5.1), whereas ACR-5 (EL 711) (Fig. 5.1E) is highly unusual because it is friable and exhibits extremely high micro-porosity and concomitantly low density. ACR-5 (EL 711) contains many foraminifera and other planktonic organisms with few inclusions of carbonate skeletal materials. The foraminifera and other planktonic organisms with skeletal carbonate are bound together and cemented by fine-grained authigenic calcite (Fig. 5.2E). In this study, the dominant authigenic mineral of ACR is fine-grained calcite. Aragonite, dolomite, pyrite, barite, quartz, and mica are also identified.

Two samples of ACR-1 (MC 118) (Fig. 5.2A) and ACR-2 (MC 118) (Fig. 5.2B) are densely cemented and homogeneous in the matrix. ACR-1 (MC 118) is completely cemented by almost totally fine-grained calcite with inclusions of pyrite, whereas ACR-2 (MC 118) contains fine-grained calcite and aragonite with the inclusions of shell fragments and debris (Figs. 5.2A and 5.2B). Both samples contain oil stains. Two samples of ACR-3 (VN 945) (Fig. 5.2C) and ACR-4 (VN 945) (Fig. 5.2D) are also densely cemented and extremely irregular in shape. ACR-3 (VN 945) contains normal marine carbonate without evidence of oil stain, whereas ACR-4 (VN 945) contains fragments of chemosynthetic mussels and other carbonate skeletal remains with visible oil stain (Figs. 5.2C and 5.2D). ACR-6 (AT 425) (Fig. 5.2F) is a densely cemented oil-stained cobble. It consists almost totally of fine-grained calcite with few inclusions of carbonate skeletal material (Fig. 5.2F).



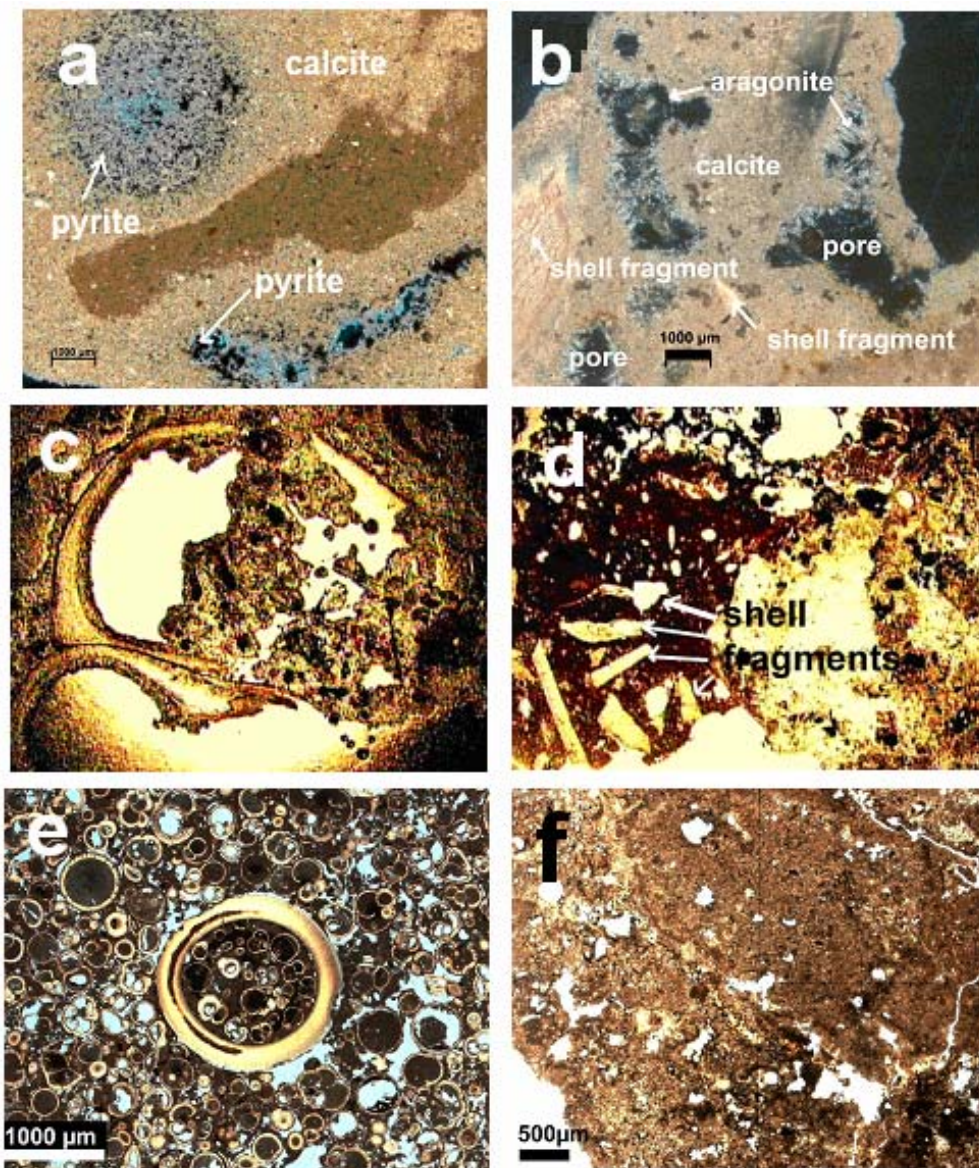


Fig. 5.2. Petrographic thin section images of authigenic carbonate rock from the Gulf of Mexico. Note that (a) and (b) are ACR-1 and ACR-2 from MC 118, respectively. (c) and (d) are ACR-3 and ACR-4 from VN 945, respectively. (e) is ACR-5 from EL 711. (f) is ACR-6 from AT 425.

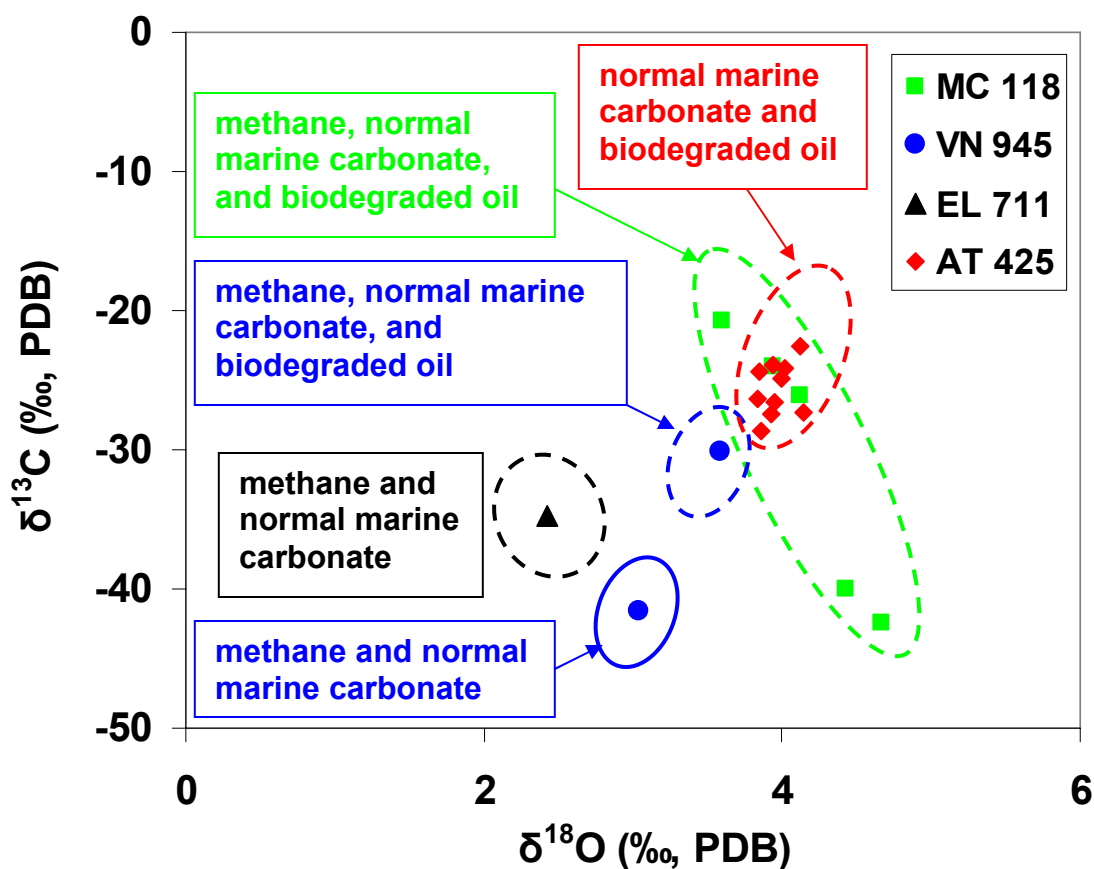


Fig. 5.3. Plot of  $\delta^{13}\text{C}$  versus  $\delta^{18}\text{O}$  of ACR from the Gulf of Mexico. This plot of  $\delta^{13}\text{C}$  versus  $\delta^{18}\text{O}$  allows us to compare isotopic properties and carbon sources of selected samples of ACR from adjacent sites in the deep water, Gulf of Mexico slope. The main source of ACR is either microbial  $\text{CH}_4$  or thermogenic hydrocarbon in the subsurface sediments.

Carbon isotopes reflect carbon sources, whereas oxygen isotopes reflect the formation temperature and the isotopic composition of source water (Friedman and O'Neil, 1977; Bohrmann et al., 1998; Greinert et al., 2001). Carbon and oxygen isotopes ( $\delta^{13}\text{C}$  and  $\delta^{18}\text{O}$ ) are widely used to distinguish between normal marine carbonate and authigenic carbonate rock derived from methane and other hydrocarbons. Large fractionations of carbon isotopes occur between carbon reservoirs during organic carbon

reminereralization (Friedman and O'Neil, 1977) with depth-related changes in the isotopic composition of dissolved inorganic carbon (DIC) (Mozley and Burns, 1993; Burns, 1998).

In this study, bulk  $\delta^{13}\text{C}$  and  $\delta^{18}\text{O}$  of ACR were measured. Measured  $\delta^{13}\text{C}$  and  $\delta^{18}\text{O}$  values of ACR are different from those of normal marine carbonates. ACR is strongly depleted in  $^{13}\text{C}$  down to  $\delta^{13}\text{C}$  of  $-42.5\text{‰}$  (up to  $-20.68\text{‰}$ ) and isotopically heavy in  $^{18}\text{O}$  up to  $\delta^{18}\text{O}$  of  $+4.67\text{‰}$  (down to  $+2.43\text{‰}$ ). ACR is derived from the microbial oxidation of methane and other hydrocarbons, which is strongly depleted in  $^{13}\text{C}$ . Therefore, if methane was the primary source of carbon to ACR, one would expect it also to be highly depleted in  $^{13}\text{C}$ . However, the  $\delta^{13}\text{C}$  values of ACR rarely correspond to those of methane or other hydrocarbons. In general, ACR is enriched in  $^{13}\text{C}$  when compared to hydrocarbon sources. Various carbon sources may affect the bulk  $\delta^{13}\text{C}$  values of ACR.

It was suggested that hydrocarbon carbon sources to ACR based on molecular and isotopic composition of vent gas or gas hydrate samples from different geological environments for ACR formation. It was hypothesized that the  $\delta^{13}\text{C}$  of ACR depleted or enriched in  $^{13}\text{C}$  reflects primarily (1) microbial oxidation of methane (2) normal marine carbonate or (3) microbial oxidation of biodegraded oil. From these, it was proposed that carbon sources to ACR were based on different isotopic values, corresponding carbonate phases, mineral compositions, and distribution of normal marine carbonates. Three groups that represent different hydrocarbon sources to ACR may be classified in this study: (1) methane and biodegraded oil, (2) methane, or (3) biodegraded oil (Fig. 5.3).

Three samples of ACR-1 (MC 118), ACR-2 (MC 118), and ACR-4 (VN 945) were derived from oxidation of methane, oxidation of biodegraded oil, and normal marine carbonate. All of the ACR samples are highly depleted in  $^{13}\text{C}$ . It was assumed that methane from vent gas was the primary source of carbon to ACR, and then one expected it to be also highly depleted in  $^{13}\text{C}$ . However, the  $\delta^{13}\text{C}$  of ACR does not closely correspond to that of the methane. ACR samples are enriched in  $^{13}\text{C}$  when compared to the methane, which is highly depleted in  $^{13}\text{C}$ . The enrichment in  $^{13}\text{C}$  of ACR is better

understood by study of petrographic thin section images. Thin sections show that several different carbon sources may affect the bulk carbon isotopes of ACR. Based on isotope values, carbonate phases, and mineral compositions, each carbon source was quantified using the mass balance equation and a point count technique in the thin section image. From these, it was proposed that the  $\delta^{13}\text{C}$  enriched in  $^{13}\text{C}$  is affected by isotopically heavy carbon derived from the oxidation of biodegraded oil.

Microbial methane oxidation may be the primary carbon source to ACR samples of ACR-3 (VN 945) and ACR-5 (EL 711). The  $\delta^{13}\text{C}$  values of ACR are highly depleted in  $^{13}\text{C}$ . ACR may be derived from the microbial oxidation of methane, which is strongly depleted in  $^{13}\text{C}$ . The percentage of normal marine carbonate in ACR was calculated to become depleted in  $^{13}\text{C}$ . Each carbon source to ACR was examined and quantified using the mass balance equation and a point count technique in the thin section images. The  $\delta^{13}\text{C}$  of microbial methane from vent gas was used to calculate the percentage of normal marine carbonate added to ACR for the mass balance equation. The result of the mass balance calculation was consistent with that of a point count analysis.

The oxidation of biodegraded oil may be the primary carbon source to ACR-6 (AT 425). In an oil-stained cobble of ACR-6 (AT 425), bulk  $\delta^{13}\text{C}$  values of ACR are in the range of  $-22.6$  to  $-28.6\text{‰}$  (Table 4.6). The mean  $\delta^{13}\text{C}$  value is  $-25.6\text{‰}$ . If thermogenic methane (mean  $\delta^{13}\text{C} = -48.8\text{‰}$  from gas hydrate, Sassen et al., 2001d) was the primary source of carbon to ACR, it should have been highly depleted in  $^{13}\text{C}$ . However, the rock was enriched in  $^{13}\text{C}$  when compared to thermogenic methane, which is highly depleted in  $^{13}\text{C}$ . Another hydrocarbon source from the oxidation of biodegraded crude oil was assumed. The  $\delta^{13}\text{C}$  of oil oxidation was in the range of  $-22.6$  to  $-28.6\text{‰}$  (mean =  $-25.6\text{‰}$ ). In addition, petrographic thin section images (Fig. 4.15) were analyzed. Petrographic thin sections show that ACR-6 (AT 425) contains almost totally fine-grained calcite with few inclusions of carbonate skeletal material. Based on those observations, it was proposed that the  $\delta^{13}\text{C}$  reflects the oxidation of biodegraded crude oil. Biodegradation is a common process in deep subsurface reservoirs of the Gulf of

Mexcio (Philippi, 1977). Carbonate isotopic properties of ACR-6 (AT 425) are similar to those of abundant biodegraded crude oil that stains the rock.

Bulk  $\delta^{18}\text{O}$  values of ACR are in the range of +2.43 to +4.67‰ (mean  $\delta^{18}\text{O} = +3.43\%$ ). The  $\delta^{18}\text{O}$  values are isotopically heavier than those of normal marine carbonates. Mozley and Burns (1993) reviewed  $\delta^{13}\text{C}$  and  $\delta^{18}\text{O}$  values for marine calcite, siderite, and dolomite from a large number of previous studies. From their review for marine calcite,  $\delta^{18}\text{O}$  is in the range of -10 to 0‰. Why are ACR samples so enriched in  $^{18}\text{O}$  with a mean  $\delta^{18}\text{O}$  of +3.43‰? Isotopically heavy values of  $\delta^{18}\text{O}$  from ACR were discussed. In this study, three likely hypotheses address the isotopically heavy  $\delta^{18}\text{O}$  values: (1) they reflect the temperature of initial formation of ACR, (2) they reflect isotopically heavy  $\delta^{18}\text{O}$  values from gas hydrate decomposition or (3) they reflect the movement of isotopically heavier water than ambient seawater from greater depth. Each hypothesis was discussed separately for the most reasonable explanation.

First, if measured  $\delta^{18}\text{O}$  values may reflect the temperature of initial formation of ACR. To calculate the temperature, the measured  $\delta^{18}\text{O}$  value in PDB to the value in SMOW was converted using the relation of  $\delta^{18}\text{O}_{\text{SMOW}} = 1.03086 \delta^{18}\text{O}_{\text{PDB}} + 30.86$  (Friedman and O'Neil, 1977). Then, using an equilibrium oxygen isotope equation (Kim and O'Neil, 1997) of  $1000 \times \ln(\alpha) = 18.03 \times (10^3 \text{ T}^{-1}) - 32.42$ , the temperature (APPENDIX A) was calculated. In general, the calculated temperatures were unrealistic, below zero Celsius. Therefore, the first hypothesis was eliminated. Then,  $\delta^{18}\text{O}$  of water in SMOW was calculated using the measured  $\delta^{18}\text{O}$  value and temperature of ACR and the equation of Kim and O'Neil (1997) to support the second hypothesis (APPENDIX A). For the calculations,  $\delta^{18}\text{O}$  value of +0.2‰ SMOW was used for seawater in the GOM (<http://data.giss.nasa.gov/o18data>; GEOSSECS Grossman and Ku, 1986) at a nearest location to the study site. Based on the calculation, it was proposed that ACR may form in heavier water.

As discussed in Chapter I, gas hydrate formation preferentially favors  $^{18}\text{O}$ , it makes the residual water  $^{16}\text{O}$  enriched (Hesse and Harrison, 1981; Ussler and Paull, 1995; Matsumoto and Borowski, 2000). Thus, water within gas hydrates is enriched in heavy oxygen ( $^{18}\text{O}$ ) relative to ambient waters. Hence, gas hydrate decomposition enriches  $^{18}\text{O}$  in residual water. Although gas hydrate water may cause an isotopically heavy  $\delta^{18}\text{O}$  value, the second hypothesis was eliminated because gas hydrate water would not cause significantly heavy oxygen isotopes (Matsumoto and Borowski, 2000; Greinert et al., 2001; Sassen and Roberts, 2004). To eliminate the second hypothesis, two examples of isotopically heavy  $\delta^{18}\text{O}$  values from gas hydrate water were provided. As discussed in Chapter I, the magnitude of the isotopically heavier values of  $\delta^{18}\text{O}$  was 0.3 to 0.6‰ SMOW at Blake Ridge Site 997 (Matsumoto and Borowski, 2000), and 0.86‰ SMOW at Hydrate Ridge (Greinert et al., 2001).

As the most likely explanation, the third hypothesis proposed that isotopically heavy  $\delta^{18}\text{O}$  values reflect the movement of isotopically heavier water than ambient seawater from greater depth. Observations consistent with the third hypothesis include (1) fractures and faults provide conduits for fluid penetration upward to the seafloor and (2) the range of  $\delta^{18}\text{O}$  values of water produced from Cenozoic hydrocarbon reservoirs in the Gulf of Mexico sedimentary basin is derived from dewatering of clastic sediments (Morton et al., 1983; Morton and Land, 1987; Land and Macpherson, 1992). Isotopic composition of ACR from the GOM is summarized in Table 5.1.

Table 5.1  
Isotopic composition of authigenic carbonate rock from the Gulf of Mexico

Measured (n)	ACR sample# from Table 3.1	$\delta^{13}\text{C}$ (‰, PDB)	$\delta^{18}\text{O}$ (‰, PDB)
MC 118-1	ACR-1	-39.96	+4.42
MC 118-2	ACR-1	-42.50	+4.67
MC 118-3	ACR-2	-24.07	+3.94
MC 118-4	ACR-2	-26.06	+4.12
MC 118-5	ACR-2	-20.68	+3.60
VN 945-1	ACR-3	-41.63	+3.04
VN 945-2	ACR-4	-30.11	+3.59
EL 711-1	ACR-5	-34.78	+2.43
AT 425-1	ACR-6	-24.34	+3.85
AT 425-2	ACR-6	-28.62	+3.86
AT 425-3	ACR-6	-26.31	+3.84
AT 425-4	ACR-6	-27.35	+4.14
AT 425-5	ACR-6	-27.43	+3.93
AT 425-6	ACR-6	-26.60	+3.95
AT 425-7	ACR-6	-24.13	+4.02
AT 425-8	ACR-6	-23.88	+3.94
AT 425-9	ACR-6	-22.55	+4.12
AT 425-10	ACR-6	-24.93	+4.00

## Offshore India

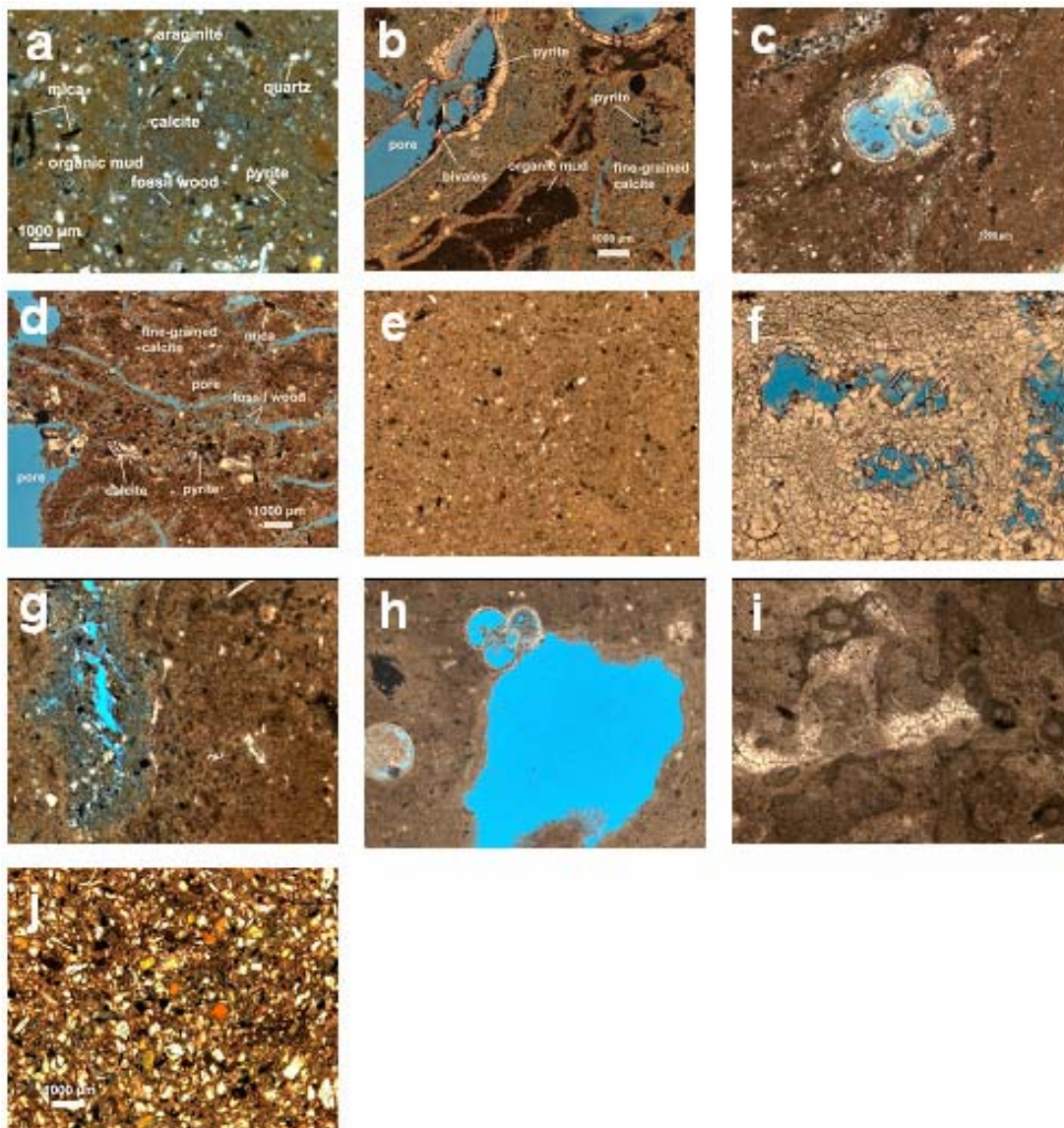


Fig. 5.4. Petrographic thin section images of authigenic carbonate rock from the Krishna-Godavari basin offshore India. Note that (a) is ACR-1 from Site 3, (b) through (d) are ACR-2, ACR-3, and ACR-4 from Site 5, respectively, (e) through (i) are ACR-5 through ACR-9 from Site 10, respectively, and (j) is ACR-10 from Site 14.



Ten samples of authigenic carbonate rock (ACR) collected from drilled cores in the Krishna-Godawari (KG) basin offshore India were characterized petrographically, mineralogically, and geochemically. ACR collected from the seafloor or chemosynthetic communities in the Gulf of Mexico (GOM) is densely cemented and extremely irregular in shape, whereas ACR recovered from the KG basin offshore India is generally highly cemented oval-shaped nodules.

The oval-shaped nodule of ACR-1 (Site 3) contains fine-grained calcite with a few inclusions of carbonate skeletal material and fossil wood fragments (Figs 4.23 and 5.4). Three samples of ACR-2, ACR-3, and ACR-4 from Site 5 are also oval-shaped smooth nodules. ACR from Site 5 contains fine-grained calcite with inclusions of massive bivalves comprising a carbonate and organic mud matrix with pore spaces or foraminifera and terrigenous organic matter such as fossil wood (Figs. 4.32 and 5.4). Five samples of ACR-5 through ACR-9 from Site 10 are highly cemented and irregularly shaped rocky nodules. They generally contain fine-grained calcite with few inclusions of pyrite and organisms comprising the mud matrix (Figs. 4.40 and 5.4). ACR-10 (Site 14) is a smooth nodule and contains fine-grained calcite mixed with fragments of carbonate skeletal material, woody debris, and sand (Figs. 4.48 and 5.4).

Measured  $\delta^{13}\text{C}$  and  $\delta^{18}\text{O}$  values of ACR from the KG basin offshore India are different from those of normal marine carbonates. The  $\delta^{13}\text{C}$  and  $\delta^{18}\text{O}$  values range up to +14.06‰ and +4.99‰, respectively, and down to -49.12‰ and +1.27‰, respectively (Table 5.2). ACR formation on the seafloor in the GOM may be controlled mainly by hydrocarbon influx and microbial processes (sulfate reduction and hydrocarbon oxidation), whereas ACR from the KG basin offshore India may form in different geochemical environments. In marine sediments, sedimentary organic matter may produce  $\text{CO}_2$  in the zone of sulfate reduction and also produce  $\text{CH}_4$  in the zone of methanogenesis (Burns, 1998; Paull et al., 2000). Those microbial processes result in organic carbon remineralization accompanied by large fractionations of carbon isotopes between carbon reservoirs. The fractionations of carbon isotopes may be controlled by a flux of methane (Borowski et al., 1996), the rate of organic carbon oxidation, or

sedimentation rate, leading to depth-related differences in the mineralogy and carbon isotopes (Mozley and Burns, 1993).

Based on the wide range in  $\delta^{13}\text{C}$  and different geochemical environments, the ten samples of ACR recovered from offshore India may be classified into five groups from A to E (Fig. 5.5) as follows.

Group A: ACR-1 (Site 3) and ACR-3 (Site 5)

Group B: ACR-2 (Site 5)

Group C: ACR-4 (Site 5)

Group D: ACR-5 through ACR-9 (Site 10)

Group E: ACR-10 (Site 14)

In Group A, the  $\delta^{13}\text{C}$  of ACR may reflect high rates of organic carbon oxidation from highly sedimentary organic matter in the zone of methanogenesis. ACR-1 (Site 3) and ACR-3 (Site 5) are highly enriched in  $^{13}\text{C}$  with  $\delta^{13}\text{C}$  values of +10.95‰ and +14.06‰, respectively. Sedimentary organic matter in marine sediments produces  $\text{CH}_4$  and  $\text{CO}_2$  (Burns, 1998; Paull et al., 2000). Oxidation of sedimentary organic matter has  $\delta^{13}\text{C}$  of  $\sim -20$ ‰ (Burns, 1998). During organic carbon remineralization, large fractionations of carbon isotopes occur between carbon reservoirs with depth-related changes in the isotopic composition of dissolved inorganic carbon (DIC) (Fig. 4.24). The  $\delta^{13}\text{C}$  of DIC decreases from  $\sim 0$ ‰ at the seafloor to  $-20$ ‰ near SMI (Claypool and Kaplan, 1974; Mozley and Burns, 1993). Below SMI,  $^{12}\text{C}$  from  $\text{CO}_2$  preferentially gets fractionated into methane and hence the DIC becomes enriched in  $^{13}\text{C}$  in the zone of methanogenesis. At these sites, in sediments with relatively high rates of organic carbon oxidation, the zone of methanogenesis is found at a shallow depth (Figs. 4.20 and 4.28).  $\text{CH}_4$  and  $\text{CO}_2$  concentrations (Figs. 4.21 and 4.22) for high rates of organic carbon oxidation at those sites were checked. The SMIs are located at shallow depths of  $\sim 12$  mbsf at Site 3 and  $\sim 24$  mbsf at Site 5 (Figs. 4.20 and 4.28). Sulfate is totally depleted by SMI, and then methanogenesis begins into the sediments. Thus,  $\text{CH}_4$  concentration

rapidly increases just below SMI, and it shows the highest value around the depth of ACR (Figs. 4.21 and 4.29). Concomitantly, CO<sub>2</sub> concentration shows low concentration at depth (Figs. 4.22 and 4.30). Based on this observation, it was proposed that the high rates of organic carbon oxidation during methanogenesis occur below SMI. It was assumed that the methanogenesis may be enough to cause isotopically heavy  $\delta^{13}\text{C}$  values at those sites.

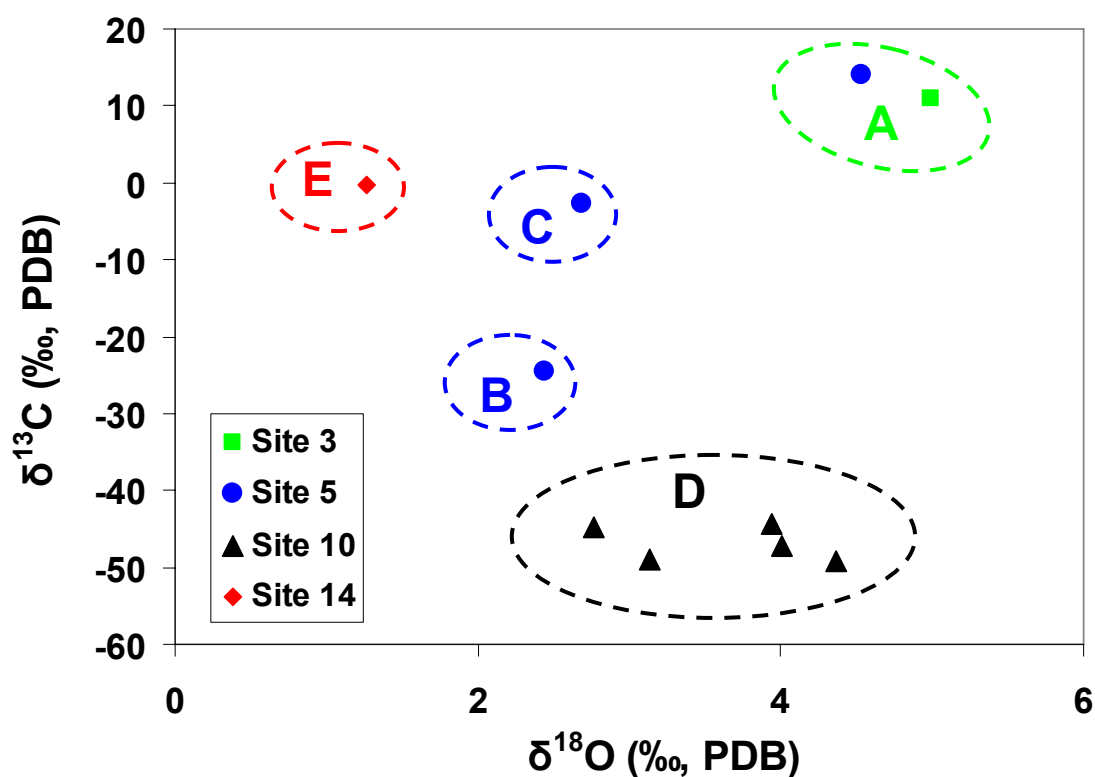


Fig. 5.5. Plot of  $\delta^{13}\text{C}$  versus  $\delta^{18}\text{O}$  of authigenic carbonate rock from the Krishna-Godawari basin offshore India. This plot of  $\delta^{13}\text{C}$  versus  $\delta^{18}\text{O}$  allows us to compare the isotopic properties of selected samples of ACR from adjacent sites in the KG basin offshore India.

The  $\delta^{13}\text{C}$  of ACR-2 (Site 5) in Group B is highly depleted in  $^{13}\text{C}$ . This site is characterized by microbial methane extremely depleted in  $^{13}\text{C}$  ( $\delta^{13}\text{C} = -69\text{‰}$ , ONGC). The SMI is located at  $\sim 24$  mbsf (Fig. 4.28) at the site, which is close to a sample depth of 37.1 mbsf. Although it was estimated that ACR-2 (Site 5) formed in the zone of methanogenesis, which means very rare or no methane oxidation, it was checked if methane was the primary carbon source to ACR-2 (Site 5). However, this hypothesis was eliminated because of lack of normal marine carbonate (Fig. 4.32). It was proposed that the  $\delta^{13}\text{C}$  of ACR-2 (Site 5) reflects organic carbon oxidation from sedimentary organic matter in the zone of methanogenesis. Although the ACR-2 (Site 5) formed below the SMI is within the zone of methanogenesis,  $\delta^{13}\text{C}$  may not be affected by methanogenesis processes. It was estimated that the methanogenesis may either not occur at all or not ever be enough to generate isotopically heavy carbon isotopes in pore waters at the depth of ACR-2 (Site 5) (Mozley and Burns, 1993). Based on the observation for ACR-2 (Site 5) and ACR-3 (Site 5), the  $\delta^{13}\text{C}$  ( $-2.8\text{‰}$ ) of ACR-4 (Site 5) in Group C may reflect the carbon source from pore waters below methanogenesis (i.g., decarboxylation process) (Fig. 4.24).

In Group D, five samples of ACR from Site 10 (ACR-5 through ACR-9) are typical of methane ( $\delta^{13}\text{C} = -69\text{‰}$ , ONGC) derived authigenic carbonate rock. ACR from Site 10 is highly depleted in  $^{13}\text{C}$  with a range of  $-44.30$  to  $-49.12\text{‰}$  (mean  $\delta^{13}\text{C} = -46.9\text{‰}$ ). The percentage of methane oxidation in ACR was calculated to become depleted in  $^{13}\text{C}$  with a mean  $\delta^{13}\text{C}$  value of  $-46.9\text{‰}$ . The calculation of mass balance with water  $\delta^{13}\text{C}$  value of  $0\text{‰}$  SMOW shows that ACR may contain  $\sim 68\%$  methane oxidation and  $\sim 32\%$  normal marine carbonate. ACR contains tiny organisms (Figs. 4.41a and 4.41c), diagenetic calcite (Figs. 4.41b and 4.41e), and foraminifera (Fig. 4.41d). In addition, petrographic thin sections show that approximately 70% methane oxidation contributed to ACR. Theoretically, some samples (ACR-5, ACR-6, and ACR-9) might form in the zone of methanogenesis because their sample depths are below the SMI, which is located at  $\sim 17.2$  mbsf at Site 10 (Fig. 4.37). However, oxidation of sedimentary organic matter has  $\delta^{13}\text{C}$  of  $\sim -20\text{‰}$  (Burns, 1998). The  $\delta^{13}\text{C}$  of DIC decreases from  $\sim 0\text{‰}$

at the seafloor to  $-20\%$  near SMI (Claypool and Kaplan, 1974; Mozley and Burns, 1993). Below SMI,  $^{12}\text{C}$  from  $\text{CO}_2$  preferentially gets fractionated into methane and hence the DIC becomes enriched in  $^{13}\text{C}$  in the zone of methanogenesis. In addition,  $\text{CH}_4$  and  $\text{CO}_2$  concentrations throughout the sediment show much scatter (Figs. 4.37, 4.38 and 4.39). Therefore, it was proposed that ACR samples from Site 10 in Group D may be affected by mostly microbial methane oxidation instead of methanogenesis processes.

In Group E, ACR-10 (Site 14) may form in sediments with relatively low rates of organic carbon oxidation in the zone of methanogenesis (Fig. 4.24). The bulk carbon ( $\delta^{13}\text{C}$ ) isotope of ACR-10 (Site 14) is  $-0.36\%$ . It was proposed that several possible explanations for low rates of organic carbon oxidation at this site: (1) stratigraphic layers are characterized by the typical sediment sequences of the basin (Fig. 4.42), (2) the major lithologies include much sand (Fig. 4.44), (3) the zone of sulfate reduction is relatively deeper, (4) alkalinity concentration gradually increases from the seafloor with a corresponding decrease in sulfate concentration in general (Fig. 4.45), (5) below the SMI, headspace  $\text{CH}_4$  concentration gradually decreases to nearly 1 mM just below the BSR (Fig. 4.46), and (6) headspace  $\text{CO}_2$  concentration gradually decreases with depth below SMI (Fig. 4.47). Based on these observations, the methanogenesis may not be enough to generate isotopically heavy  $\delta^{13}\text{C}$  in the pore waters to ACR-10 (Site 14) (Fig. 4.24).

Bulk  $\delta^{18}\text{O}$  values of ACR from the KG basin offshore India are in the range of  $+1.27$  to  $+4.99\%$  (mean  $\delta^{18}\text{O} = +3.41\%$ ). The  $\delta^{18}\text{O}$  values are isotopically heavier than those of normal marine carbonates. Why are ACR samples so enriched in  $^{18}\text{O}$  with a mean  $\delta^{18}\text{O}$  of  $+3.41\%$ ? Isotopically heavy values of  $\delta^{18}\text{O}$  from ACR was discussed. In this study, three likely hypotheses could explain the isotopically heavy  $\delta^{18}\text{O}$  values: (1) they reflect the temperature of initial formation of ACR; (2) they reflect isotopically heavy  $\delta^{18}\text{O}$  values from gas hydrate decomposition; or (3) they reflect the movement of isotopically heavier water than ambient seawater from greater depth. As in the previous section on the Gulf of Mexico, each hypothesis was discussed separately.

The first hypothesis is that the measured  $\delta^{18}\text{O}$  value reflects the temperature of initial formation of ACR. To calculate the temperature, the measured  $\delta^{18}\text{O}$  in PDB to the value in SMOW was converted using the relation of  $\delta^{18}\text{O}_{\text{SMOW}} = 1.03086 \delta^{18}\text{O}_{\text{PDB}} + 30.86$  (Friedman and O'Neil, 1977). Then, using an equilibrium oxygen isotope equation (Kim and O'Neil, 1997) of  $1000 \times \ln(\alpha) = 18.03 \times (10^3 \text{ T}^{-1}) - 32.42$ , the temperature was calculated (APPENDIX B).

However, the first hypothesis was eliminated because the calculated temperature for seawater was unrealistic or unreasonable for the environment. Then,  $\delta^{18}\text{O}$  water value in SMOW was calculated using the measured  $\delta^{18}\text{O}$  and temperature of ACR with the equation of Kim and O'Neil (1997). The  $\delta^{18}\text{O}$  value of +0.15‰ SMOW was applied for Indian Ocean water (<http://data.giss.nasa.gov/o18data>, GEOSECS Ostlund et al., 1987) at a nearest location to the study site. Although gas hydrate water may cause an isotopically heavy  $\delta^{18}\text{O}$  value, the second hypothesis for isotopically heavy  $\delta^{18}\text{O}$  water resulting from gas hydrate decomposition was eliminated. This is because hydrate water would not cause significant heavy oxygen isotopes (Matsumoto and Borowski, 2000; Greinert et al., 2001; Sassen and Roberts, 2004). To eliminate the second hypothesis, two examples of isotopically heavy  $\delta^{18}\text{O}$  water values from hydrate water were provided. The third hypothesis proposed that the  $\delta^{18}\text{O}$  value may be affected by the migration and movement of isotopically heavy water from greater depth. The isotopically heavy water from greater depth has  $\delta^{18}\text{O}$  values ranging +3.3 to +5.1‰ (Land and Macpherson, 1992) as produced from Cenozoic hydrocarbon reservoirs in the Gulf of Mexico sedimentary basin. In this section,  $\delta^{18}\text{O}$  values of isotopically heavy water from greater depth in the Gulf of Mexico were used alternatively.

Isotopic compositions of ACR from the KG basin offshore India are summarized in Table 5.2. Calculated oxygen isotopes and temperatures are also summarized in Table 5.3.

Table 5.2  
Isotopic composition of authigenic carbonate rock from the KG basin offshore India

Sample#	Site#	Hole#	Sample depth (mbsf)	$\delta^{13}\text{C}$ (‰)	$\delta^{18}\text{O}$ (‰)
ACR-1	Site 3	B	56.2	+10.95	+4.99
ACR-2	Site 5	C	37.1	-24.62	+2.44
ACR-3	Site 5	C	40.0	+14.06	+4.54
ACR-4	Site 5	C	110.2	-2.80	+2.69
ACR-5	Site 10	B	22.3	-44.90	+2.77
ACR-6	Site 10	B	31.4	-44.30	+3.94
ACR-7	Site 10	D	16.2	-47.16	+4.00
ACR-8	Site 10	D	16.5	-49.12	+4.36
ACR-9	Site 10	D	43.2	-49.06	+3.13
ACR-10	Site 14	A	109.5	-0.36	+1.27

Table 5.3  
Calculated oxygen isotopes and temperatures of authigenic carbonate rock from the KG basin offshore India

Sample#	Site#	Sample depth (mbsf)	Measured $\delta^{18}\text{O}_{\text{ACR}}$ (‰, PDB)	Calculated temp. (°C)	Temperature at sample depth (°C)	Calculated $\delta^{18}\text{O}_{\text{H}_2\text{O}}$ (‰, SMOW)
ACR-1	Site 3	56.2	+4.99	-6.6	8.69	+3.83
ACR-2	Site 5	37.1	+2.44	3.8	8.60	+1.26
ACR-3	Site 5	40.0	+4.54	-4.8	8.73	+3.39
ACR-4	Site 5	110.2	+2.69	2.7	11.96	+2.26
ACR-5	Site10	22.3	+2.77	2.4	7.50	+1.34
ACR-6	Site10	31.4	+3.94	-2.4	7.91	+2.60
ACR-7	Site10	16.2	+4.00	-2.7	7.23	+2.50
ACR-8	Site10	16.5	+4.36	-4.1	7.24	+2.86
ACR-9	Site10	43.2	+3.13	0.9	8.44	+1.91
ACR-10	Site14	109.5	+1.27	8.9	11.97	+0.85



## CHAPTER VI

### CONCLUSIONS AND SUGGESTIONS FOR FUTURE RESEARCH

Hydrocarbon gas venting, seepage, free gas, and gas hydrate are associated with hydrocarbon-derived authigenic carbonate rock (ACR). Petrographic, mineralogic, and geochemical studies were used to characterize the precipitation of ACR. Six samples collected from 30 cm push cores at the seafloor in the Gulf of Mexico (GOM) and ten samples collected from drilled cores in the Krishna-Godawari (KG) basin offshore India were characterized.

ACR samples are gray to light brown in color but often coated by dark brown, exhibiting extremely irregular shapes. ACR collected from the seafloor in the GOM are generally densely cemented, whereas one sample of ACR-5 (EL 711) is quite unusual because it is friable and exhibits extremely high microporosity and low density. ACR-5 (EL 711) contains many foraminifera and other planktonic organisms with few inclusions of carbonate skeletal materials. The foraminifera and other planktonic organisms with skeletal carbonate are bound together and cemented by fine-grained authigenic calcite. The dominant authigenic mineral is fine-grained calcite. Aragonite, dolomite, pyrite, barite, quartz, and mica are also present. ACR collected from the seafloor or chemosynthetic communities in the GOM is densely cemented and extremely irregular in shape, whereas ACR collected from the KG basin offshore India is generally oval-shaped nodules but is also highly cemented.

Bulk carbon and oxygen ( $\delta^{13}\text{C}$  and  $\delta^{18}\text{O}$ ) isotopes of ACR recovered from the GOM are different from those of normal marine carbonates. ACR is strongly depleted in  $^{13}\text{C}$  ( $\delta^{13}\text{C}$  of  $-42.5\%$  to  $-20.68\%$ ) and enriched in  $^{18}\text{O}$  ( $\delta^{18}\text{O}$  of  $+4.67\%$  to  $+2.43\%$ ). ACR may be derived from the microbial oxidation of methane and other hydrocarbons, which is strongly depleted in  $^{13}\text{C}$ . Therefore, if methane was the primary source of carbon in ACR, one would expect it also to be highly depleted in  $^{13}\text{C}$ . However, the  $\delta^{13}\text{C}$  values of ACR rarely correspond to those of methane or other hydrocarbons. In general,

ACR is enriched in  $^{13}\text{C}$  when compared to hydrocarbon sources because various carbon sources may affect the bulk  $\delta^{13}\text{C}$  values of ACR.

It was proposed that hydrocarbon sources to ACR are based on molecular and isotopic composition of vent gas or gas hydrate samples from different geological environments for the formation of ACR. Other carbon sources to ACR depend on different isotopic values, corresponding carbonate phases, mineral compositions, and distribution of normal marine carbonates. Primary hydrocarbon sources to ACR may be classified into (1) methane and biodegraded oil, (2) methane, or (3) biodegraded oil.

Bulk  $\delta^{18}\text{O}$  values of ACR recovered from the GOM are in the range of +2.43 to +4.67‰ (mean  $\delta^{18}\text{O} = +3.43\%$ ). The  $\delta^{18}\text{O}$  values are isotopically heavier than those of normal marine carbonates. ACR samples are highly enriched in  $^{18}\text{O}$  with a mean  $\delta^{18}\text{O}$  of +3.43‰. Three hypotheses could explain the isotopically heavy  $\delta^{18}\text{O}$  values: (1) they reflect the temperature of initial formation of ACR, (2) they reflect isotopically heavy  $\delta^{18}\text{O}$  values from gas hydrate decomposition, or (3) they reflect the movement of isotopically heavier water than ambient seawater from greater depth. The third hypothesis appears to be the most likely explanation and is consistent with data from Cenozoic hydrocarbon reservoirs in the Gulf of Mexico sedimentary basin (Land and Macpherson, 1992). The same model may explain the isotopically heavy ACR samples recovered from offshore India.

Wide ranges in  $\delta^{13}\text{C}$  and  $\delta^{18}\text{O}$  values were observed in ACR recovered from offshore India with  $\delta^{13}\text{C}$  and  $\delta^{18}\text{O}$  values up to +14.06‰ and +4.99‰, respectively, and with  $\delta^{13}\text{C}$  and  $\delta^{18}\text{O}$  values down to -49.12‰ and +1.27‰, respectively. ACR formation on the seafloor in the GOM may be controlled by mainly hydrocarbon influx and microbial processes (sulfate reduction and hydrocarbon oxidation), whereas ACR from the KG basin offshore India may form in different geochemical environments. Based on the wide range in  $\delta^{13}\text{C}$  and different geochemical environments, ACR into five groups from group A to E are classified.

In Group A, the  $\delta^{13}\text{C}$  of ACR may reflect high rates of oxidation of sedimentary organic matter in the zone of methanogenesis. ACR samples are enriched in  $^{13}\text{C}$  with

$\delta^{13}\text{C}$  values of +10.95‰ and +14.06‰. At these sites, in sediments with relatively high rates of organic carbon oxidation, the zone of methanogenesis is found at a shallow depth. The SMI is located at shallow depths. Sulfate is totally depleted by SMI, and then methanogenesis begins in the sediments. Thus,  $\text{CH}_4$  concentration rapidly increases just below SMI, and it shows the highest value around the depth of ACR. Concomitantly,  $\text{CO}_2$  concentrations are low at that depth. It was proposed that the high rates of organic carbon oxidation during methanogenesis occur below SMI. The methanogenesis may be enough to cause isotopically heavy  $\delta^{13}\text{C}$  values.

The  $\delta^{13}\text{C}$  of ACR in Group B is highly depleted in  $^{13}\text{C}$ . It was proposed that the  $\delta^{13}\text{C}$  of ACR reflects organic carbon oxidation from sedimentary organic matter in the zone of methanogenesis. Although ACR were formed below SMI is within the zone of methanogenesis,  $\delta^{13}\text{C}$  may not be affected by methanogenesis processes.

Methanogenesis may not be extensive enough to generate isotopically heavy carbon isotopes in pore waters at depth. Based on observations of Group B, ACR in Group C may reflect the carbon source from pore waters below methanogenesis (i.e., decarboxylation).

In Group D, ACR are typical of methane ( $\delta^{13}\text{C} = -69\text{‰}$ , ONGC) derived authigenic carbonate rock. All of ACR is highly depleted in  $^{13}\text{C}$  with a range of  $-44.30$  to  $-49.12\text{‰}$  (mean  $\delta^{13}\text{C} = -46.9\text{‰}$ ). Some samples might theoretically form in the zone of methanogenesis because their sample depths are below the SMI. However, oxidation of sedimentary organic matter has  $\delta^{13}\text{C}$  of  $\sim -20\text{‰}$  (Burns, 1998). The  $\delta^{13}\text{C}$  of DIC decreases from  $\sim 0\text{‰}$  at the seafloor to  $-20\text{‰}$  near SMI (Claypool and Kaplan, 1974; Mozley and Burns, 1993). Below SMI,  $^{12}\text{C}$  from  $\text{CO}_2$  preferentially gets fractionated into methane and hence the DIC becomes enriched in  $^{13}\text{C}$  in the zone of methanogenesis. In addition,  $\text{CH}_4$  and  $\text{CO}_2$  concentrations throughout the sediment show much scatter. Therefore, it was proposed that ACR in Group D may be affected by mostly microbial methane oxidation instead of the methanogenesis process.

In Group E, ACR may form in sediments with relatively low rates of organic carbon oxidation in the zone of methanogenesis. The bulk carbon ( $\delta^{13}\text{C}$ ) isotope of ACR

is  $-0.36\text{‰}$ . Several possible explanations for low rates of organic carbon oxidation at this site were proposed: (1) stratigraphic layers are characterized by the typical sediment sequences of basin; (2) the major lithologies include much sand; (3) the zone of sulfate reduction is relatively deeper; (4) alkalinity concentration gradually increases from the seafloor with a corresponding decrease in sulfate concentration in general; (5) below the SMI, headspace  $\text{CH}_4$  concentration gradually decreases to nearly 1 mM just below the BSR; and (6) headspace  $\text{CO}_2$  concentration gradually decreases with depth below SMI. Based on these observations, the methanogenesis may not be enough to generate isotopically heavy  $\delta^{13}\text{C}$  in the pore waters to ACR with relatively low rates of organic carbon oxidation in the zone of methanogenesis.

Clearly, more research on the microbial origin of carbonate mineralization is needed. For example, at the VN 945 site in the GOM, the  $\delta^{13}\text{C}$  of ACR-4 (VN 945) may involve a physical mixture of isotopically light carbon from microbial methane oxidation and degraded crude oil oxidation. Although oil biodegradation is a common process in deep subsurface reservoirs of the GOM, more studies are needed around the world in diverse geological environments. Few publications address the biodegradation of oil in the deep sea. Further study of the mixture of carbon from methane and degraded oil oxidation may be valuable. In this study, it is proposed that heavy  $\delta^{18}\text{O}$  values are generally affected by isotopically heavier water from greater depth in geologic sections in both study sites in the GOM and in the KG basin offshore India. Direct evidence of the isotopically heavy water for ACR samples in the GOM was provided. However, direct evidence of isotopically heavy water for ACR from offshore India is not available.

The precipitation of hydrocarbon-derived ACR is important because ACR sequesters enormous quantities of carbon as part of the global carbon cycle (; Houghton et al., 1996; Judd et al., 2002; Dickens, 2003; Sassen et al., 2006). Designing programs to sequester carbon dioxide ( $\text{CO}_2$ ) as carbonate rock may be an outstanding issue for future industrial operations.

## REFERENCES

- Aharon, P., 2000. Microbial processes and products fueled by hydrocarbons at submarine seeps. In: Riding, R. and Awramik, S.M. (Eds.), *Microbial Sediments*, Springer-Verlag, 270-281.
- Aharon, P., Fu, B., 2000. Microbial sulfate reduction rates and sulfur and oxygen isotope fractionations at oil and gas seeps in deepwater Gulf of Mexico. *Geochim. Cosmochim. Acta*, 233-246.
- Aharon, P., Schwarcz, H.P., Roberts, H.H., 1997. Radiometric dating of hydrocarbon seeps in the Gulf of Mexico. *GSA Bulletin*, 568-579.
- Baker, P. A., Burns, S. J., 1985. The occurrence and formation of dolomite in organic-rich continental margin sediments. *AAPG Bull.*, 1917-1930.
- Barker, J.F., Fritz, P., 1981. Carbon isotope fractionation during microbial methane oxidation. *Nature* 293, 289-291.
- Berner, R.A., 1964. Stability fields of iron minerals in anaerobic marine sediments. *Geology* 72, 826-834.
- Berner, R.A., 1970. Sedimentary pyrite formation. *Amer. J. Sci.* 268, 1-23.
- Biksham, G., Subrahmanyam, V., 1988. Sediment transport of the Godawari River Basin and its controlling factors, *J. Hydrol.*, 275-290.
- Bohrmann, G., Greinert, J., Suess, E., Torres, M., 1998. Authigenic carbonate from the Cascadia subduction zone and their relation to gas hydrate stability. *Geology* 26, 647-650.
- Borowski, W.S., Paull, C.K., Ussler III, W., 1996. Marine pore-water sulfate profiles indicate in situ methane flux from underlying gas hydrate. *Geology* 24, 655-658.
- Burns, S. J., 1998. Carbon isotopic evidence for coupled sulfate reduction-methane oxidation in Amazon Fan sediments. *Geochimica et Cosmochimica Acta*, 797-804.

- Castellini, D.G., Dickens, G.R., Synder, G.T., Ruppel, C.D., 2006. Barium cycling in shallow sediment above active mud volcanoes in the Gulf of Mexico. *Chem. Geol.* 226, 1-30.
- Cavagna, S., Clari, P., Martire, L., 1999. The role of bacteria in the formation of cold seep carbonates: geological evidence from "Montferrato" (Tertiary, NW Italy). *Sedimentary Geology* 126, 253-270.
- Chapelle, F.H., O'Neill, K., Bradley, P.M., Methé, B.A., Ciufo, S.A., Knobel, L.L., Lovley, D.R., 2002. A hydrogen-based subsurface microbial community dominated by methanogens. *Nature*, 415, 312-315.
- Chen, D.F., Feng, D., Su, Z., Song, Z.G., Chen, G.Q., Cathles III, L.M., 2006. Pyrite crystallization in seep carbonates at gas vent and hydrate site. *Materials Science and Engineering C26*, 602-605.
- Claypool, G.E., Kaplan, I.R., 1974. The origin and distribution of methane in marine sediments. In: Kaplan, I. R. (Ed.), *Natural Gases in Marine Sediments*, New York (Plenum), 99-139.
- Collett, T., Riedel, M., Cochran, J., Boswell, R., Presley, J., Kumar, P., Sathe, A., Sethi, A., Lall, M., Sibal, V., the NGHP Expedition 01 Scientists, 2006. Indian National Gas Hydrate Program. Expedition 01 Initial Reports.
- Curray, J.R., Emmel, F.J., Moore, D.G., Raitt, R.W., 1982. Structure, Tectonics and Geological History of the Northeastern Indian Ocean, 399-450.
- Curray, J.R., 1991. Possible greenschist metamorphism at the base of a 22 km sedimentary section, Bay of Bengal. *Geology* 19, 1097-1100.
- Curray, J. R., Emmel, F. J., Moore, D. G., 2003. The Bengal Fan: morphology, geometry, stratigraphy, history and processes. *Marine and Petroleum Geology*, 1191-1223.
- Dickens, G.R., 2001. Sulfate profiles and barium fronts in sediment on the Blake Ridge: present and past methane fluxes through a large gas hydrate reservoir. *Geochim. Cosmochim. Acta*, 529-543.

- Dickens, G.R., 2003. Rethinking the global carbon cycle with a large, dynamic and microbially mediate gas hydrate capacitor. *Earth Planet. Sci. Lett.* 213, 169-183.
- Feely, H. W., Kulp, J.L., 1957, Origin of Gulf Coast salt-dome surfur deposits. *Bull. Am. Assoc. Pet. Geol.*, 1802-1853.
- Friedman, I., O'Neil, J.R., 1977. Compilation of stable isotope fractionation factors of geochemical interest (Data of Geochemistry, Sixth Edition, Chapter KK): U.S. Geological Survey Professional Paper 440-KK, pp. 12.
- Fu, B., Aharon, P., Byerly, G.R., Roberts, H.H., 1994. Barite chimneys on the Gulf of Mexico slope: initial report on their petrography and geochemistry. *Geo. Mar. Lett.* 14, 81-87.
- Fu, B., Aharon, P., 1998. Sources of hydrocarbon-rich fluids advecting on the seafloor in the northern Gulf of Mexico. *Trans.-Gulf Coast Assoc. Geol. Soc.*, 73-81.
- Gieskes, J., Mahn, C., Day, S., Martin, J.B., Greinert, J., Rathburn, A.E., McAdoo, B, 2005. A study of the chemistry of pore fluids and authigenic carbonates in methane seep environments, Kodiak Trench, Hydrate Ridge, Monterey Bay and Eel River Basin. *Chem. Geol.* 220, 329-345.
- Hesse, R., Harrison, W.E., 1981. Gas hydrates (clathrates) causing pore water freshening and oxygen isotope fractionation in deep-water sedimentary sections of terrigenous continental margin. *Earth Planet. Sci. Lett.*, 453-462.
- Houghton, J.T., Meira Filho, L.G., Callander, B.A., Harris, N., Kattenberg, A., Maskell, K., 1996. *Climate Change 1995: The Science of Climate Change*. Cambridge University Press for the Intergovernmental Panel on Climate Change, Cambridge.
- Hudson, J.D., 1977. *Marine Carbonates*. Springer-Verlag New York, 30-33.
- Iversen, N., Jørgensen, B.B., 1985. Anaerobic methane oxidation rates at the sulfate-methane transition in marine sediments from Kattegat and Skagerrak (Denmark). *Limnol. Oceanogr.* 30, 944-955.
- Judd, A.G., Hovland, M., Dimitrov, L.I., Gil, S.G., Jukes, V., 2002. The geological methane budget at Continental Margins and its influence on climate change. *Geofluids* 2, 109-126.

- Jung, W., Sassen, R., 2006. Authigenic carbonate rock from geologic settings with and without gas hydrate from the Gulf of Mexico. AAPG 2007 Annual Conference, Long Beach, California, 1-4 April.
- Kastner, A., 1999. Oceanic minerals: their origin, nature of their environment, and significance. *Proc. Natl. Acad. Sci.* 96, 3380-3387.
- Kim, S., O'Neil, J.R., 1997. Equilibrium and non equilibrium oxygen isotope effects in synthetic carbonates. *Geochim. Cosmochim. Acta*, 3461-3475.
- Kvenvolden, K.A., 1995. A review of the geochemistry of methane in natural gas hydrate. *Org. Geochem.*, 997-1008.
- Kvenvolden, K.A., Lorenson, T.D., 2001. The global occurrence of natural gas. In: Paull, C.K., Dillon, W.P. (Eds.), *Natural Gas Hydrate: Occurrence, Distribution and Detection*, Am. Geophys. Union, Geophysical Monograph, Washington DC, vol. 124, pp. 3-18.
- Land, L.S., Macpherson, G.L., 1992. Origin of saline formation waters, Cenozoic section, Gulf of Mexico sedimentary basin. *American Association of Petroleum Geologists Bulletin*, 1344-1362.
- MacDonald, I.R., Boland, G.S., Baker, J.S., Brooks, J.M., Kennicutt II, M.C., Bidigare, R.R., 1989. Gulf of Mexico hydrocarbon seep communities: II. Spatial distribution of seep organisms and hydrocarbons at Bush Hill. *Mar. Biol.* 101, 235-247.
- Malone, M.J., Baker, P., Burns, S., Swart, P., 1990. Geochemistry of periplatform carbonate sediments, Ocean Drilling Program Site 716 (Maldives Archipelago, Indian Ocean), in Duncan, R., Backman, J., Peterson, L.C., et al. (Eds.), *Proc. Ocean Drill. Program: Sci. Results*, Ocean Drilling Program, Texas A&M University, College Station, vol. 115, pp. 647-659.
- Malone, M.J., Claypool, G., Martin, J.B., Dickens, G.R., 2002. Variable methane fluxes in shallow marine systems over geologic time: the composition of pore waters and authigenic carbonates on the New Jersey shelf. *Marine Geology* 189, 173-194.



- Matsumoto, R., Borowski, W.S., 2000. Gas hydrate estimates from newly determined oxygen isotopic fractionation ( $\alpha_{GH-IW}$ ) and  $\delta^{18}O$  anomalies of the interstitial water: Leg 164, Blake Ridge. In: Paull, C.K., Matsumoto, R., Wallace, P.J., Dillon, W.P. (Eds.), Proc. Ocean Drill. Program: Sci. Results, Ocean Drilling Program, Texas A&M University, College Station, vol. 164, pp. 59-66.
- Mazzini, A., Svensen, H., Hovland, M., Planke, S., 2006. Comparison and implications from strikingly different authigenic carbonates in a Nyegga complex pockmark, G11, Norwegian Sea. *Marine Geology*, 89-102.
- Milkov, A.V., 2005. Molecular and stable isotope compositions of natural gas hydrates: a revised global dataset and basic interpretations in the context of geological settings. *Organic Geochemistry*, 681-702.
- Morton, R.A., Han, J.H., Posey, J.S., 1983. Variations in chemical compositions of Tertiary Formation waters, Texas Gulf Coast, in consolidation of geologic studies of geopressured geothermal resources in Texas: Texas Bureau of Economic Geology report to the U.S. Department of Energy, Contract No. DE-AC08-79ET2711, pp. 63-135.
- Morton, R.A., Land, L.S., 1987. Regional variations in formation water chemistry, Frio Formation (Oligocene), Texas Gulf Coast. *American Association of Petroleum Geologists Bulletin*, 191-206.
- Mozley, P.S., Burns, S.J., 1993. Oxygen and carbon isotopic composition of marine carbonate concretions: an overview. *Journal of Sedimentary Petrology*, 73-83.
- Neurauter, T.W., Bryant, W.R., 1990. Seismic expression of sedimentary volcanism on the continental slope, northern Gulf of Mexico. *Geo-Marine Letters* 10, 225-231.
- Paull, C.K., Hecker, R., Commeau, R., Fredman, R.P., Lyne, R.P., Neumann, Corso, W.P., Golubic, S., Hook, J.E., Sikes, E., Currey, J., 1984. Biological communities at the Florida Escarpment resemble hydrothermal vent taxa. *Science* 226, 965-967.
- Paull, C.K., Lull, A.J.T., Toolin, L.J., Linick, T., 1985. Stable isotope evidence for chemosynthesis in an abyssal seep community. *Nature* 317, 709-711.

- Paull, C.K., Lorenson, T.D., Borowski, W.S., Ussler III, W., Olsen, K., Rodriguez, N.M., 2000. Isotopic composition of CH<sub>4</sub>, CO<sub>2</sub> species, and sedimentary organic matter within samples from the Blake Ridge: gas source implications. In: Paull, C.K., Matsumoto, R., Wallace, P.J., Dillon, W.P. (Eds.), Proc. Ocean Drill. Program: Sci. Results, Ocean Drilling Program, Texas A&M University, College Station, vol. 164, pp. 67-78.
- Peckmann, J., Reimer, A., Luth, U., Luth, C., Hansen, B.T., Heinicke, C., Hoefs, J., Reitner, J., 2001. Methane-derived carbonates and authigenic pyrite from the northwestern Black Sea. *Marine Geology*, 129-150.
- Philippi, G.T., 1977. On the depth, time, and mechanism of origin of the heavy to medium-gravity naphthenic crude oils. *Geochim. Cosmochim. Acta* 41, pp. 33-52.
- Posey, H.H., Price, P.E., Kyle, J.R., 1987. Mixed carbon sources for calcite cap rocks of Gulf Coast salt domes. In: Lerche, I., O'Brien, J.J. (Eds.), *Dynamical Geology of Salt and Related Structures*, Academic Press, New York, pp. 593-630.
- Powell, C.M., Roots, S.R., Veevers, J. J., 1988. Pre-breakup continental extension in East Gondwanaland and the early opening of the eastern Indian Ocean. *Tectonophys.*, 261-183.
- Reeburgh, W.S., 1976. Methane consumption in Cariaco Trench waters and sediments. *Earth Planetary Sci. Lett.* 28, 337-344.
- Reeburgh, W.S., 1980. Anaerobic methane oxidation: rate depth distributions in Skan Bay sediments. *Earth Planetary Sci. Lett.* 47, 345-352.
- Ripmeester, J.A., Tse, J.S., Ratcliffe, C.I., Powell, B.M., 1987. A new clathrate hydrate structure, *Nature*, 135.
- Roberts, H.H., Aharon, P., Carney, R., Larkin, J., Sassen, R., 1990. Seafloor response to hydrocarbon seeps, Louisiana continental slope. *Economic Geology* 92, 863-879.
- Roberts, H.H., Aharon, P., 1994. Hydrocarbon-derived buildups of the northern Gulf of Mexico: a review of submersible investigations. *Geo. Mar. Lett.* 14, 135-148.
- Roberts, H.H., Carney, R., 1997. Evidence of episodic fluid, gas, and sediment venting on the northern Gulf of Mexico slope. *Econ. Geol.* 92, 863-879.

- Rodriguez, N.M., Paull, C.K., and Borowski, W.S., 2000. Zonation of authigenic carbonates within gas hydrate-bearing sedimentary sections on the Blake Ridge: offshore southeastern North America. In: Paull, C.K., Matsumoto, R., Wallace, P.J., Dillon, W.P. (Eds.), Proc. Ocean Drill. Program: Sci. Results, Ocean Drilling Program, Texas A&M University, College Station, vol. 164, pp. 301–312.
- Salvador, A., 1987. Late Triassic-Jurassic paleogeography and origin of Gulf of Mexico basin. American Association of Petroleum Geologists Bulletin, 419-451.
- Sansone, F., Martens, C.S., 1982. Volatile fatty acid cycling in organic-rich marine sediments. *Geochim. Cosmochim. Acta*, 1575-1589.
- Sassen, R., 1980. Biodegradation of crude oil and mineral deposition in a shallow Gulf Coast salt dome. *Organic Geochemistry*, 153-166.
- Sassen, R., Roberts, H.H., Robert, C., Aharon, A., Larkin, J., Chinn, E.W., Carney, R., 1993. Chemosynthetic bacterial mats at cold hydrocarbon seeps, Gulf of Mexico continental slope. *Org. Geochem.* 20, 77-89.
- Sassen, R., Joye, S., Sweet, S.T., DeFreitas, D.A., Milkov, A.V., MacDonald, I.R., 1999. Thermogenic gas hydrates and hydrocarbon gases in complex chemosynthetic communities, Gulf of Mexico continental slope. *Org. Geochem.* 30, 485-497.
- Sassen, R., Losh, S.L., Cathles III, L., Roberts, H.H, Whelan, J.K., Milkov, A.V., Sweet, S.T., DeFreitas, D.A., 2001a. Massive vein-filling gas hydrate: relation to ongoing gas migration from the deep subsurface in the Gulf of Mexico. *Marine and Petroleum Geology* 18, 551-560.
- Sassen, R., Sweet, S.T., DeFreitas, D.A., Alejandro Morelos, J., Milkov, A.V., 2001b. Gas hydrate and crude oil from the Mississippi Fan Foldbelt, downdip, Gulf of Mexico Salt Basin: significance to petroleum system. *Organic Geochemistry* 32, 999-1008.
- Sassen, R., Sweet, S.T., Milkov, A.V., DeFreitas, D.A., Kennicutt II, M.C., 2001c. Thermogenic vent gas and gas hydrate in the Gulf of Mexico slope: Is gas hydrate decomposition significant? *Geology* 29, 107-110.

- Sassen, R., Sweet, S.T., Milkov, A.V., DeFreitas, D.A., Kennicutt II, M.C., 2001d. Stability of thermogenic gas hydrate in the Gulf of Mexico: constraints on models of climate change. In: Paull, C.K., Dillon (Eds.), *Natural Gas Hydrates: Occurrence, Distribution, and Detection*. American Geophysical Union, Washington DC, 131-143.
- Sassen, R., Milkov, A.V., DeFreitas, D.A., Sweet, S.T., 2002. Molecular and isotopic properties of high flux gas seeps, Northwestern Gulf of Mexico. *AAPG Bull.*, 13 (supplement).
- Sassen, R., 2004. *Organic Biogeochemistry of Chemosynthetic Communities on the Lower Slope of the Gulf of Mexico*, Geochemical and Environmental Research Group (GERG), Texas A&M University, College Station, GERG Technical Report, #04-009, pp.17-19.
- Sassen, R., Roberts, H.H., 2004. Site selection and characterization of vent gas, gas hydrate and associated sediments, DOE Report# DE-FC26-02NT41628, pp. 21.
- Sassen, R., Roberts, H.H., Robert, C., Milkov, A.V., DeFreitas, D.A., Lanoil, B., Zhang, C., 2004a. Free hydrocarbon gas, gas hydrate, and authigenic minerals in chemosynthetic communities of the northern Gulf of Mexico continental slope: relation to microbial processes. *Chem. Geol.* 205, 195-217.
- Sassen, R., Jung, W., Zhang, C., DeFreitas, D.A., 2004b. Carbon sources to authigenic carbonate rock at chemosynthetic communities: lower slope of the Gulf of Mexico. AGU Fall Meeting 2004, San Francisco, CA, 13-17 December.
- Sassen, R., Roberts, H.H., Jung, W., Lutken, C.B., DeFreitas, D.A., Sweet, S.T., Guinasso, N.L., 2006. The Mississippi Canyon 118 gas hydrate site: a complex natural system. 2006 Offshore Technology Conference, Paper OTC 18132, Houston, Texas, 1-4 May, 1-6.
- Sastri, V.V., Venkatachala, B.S., Narayanan, V., 1981. The evolution of the east coast of India. *Paleogeogr., Paleoclim., Paleoeco.*, 23-54.
- Schoell, M., 1980. The hydrogen and carbon isotopic composition of methane from natural gases of various origins. *Geochim. Cosmochim. Acta* 44, 649-661.

- Schoell, M., 1983. Genetic characterization of natural gases, AAPG Bull., 2225-2238.
- Scotese, C.R., Gahagan, L.M., Larson, R.L., 1988. Plate tectonic reconstruction of the Cretaceous and Cenozoic ocean basins, Tectonophys., 27-48.
- Sen Gupta, B.K., Aharon, P., 1994. Benthic foraminifera of bathyal hydrocarbon vents of the Gulf of Mexico: initial report on communities and stable isotopes. Geo-Marine Letters, 88-96.
- Sloan, E.D., 1998. Clathrate Hydrates of Natural Gases (2nd ed.). New York, Dekker, pp. 705.
- Taylor, K.G., Curtis, C.D., 1995. Stability and facies association of early diagenetic mineral assemblages: an example from a Jurassic ironstone-mudstone succession. UK. J. Sediment. Petrol. A65, 358-368.
- Thauer, R.K., 1998. Biochemistry of methanogenesis: a tribute to Marjory Stephenson. Microbiology 144, 2377-2406.
- Thomsen, T.R., Finster, K., Ramsing, N.B., 2001. Biogeochemical and molecular signatures of anaerobic methane oxidation in a marine sediment. Appl. Environ. Microbiol. 67, 1646-1656.
- Tissot, B.P., Welte, D.H., 1984. Petroleum Formation and Occurrence (2nd ed.), Springer-Verlag, Heidelberg.
- Torres, M.E., Bohrmann, G., Suess, E., 1996a. Authigenic barites and fluxes of barium associated with fluid seeps in the Peru subduction zone. Earth Planet. Sci. Lett. 144, 469-481.
- Torres, M.E., Brumsack, H.J., Bohrmann, G., Emeis, K.C., 1996b. Barite fronts in continental margin sediments: a new look at barium remobilization in the zone of sulfate reduction and formation of heavy barites in diagenetic fronts. Chem. Geol. 127, 125-139.
- Ussler III, W., Paull, C.K., 1995. Effects of ion exclusion and isotopic fractionation on pore water geochemistry during gas hydrate formation and decomposition. Geo-Mar. Lett., 15, 37-44.

- Valentine, D.L., Reeburgh, W.S., 2000. New perspectives on anaerobic methane oxidation. *Environmental Microbiology* 2, 477-484.
- Valentine, D.L., 2002. Biogeochemistry and microbial ecology of methane oxidation in anoxic environments: a review. *Antonie van Leeuwenhoek*, 81, 271-282.
- von Stackelberg, M., Müller, H.R., 1954. Feste Gashydrate, *Z. für Elektrochemie*, 25.
- Whiticar, M. J., Faber, E., Schoell, M., 1986. Biogenic methane formation in marine and freshwater environments. CO<sub>2</sub> reduction vs. acetate fermentation-isotope evidence. *Geochim. Cosmochim. Acta*, 693-709.
- Whiticar, M. J., 1999. Carbon and hydrogen isotope systematics of bacterial formation and oxidation of methane. *Chemical Geology*, 291-314.
- Worrall, D.M., Snelson, S., 1989. Evolution of the northern Gulf of Mexico with emphasis on Cenozoic growth faulting and the role of salt. In: Bally, A.W., Palmer, E.R. (Eds.), *The geology of North America – An overview*: Boulder, Colorado Geological Society of America, 97-138.

## APPENDIX A

Equilibrium temperature can be calculated from an equilibrium oxygen isotope equation between calcite and water (Eq. A.1) (Kim and O'Neil, 1997). For the calculations, oxygen isotope values measured in PDB are converted to SMOW using the relation of  $\delta^{18}\text{O}_{\text{SMOW}} = 1.03086 \delta^{18}\text{O}_{\text{PDB}} + 30.86$  (Friedman and O'Neil, 1977).

$$1000 \ln \alpha = 18.03 (10^3 \text{ T}^{-1}) - 32.42 \quad (\text{A.1})$$

$$\alpha = (1000 + \delta^{18}\text{O}_{\text{calcite}}) / (1000 + \delta^{18}\text{O}_{\text{water}}) \quad (\text{A.2})$$

$$\delta^{18}\text{O}_{\text{SMOW}} = 1.03086 \delta^{18}\text{O}_{\text{PDB}} + 30.86 \quad (\text{A.3})$$

where  $\alpha$  is the fractionation factor (Eq. A.2) and T is temperature in kelvin.

At the MC 118 site,  $\delta^{18}\text{O}$  value of +4.15‰ was measured and a seafloor temperature of +5.7°C was calculated. To calculate the equilibrium temperature, the measured  $\delta^{18}\text{O}$  value of +4.15‰ in PDB to the value in SMOW were converted from Eq. (A.3) as shown below.

$$\delta^{18}\text{O}_{\text{SMOW}} = 1.03086 (4.15) + 30.86 = 35.14$$

From Eq. (A.2), the fractionation factor ( $\alpha$ ) is 1.03514, as shown below.

$$\alpha = (1000 + 35.14) / (1000 + 0.0) = 1.03514$$

Thus, the equilibrium temperature of -3.9°C was calculated from Eq. (A.1), with water  $\delta^{18}\text{O} = +0.2\text{‰}$ .

The water  $\delta^{18}\text{O}$  value of +0.2‰ (SMOW) is for seawater (<http://data.giss.nasa.gov/o18data>; GEOSECS Grossman and Ku, 1986) in the Gulf of Mexico at a nearest location (latitude: 27.52°N and longitude: 95.00°E, water depth: 799 m) to the study site of MC 118 (latitude: 28° 51.4'N and longitude: 88° 29.5'E, water depth: 890 m).

Because this calculated temperature of  $-3.9^\circ\text{C}$  for seawater is too cold for the environment,  $\delta^{18}\text{O}$  of water using the measured  $\delta^{18}\text{O}$  value and temperature of the ACR sample was calculated.

From Eqs. (A.1) and (A.2), water  $\delta^{18}\text{O}$  of +2.3‰ (SMOW) with a fractionation factor of 1.03276 was calculated.

$$1000 \ln(\alpha) = 18.03 [10^3 (5.7^{-1})] - 32.42 \quad (\text{A.1})$$

$$1.03276 = (1000 + 4.15) / (1000 + \delta^{18}\text{O}_{\text{water}}) \quad (\text{A.2})$$

$$\alpha = \text{EXP}[(18.03 \times 1000 / (273.15 + 5.7) - 32.42) / 1000] = 1.03276$$

$$\delta^{18}\text{O}_{\text{water}} = (1000 + 35.14) / 1.03276 - 1000 = +2.3$$

Thus, ACR may form in heavier water of +2.3‰ (SMOW).



## APPENDIX B

Equilibrium temperature with an equilibrium oxygen isotope equation between calcite and water was calculated (Eq. A.1) (Kim and O'Neil, 1997). For the calculations, oxygen isotope values measured in PDB were converted to SMOW using the relation of  $\delta^{18}\text{O}_{\text{SMOW}} = 1.03086 \delta^{18}\text{O}_{\text{PDB}} + 30.86$  (Friedman and O'Neil, 1977).

ACR sample #3-1 from Site 3 in the Krishna-Godawari basin offshore India has  $\delta^{18}\text{O}$  value of +4.99‰. According to the geothermal gradient (3.9°C/100 m), depth =  $25.641 \times -166.67$ , the temperature at sample depth was calculated:  $56.2 = 25.641 \times -166.67$ , where  $\times$  is the temperature at sample depth. Here  $\times = 8.69^\circ\text{C}$ .

$$1000 \ln \alpha = 18.03 (10^3 \text{ T}^{-1}) - 32.42 \quad (\text{A.1})$$

$$\alpha = (1000 + \delta^{18}\text{O}_{\text{calcite}}) / (1000 + \delta^{18}\text{O}_{\text{water}}) \quad (\text{A.2})$$

$$\delta^{18}\text{O}_{\text{SMOW}} = 1.03086 \delta^{18}\text{O}_{\text{PDB}} + 30.86 \quad (\text{A.3})$$

where  $\alpha$  is the fractionation factor (A.2) and T is temperature in kelvin.

At Site 3, there are a measured  $\delta^{18}\text{O}$  value of +4.99‰ and a calculated temperature of +8.69°C from geothermal gradient.

$\delta^{18}\text{O}$  value of +0.15‰ was used for seawater (<http://data.giss.nasa.gov/o18data>; GEOSECS Ostlund et al., 1987) in the Indian Ocean at a nearest location (latitude: 12.53°N and longitude: 84.51°E, water depth: 1,190 m) to the study of Site 3 (15° 53.90'N and 81° 53.97'E). To calculate the equilibrium temperature, the measured  $\delta^{18}\text{O}$  value of +4.99‰ in PDB to the value in SMOW was converted from Eq. (A.3).

$$\delta^{18}\text{O}_{\text{SMOW}} = 1.03086 (4.99) + 30.86 = 36.004 \quad (\text{A.3})$$

From Eq. (A.2), the fractionation factor ( $\alpha$ ) is 1.03585, as shown below.

$$\alpha = (1000 + 36.004) / (1000 + 0.15) = 1.03585 \quad (\text{A.2})$$

Thus, the equilibrium temperature of  $-6.6^{\circ}\text{C}$  was calculated from Eq. (A.1). Because this calculated temperature of  $-6.6^{\circ}\text{C}$  for seawater is too cold for the environment, the  $\delta^{18}\text{O}$  of water was calculated using the measured  $\delta^{18}\text{O}$  value and temperature of the ACR sample. From Eqs. (A.1) and (A.2), water  $\delta^{18}\text{O}$  of  $+3.83\text{‰}$  (SMOW) was calculated with fractionation factor of 1.03206.

$$\alpha = \text{EXP}[(18.03 \times 1000 / (273.15 + 8.69) - 32.42) / 1000] = 1.03206 \quad (\text{A.1})$$

$$\delta^{18}\text{O}_{\text{water}} = (1000 + 36.004) / 1.03206 - 1000 = 3.83 \quad (\text{A.2})$$

Thus, ACR may form in heavier water of  $+3.83\text{‰}$  (SMOW).

**VITA**

Name: Woodong Jung

Email address: jwoodong@gmail.com

Permanent Address: 7-20 Shinsa-dong, Eunpyeong-gu,  
Seoul, 122-080  
Republic of Korea (South Korea)

Education: B.S., Mechanical Engineering, 1984  
Hanyang University, Korea  
M.S., Mechanical Engineering, 1987  
Chungang University, Korea  
M.S., Petroleum Engineering, 2002  
Texas A&M University, U.S.A.

Professional Experience: Korea Gas Technology Corporation  
Dong-Ah Engineering & Construction Co.